UNIVERSITY OF NAPLES

"FEDERICO II"

PhD in Chemical Sciences

XXXI Cycle

2015-2018

Eumelanin exploitation in bioelectronics: ionic-electronic charge transport in eumelanin organic thin films

Dr Ludovico Migliaccio

Supervisors

Dr Alessandro Pezzella (University Tutor)

Dr Paolo Tassini (ENEA Tutor)

Assessor	PhD Coordinator
Prof. Antonio Roviello	Prof. Luigi Paduano

Index

Aknowledgements

First of all I would like to thank my two tireless supervisors, Alessandro Pezzella and Paolo Tassini without whom every single experiment would have been difficult and with complicated scientific answers. I still know I have to learn a lot from them, but during these years I have tried to steal a lot of ideas that I hope will serve me for my future as a researcher. Furthermore, it is a duty to thank Mariagrazia Maglione and Paola Manini who also helped me in situations that were outside the experiments related to my PhD topic and that were always on the front line during the entire journey.

A small parenthesis of my Ph.D, which turned out to be a modification of my life, was the experience as a visiting student at the LOE group in Norrköping (Sweden), for which opportunity I thank Alessandro Pezzella who believed in me, and it is also a duty to thank Eric Głowacki, a big scientist and also a good friend, who was my supervisor during this period, and his group that welcomed me and considered me an integral part of the team. For all the things that they have done, it is more than fair to thank them individually, so I would like to thank Vedran Đerek, one of the most meticulous scientists I have ever met in my path, practically a “factotum” with an uncommon brain. I would also like to thank Marie Jakešová, a true friend and a wonderful person, not only scientifically but also humanly. And I also thank Maciej Gryszel, my experiment collegue, with whom, despite the countless moments of desolation, we were also able to laugh during the experiments. It was a really nice period that made me stronger. It was not easy for me to fight against the cold, the snow, the dark and so on, for me that if I look out of the office I see the sea, but it helped me to improve myself because I am of the opinion that before being a good scientist, you have to be a good person and appreciate the things you have in front of you. For this I would like to thank the biggest piece of my heart, my "Bella famiglia", that has been beside me from the happiest days to the saddest

ones of this journey. It was not easy for them to fight against my ugly behaviour resulting from days of inconclusive experiments, but they never made me weigh and I take this opportunity to apologize to them of my attitude. But one of the best moments of the day was to come back home, my fortress, with my trusted and loved people, so I would like to thank them by giving a few lines from the opening speech of the film "Patch Adams", which I saw when I was in Sweden and immediately I shared that thought and meaning attributed to home and in my case family:

“All of life is a coming home. Salesmen, secretaries, coal miners, beekeepers, sword swallowers, all of us. All the restless hearts of the world, all trying to find a way home. It's hard to describe what I felt like then. Picture yourself walking for days in the driving snow; you don't even know you're walking in circles. The heaviness of your legs in the drifts, your shouts disappearing into the wind. How small you can feel, and how far away home can be. Home. The dictionary defines it as both a place of origin and a goal or destination. And the storm? The storm was all in my mind. Or as the poet Dante put it: In the middle of the journey of my life, I found myself in a dark wood, for I had lost the right path. Eventually I would find the right path, but in the most unlikely place.”

Of course I would like to thank my old date friends, Antonio, Carlo and Nicola who have always supported me in everything I have done, believing in me and strengthening my constancy and audacity in my activities.

Finally I thank "you", THE MUSIC, the perfect accompanying lady of every single moment of my life. I consider myself to be a rather solitary person, but the music and the Guitar have softened me and they are a company that never tires, from racing to take trains, to long walks back home, to air flights, to countless experiments.

The music sensitizes, listen to it, let it be said by a lonely lab rat like me.

Abstract

Eumelanin, the mammal pigment originating via the oxidative polymerization of 5,6-dihydroxyindole (DHI) and/or 5,6-dihydroxyindole-2 carboxylic acid (DHICA), for more than forty years have been the focus of uncommon interest in biomedical research due to their central relevance to skin and eye photoprotection.

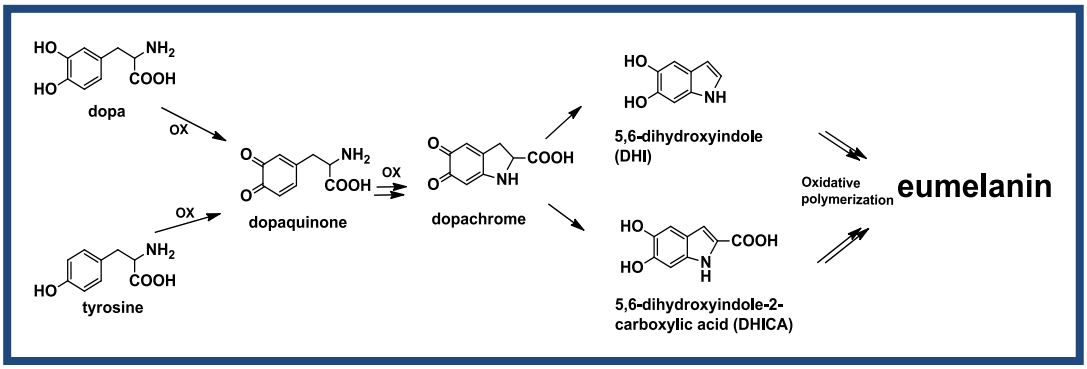

During the last two decades, several peculiar properties of eumelanin-inspired polymers have attracted the attention of the materials science community too, following the realization of device quality thin films through controlled polymerization of DHI and derivatives. The properties of these materials include: a) broadband optical absorption in the UV-visible range; b) efficient UV-dissipative mechanisms; c) photoconductivity in the solid state; d) electronic-ionic hybrid conduction properties.

Anyway, despite a burst of interest in the use of synthetic eumelanin for organic electronics and bioelectronics, the implementation of competitive eumelanin based technology has so far been hindered by several drawbacks. These ones include: complete insolubility in all solvents, preventing the development of standardized and reproducible synthetic procedures, low conductivity, and the lack of a solid

conceptual frame of structure–property–function relationships. In particular, the high molecular heterogeneity of the eumelanin, whose impact on their electrical performances has not been still systematically assessed, generates several critical consequences like, for example, the lack of well-defined HOMO–LUMO gaps.

This PhD project aims to identify Structure Property Function relationships in order to propose a mechanistic model describing the ionic-electronic charge transport in eumelanin thin films and finally fabricate eumelanin based devices.

In Chapter 1, is described an overview related to the physico-chemical properties of Eumelanin and the different methods used to obtain it , and this chapter will present also a description related to the recent explosion of interest for Eumelanin applications in bio-electronics and organic-electronics fields that will be one of the main focus with which this thesis will deal.

In Chapter 2, to increase the eumelanin conductivity performances, hybrid materials were designed, adding eumelanin to conductive materials (in this case, PEDOT:PSS (poly(3,4-ethylenedioxythiophene):polystyrene sulfonate)). Resulting material properties have been studied through spectroscopic characterizations, and by means of X-rays, SEM, UV-VIS, contact angle, profilometry, and electrical measurements on different devices architectures.

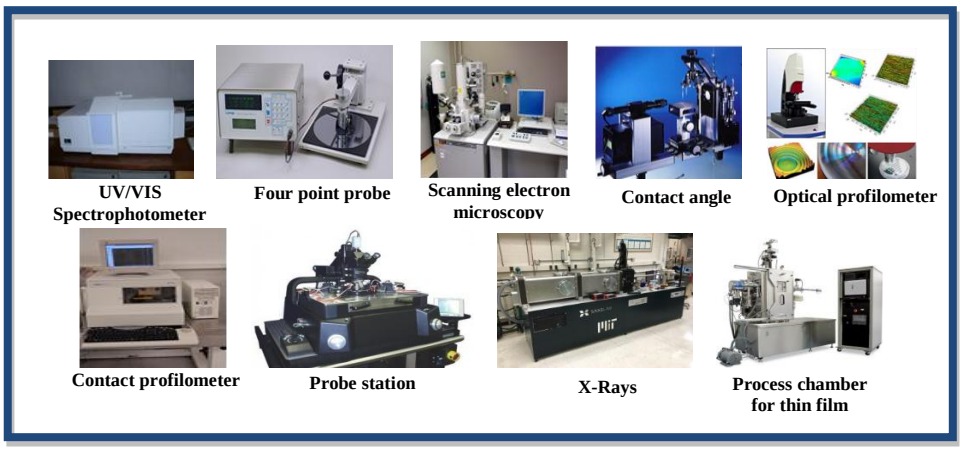

Figure 1: Part of the instruments used to characterize material properties

Thin films are ideal candidates to be studied, because they are easily accessible to chemical and morphological characterizations and potentially susceptible to device applications. The first step in the PhD study has involved the design and characterization of hybrids made from blends of Clevios™ PEDOT:PSS PH1000, a conductive polymer, and melanin pigments. The aim of this blend is to have a material which is conductive or satisfactorily conductive as the PEDOT:PSS and, at the same time, resistant to the possible conditions under which the PEDOT: PSS is unstable, for example, exposure to water and other degrading agents such as oxygen. The melanin is able to ensure factors such as stability to degrading agents, but also adhesion to the substrate, which does not make the PEDOT:PSS.

The designed and prepared blends differ in the variable DHI / PEDOT:PSS ratio; the solvent used for the solubilization of the DHI was found to be the propan-2-ol. The blends were prepared in the presence and in the absence of a secondary dopant. A primary dopant differs from a secondary dopant (better defined as "additive") since the former has a reversible effect, while the effect of the secondary doping is permanent and remains even when the additive is removed. Here, the agent of the secondary doping was dimethylsulfoxide (DMSO).

Capitalizing on a recently developed protocol to prepare high quality eumelanin coatings, herein it is reported the design and the integration of standard commercial PEDOT:PSS with eumelanin pigment (see chapter 2). During this study, were prepared different blends with different DHI/PEDOT ratios in order to understand and define an electrical conductivity trend, with eumelanin content increase in the chemical system. The study of electrical properties of these blends was mandatory in order to define and satisfy a good blend able to work as polymeric anode in an Organic light emitting diode device (OLED) that is one of the ideas of application of this material for organic-electronics and bio-electronics purposes. The blend used is the one with DHI/PEDOT ratio = 0.4 w/w. This blend has allowed to get water stable transparent thin films, capable to operate as electrodes for organic devices, complementing the PEDOT:PSS electronic conductivity with *the* peculiar

eumelanin properties, including adhesion, water stability and ionic-electronic conductivity.

As a proof of concept, an unprecedented ITO (Indium tin oxide)-free organic light emitting diode (OLED) implementing an eumelanin-PEDOT layer as the anode was fabricated and characterized. To the best of our knowledge, this is the first evidences of an OLED device based on an anode layer integrating eumelanin. To prepare the mixture of eumelanin and PEDOT:PSS (Eu-PH), a protocol involving in situ eumelanin generation was designed. This approach allowed not only to circumvent the actual insolubility of eumelanin in any solvent, but also to gain over the PEDOT molecular organization. The target was to obtain a material with good conductivity (not less than 300 $S*cm^{-1}$) and a work function at least comparable with the ITO (whose commonly reported around 4.4÷4.7 eV) or larger for an efficient hole injection, to be effectively used as the anodic material in organic electronic devices. The Eu-PH thin films were thus obtained by exposing the DHI-PEDOT:PSS films, obtained via spin-coating onto glass substrates, for 1 h to air-equilibrated gaseous ammonia (AISSP (Ammonia induced solid state polymerization) protocol)), from an ammonia solution (28% in water) inside a sealed chamber at 1 atm pressure and at controlled temperature (25°C÷ 40°C).

For the OLEDs, a hole injection layer (HIL), CLEVIOS PEDOT:PSS PVP Al 4083, used *as-is*, was deposited via dip-coating (thickness 90 nm). Final steps of the OLEDs fabrication were carried out under inert atmosphere. All the substrates were loaded into a glove box system (N_2 atmosphere, O_2 < 1 ppm, H_2O < 1 ppm), and transferred into an in-line evaporation chamber. The active area of the devices was 7 x 10^{-6} m^2. The final OLED architecture includes: the glass substrate; the anode (ITO; or CLEVIOS PH 1000; or Eu-PH); the HIL; the HTL; the ETL-EML and the cathode.

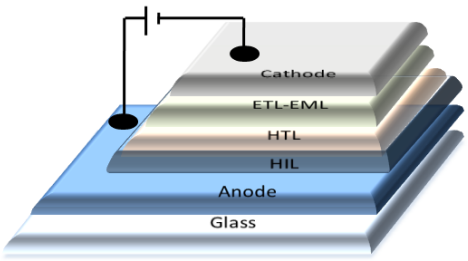

Figure 2: Schematic section of the OLED devices prepared

Because a more in-depth investigation is required to fully address the eumelanin-PEDOT integration, the effect of the eumelanin on conductivity of the blends was thus related to structural features observed in Wide Angle X-ray Scattering (WAXS) and X-ray diffraction (XRD) patterns of films with different eumelanin content and fixed PEDOT:PSS ratio. Analysis of free-standing films in transmission geometry (WAXS) allowed to get rid of substrate scattering contribution, and mainly probe crystallographic directions parallel to the film plane. On the other hand, reflection geometry (XRD, GIWAXS) allowed probing structural order in both directions, in and out of the film plane, and can be used for the as-prepared films, laying on glass substrates, to better relate structural and electrical properties. The effect of the eumelanin integration within PEDOT:PSS layers was investigated in terms of the changes in the hierarchical structure of the PEDOT:PSS films. The results of the X-ray scattering characterization clearly demonstrate that the presence of the eumelanin affects the PEDOT component of the blend, inducing an overall increase of the crystalline order at low eumelanin contents. This effect is associated with a smaller distance between the PEDOT chains. Moreover, when eumelanin percent content increases, a less steep decay of the blend conductivity was observed, than the one expected on the basis of the data reported on the conductivity of PEDOT ternary mixtures. At the same time, the introduction of the eumelanin gives noteworthy properties to the Eu-PH blend, including a strong adhesion on inorganic substrates, and water stability, which open

to an efficient exploitation of the Eu-PH for conductive coatings within biointerfaces for application in bioelectronics.
As said, higher values of the eumelanin electrical conductivity are needed for applications in organic electronics, thus several studies explored the integration of the pigment with conductive materials. But, these approaches actually modify the chemistry of the layers. Other approaches also exploited severe modifications of the eumelanin-like materials to gain a graphene-like material, as for example by pyrolitic treatment of polydopamine under hydrogen atmosphere.

The mechanism of charge transport in eumelanin is still not fully clear, but several evidences are concurring to sustain a hybrid ionic-electronic behaviour, where the electronic contribution depends on the presence, extent and the redox properties of the delocalized aromatic systems, while the ionic part is largely dictated by the hydration level of the pigment (i.e. humidity in the measuring environment). Basing on the concurring evidences disclosing the correlation between the chemical physical properties of the eumelanins and the polyindole π-system staking, as well as the packing of the molecular constituents within the pigment, we speculated about the modulation of the electronic conductivity, by acting on the polyindole packing in eumelanin thin films. Here (Chapter 3), preparation and characterization of eumelanin thin films showing conductivity up to 318 S/cm are discussed. Highly conductive films were prepared via the oxidative polymerization of films of 5,6-dihydroxyindole (DHI), the ultimate monomer precursor in the formation pathways of natural and synthetic eumelanins, then treated under high vacuum thermal annealing. We name the obtained material as High Vacuum Annealed Eumelanin, HVAE.

During the 3rd year of the PhD course, I have had a research visiting period in the Laboratory of Organic Electronics of the University of Linköping in Norrköping under the supervision of Dr. Eric Daniel Głowacki. During this

time, I worked on a project concerning the photo(electrochemical) properties of the eumelanin. We report (see Chapter 4) that eumelanin is a photo-catalytic material. Though photoconductivity of eumelanin and its photochemical reactions with oxygen have been known for some time, eumelanins have not been regarded as photofaradaic materials. We found that eumelanin shows photocathodic behaviour for both the oxygen reduction reaction and the hydrogen evolution reaction. Eumelanin films irradiated in aqueous solutions at pH 2 or 7 with simulated solar light, photochemically reduce oxygen to hydrogen peroxide with accompanying oxidation of sacrificial oxalate, formate, or phenol. Auto-oxidation of the eumelanin competes with oxidation of donors. Deposition of thin films on electrodes yields photoelectrodes with higher photocatalytic stability, compared with the case of pure photocatalysis, implicating the successful transport and extraction of holes from the eumelanin layer. These results open up new potential applications for eumelanin as a photocatalytically-active biomaterial, and inform the growing fundamental body of knowledge about the physical chemistry of the eumelanin.

From all of this work, as result of this finding, we demonstrate new potentialities of Eumelanin in organic-electronics and bio-electronics field, developing new methods and new recipes either to increase electrical conductivity in order to exploit this material for several applications and purposes either to use it as photocatalytically-active material. Although a conclusive picture about the conductor vs semiconductor behavior of the eumelanins and insights about the mobility of charge carriers will require further investigations, results related to annealed thin films of Eumelanin, here reported, radically modify the actual picture of the eumelanin charge transport properties, reversing the paradigm according to which eumelanin conductivity increases with the water content of the pigment. Indeed, when

eumelanin molecular constituents are rearranged in conductive layers, the contribution of electronic current is demonstrated to be largely preeminent with respect to the ionic one, allowing to get unprecedented conductivity and to consider the mammalian pigment as an actual conductor.

1. Introduction

1.1 Introduction on melanins

The term Melanins (μέλας = black)[1] has been used since 1840 to denote the broad class of pigments found throughout nature, from human beings to invertebrates, plants and fungi.

Melanin is a predominantly indolic macromolecule[2]. There are many different types of melanin, including eumelanin, pheomelanin, neuromelanin and allomelanin. Eumelanin and pheomelanin are both found in the skin, hair and eyes of many animal species, including humans, where they act as photo-protectants (absorbing harmful ultraviolet and visible radiation).

Eumelanin is known to be a macromolecule built up from 5,6-dihydroxyindole (DHI) and 5,6-dihydroxyindole-2-carboxylic acid (DHICA), and is black to brown in colour[3]. Eumelanin is the most extensively studied of all melanins since it is the primary pigment found in human skin, although it also forms the major component of squid ink and is responsible for the dark colouration in feathers[4]. Pheomelanin is a sulfur containing macromolecule composed of 1,4-benzothiazine units, and is red to yellow in colour (pheomelanin is responsible for the colouration of human red hair and chicken feathers[5, 6]). This thesis deals essentially with eumelanins.

The other varieties of melanins (including allomelanins and neuromelanins) will not be described in this thesis, but briefly allomelanins are pigments

nitrogen free found largely in plants such as certain fungi and seeds, and also in soil. Neuromelanins are found in the brainstem and inner ear of humans and higher primates where its role is unknown, although it is thought to have some biological significance; neuromelanin is decreased or absent in individuals with Parkinson's disease, for example[7, 8]. It is not clear whether the relationship between neuromelanin and Parkinson's disease is causal, although it is suggested that the pigment might modulate neurotoxic processes through interaction through iron, binding of drugs or reaction with free radicals and free radical producing species[9]. Additionally, albinism often leads to deafness in animals, suggesting biological functionality[10].

1.2 Interest in melanins

Paradoxically, although melanin is a photoprotectant, it has also been implicated in the chain of events that lead to malignant melanoma skin cancer[11-13], although this link is very poorly understood. Highly pigmented skin is more protected from carcinogenesis than un-pigmented skin[14], but it has been suggested that pheomelanin may actually function as a photosensitizer[15], and has been shown to actually enhance DNA damage in cells in response to ultraviolet radiation[16, 17]. The skin is the most common site of cancer in humans[14], and although melanoma is one of the rarer types of skin cancer, it causes the majority of skin cancer related deaths[18]. According to the World Heath Organisation, approximately 48,000 melanoma related deaths occur each year[19]. This makes understanding the biological functionality of melanin and its role in melanoma a health priority, particularly for countries with high levels of solar radiation such as Australia. Melanin also plays a central role in a variety of highly visible and inconvenient pigmentary disorders such as albinism and vitiligo[20].

Melanin is also of interest as a model system for understanding disorder in biological systems. Disorder is thought to be an essential part of the biological functionality of melanin, which is unlike other much more thoroughly studied biomolecular systems such as DNA and proteins. Disordered systems in biology have yet to receive a great deal of attention, likely due to the difficulties inherent in studying them. This makes melanin a fascinating novel system with the potential for development of techniques applicable to a wide range of important biosystems[21-23].

As a third point of interest, melanins exhibit interesting physical and chemical properties such as anti-oxidant and free-radical scavenging

behaviour, metal and drug binding properties[24-27], broad band ultraviolet and visible absorption and strong non-radiative relaxation of photo-excited electronic states[28]. These physical chemical properties, together with the natural pigment bio-compatibility, are the basis for the great interest in the realization of eumelanin based electronic devices. Possible examples include highly efficient broadband single photon counters (superconductor based bolometers with a thin eumelanin film as the sensitising pigment), extremely sensitive humidity sensors (based on the extreme sensitivity of eumelanin solid state conductivity to hydration), organic semiconductor electronics and solar cells[29, 30]. Despite a burst of interest in the use of synthetic eumelanins and related biopolymers for organic electronics and bioelectronics, the implementation of competitive eumelanin based technology has so far been hindered by several drawbacks, expecially related to the low conductivity of the material. One of the main focuses with which this thesis will deal is thus related to the possibility to modulate the electrical conductivity of this bio-polymer in order to make it suitable for its application as material for devices fabrication.

1.3 Synthesis of eumelanins

Biochemically, eumelanin is derived from tyrosine in a reaction catalysed by the enzyme tyrosinase, as outlined in the scheme depicted in scheme 1.1. Analysis of this synthetic process and final eumelanin structure is extremely difficult due to the highly unstable nature of the reaction intermediates, and extremely stable and insoluble nature of the final product[31]. Nevertheless, intermediates have been identified, largely due to the pioneering work of Raper and Mason[32]. The enzyme tyrosinase acts on dopa and tyrosine to produce dopaquinone, which reacts to form dopachrome (a red compound). Dopachrome is rather stable, but will spontaneously decompose to form DHI (5,6-dihydroxyindole), giving off CO_2. If the enzyme dopachrome tautomerase is present (Dct), dopachrome will instead tautomerise to give mostly DHICA (5,6-dihydroxyindole-2-carboxylic acid), retaining the carboxylic acid group[33]. Hence the availability of Dct will determine the relative amounts of DHI and DHICA produced, and therefore the ratio of these components in the final eumelanin macromolecule. This ratio will also be affected by other enviromental factors, and hence varies widely depending upon the source of the eumelanin under study[34]. It is widely accepted that eumelanin is a heterogeneous macromolecule of DHI and DHICA. Melanin must be extracted from biological systems for study, and the extensive amount of bound protein must be removed. This is often achieved via harsh processes such as acid/base treatment, which is known to severly disrupt the properties of the pigment[35].

Much milder enzymatic methods are also available to extract melanin from hair, skin and eye tissue yielding melanin that is closer to its natural state[36]. It has become common practice to use eumelanin extracted from the ink sac of

the cuttlefish Sepia officinalis as a model eumelanin pigment since it is readily available and easily extracted via mild techniques which yield a uniform black pigment that is appropriate for use as a standard[37]. Material that is termed 'synthetic melanin' is also often used as a standard for natural melanins. Synthetic melanin is formed under a variety of conditions in vitro including:

• Biomimetic conditions - oxidation by DHI with enzyme tyrosinase in aqueous buffer at neutral pH. This would seem to be the best synthetic method since it is closest to the natural system, but unexpectedly eumelanin formation occurs very slowly under these conditions, even in the presence of large amounts of enzyme[38]. Additionally, it is challenging to control and measure the activity of tyrosinase during this reaction, giving poor reproducibility[3]. Enzymatic preparations may also be performed with the alternate substrates of dopa and tyrosine.

• Autoxidative dopa eumelanin may be prepared by simply allowing alkaline solutions of dopa to come into contact with air. The solution may then be acidified to precipitate the eumelanin[31].

• A peroxidase/H_2O_2 couple induces a complete and rapid conversion of DHI to eumelanin in aqueous buffer at biomimetic pHs[39]. Similarly, a synthetic eumelanin is commercially available that has been prepared by persulfate or peroxide oxidation of tyrosine[31].

The resulting black pigments show great similarity to natural eumelanin, although proof that they are identical to natural eumelanin remains lacking[3]. Synthetic eumelanin is convenient as a model system for pioneering new methods or theories to treat this difficult material, and since they are produced under controlled conditions and contain known monomeric units they offer advantages for analysis over the more complex naturally extracted melanins. Throughout this thesis we use DHI eumelanin as a synthetic analogue for natural eumelanin in the way to be able to circumvent the

multiple problems related with the low processability of the Eumelanin following the monomer route[40] as will be described in 1.5.

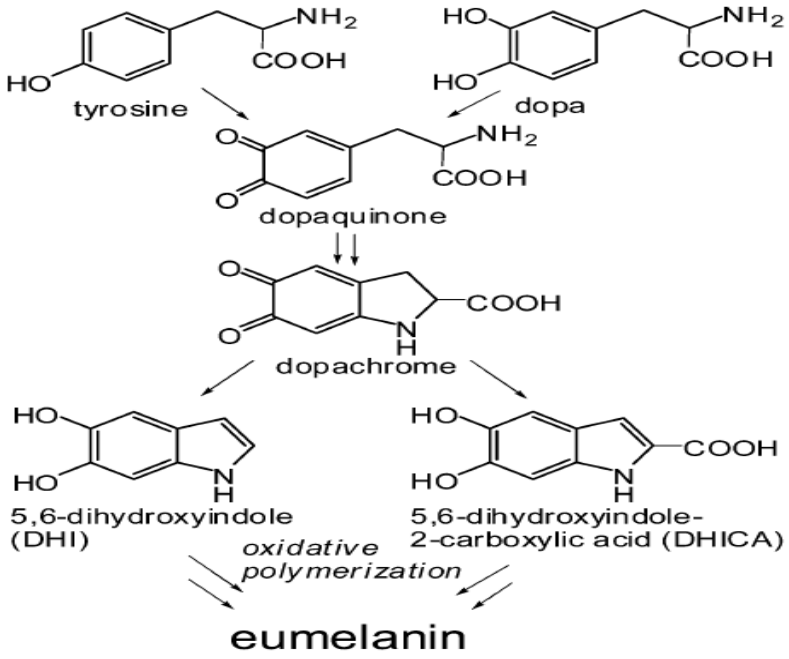

Scheme 1.1. Schematic view of eumelanin synthesis from tyrosine or dopa. Representative intermediates in the process are highlighted.

1.4 Eumelanin physicochemical properties

Working on eumelanins has usually been regarded as an intriguing, though experience[40]. This is due to several challenging features of the system, including almost complete insolubility in all solvents, an amorphous particulate character, and extreme molecular heterogeneity. Eumelanin does however possess a number of physicochemical properties[28] that can be used to identify and quantify the system, such as a persistent electron paramagnetic resonance (EPR) signal, broadband monotonic optical absorption, peculiar excitation and emission properties[41, 42], and time dependent photodynamics[43-45]. Standard vibrational methods such as infrared absorption and Raman spectroscopy[46, 47] and more recently inelastic neutron scattering spectroscopy[48] have also been applied with varying degrees of success to study the vibrational finger-print of eumelanin precursors. Controlled chemical degradation giving traces of pyrrolic acids has been exploited mainly for pigment analysis in tissues[49, 50] yielding only limited information as to the basic aspects of eumelanin primary-level structure[3]. Yet to-date eumelanins fundamental structure (if indeed the term “structure” can rightly be applied to such a highly heterogeneous material), is still under intense scrutiny[40, 51].

These properties – which include features such as anti-oxidant and free-radical scavenging behaviour, broad band UV and visible absorption and strong non-radiative relaxation of photo-excited electronic states – are defined by the molecular, supramolecular and aggregate-level structure. Establishing the relationships which link structure and properties is a common goal in many branches of materials physics and chemistry. Understanding how these structure–property relationships define biological

function is the realm of molecular biophysics and molecular biology. The ultimate goal of melanin research is to link all these facets together to gain a full mapping of how molecular and cellular scale structure relate to macroscopically observable properties and functions. Such a process will allow us to understand melanin related disease states, and create meaningful medical interventions. Exactly this process has led to the genomics and proteomics revolutions of the last decade.

1.5 Eumelanin-based organic (bio) electronics

The pigment melanin, more precisely eumelanin, was reported to have semiconducting properties already in the 1960's and 70's[56-59]. Properties of eumelanin that caught the attention of material scientists and physicists include a persistent electron spin resonance signal, indicating stable free radicals[60], strong optical absorption with a featureless spectrum[61], and the hydration-dependent (photo-)conductivity of eumelanin pellets. These properties were mostly explained within the framework of the amorphous semiconductor model, building on the discovery of reversible threshold switching of eumelanin pellets by McGinness in 1974[59]. Most recent works referring to the electrical properties of eumelanin still consider eumelanin as an amorphous semiconductor[54, 61-65]. However, there have also been reports about mobile ions, in particular protons, in eumelanin[67-69]. In 2012, Mostert et al. resumed the debate on the origin of the electrical conductivity of eumelanin[68a]. Their work on eumelanin pellets seems to disprove the amorphous semiconductor model and suggests that both electrons and protons are mobile in eumelanin pellets.

Santato et al. have elaborated a charge transport model in a series of papers showing the relationship between protons as the major charge carrier and the paramagnetic species observed in eumelanin[68b]. Definitive proof of electron and proton transport over device-relevant distances, insights into the relative contribution of electrons and protons to the electrical current at different sample hydration states, and a new model for the charge carrier transport mechanism in eumelanin are still missing to date. In particular, reports on the electrical properties of hydrated eumelanin films are very sparse. The characterization of eumelanin is complicated by its high degree of chemical

and structural disorder and its insolubility in common solvents[70]. Furthermore, many properties of eumelanin are strongly affected by hydration[71]. The structure of eumelanin depends on (bio-)synthetic conditions and precursors[70, 72]. Chemical and structural disorder also implies energetic disorder and makes any structure-property correlation challenging. The insoluble nature of eumelanin defies many conventional techniques for the characterization of organic molecules and it is furthermore an obstacle for the preparation of eumelanin thin films. Indeed, strategies for the solution processing of eumelanin films have been suggested only recently[73, 74]. Thin films enable the use of a wider range of characterization techniques and facilitate the integration in device architectures. The next step in this line of research is to optimize film processing, characterize film structure and functional properties, and to investigate the interaction of eumelanin thin films with other device components. The development of organic bioelectronics revived the interest in eumelanin as a functional material[53, 54, 75, 76]. The electrical and chemical properties of eumelanin in combination with its intrinsic biocompatibility have encouraged researchers to explore the use of eumelanin in tissue engineering[65], biocompatible batteries[77], memory devices[78], and sensors[66, 79]. The possibility of mixed ionic-electronic conduction makes eumelanin an interesting candidate for ion-to-electron transduction[68].

1.6 Thin film fabrication

The employment of eumelanin in organic electronics requires effective technologies for device fabrication, in particular thin film preparation. A milestone in film fabrication is given by the report on device-quality synthetic melanin thin films by Bothma and de Boor in 2008[74], using eumelanin solution obtained by alkaline treatment. It has to be noted here that such treatments also produce serious chemical modification in the structural backbone of the pigment[80, 81]. A number of other papers also report melanin film preparation by spin-cast procedures.

Generally, these procedures require alkaline treatment of eumelanin samples[69, 82] or very harsh synthetic procedure such as benzoyl peroxide-promoted oxidation of L-DOPA in dimethyl sulfoxide (DMSO) over days[83, 84]. Bettinger and Bruggeman reported good biocompatibility of eumelanin films spin-cast from either alkaline solution or DMSO[66].

More recently, a series of studies addressed novel technologies for film preparation. Abbas and Ali reported the use of electrospray deposition[86]. A similar procedure has been adopted previously[62]. The first deposition of biomimetically prepared eumelanins was achieved by the use of laser deposition matrix-assisted pulsed laser evaporation (MAPLE), as reported by Bloisi and Pezzella, yielding melanin films featuring a high structural integrity at the molecular level[87, 88].

Electrochemical methods were also used for the self-assembly of eumelanin films on Au and graphite surfaces, using alkaline suspensions of eumelanin aggregates[79, 84, 89]. A totally different approach is the polymerization of melanin precursors on substrates. Subianto and Will obtained eumelanin free-standing films by electrochemical oxidation of DOPA solution on

indium tin oxide (ITO) glass electrode[90]. Electrochemical polymerization of DHI on ITO substrates was obtained by using cyclic voltammetry and constant potential methods[84]. Also, dopamine was used as precursor to obtain films of melanin-like polymers, namely, polydopamine. By simple immersion in dopamine solution, a large variety of substrates could be coated[91]. The thickest films were produced in alkaline medium[85, 92].

These works demonstrate the significant progress made in eumelanin film fabrication during the last years. In this thesis the approach used for the fabrication of eumelanin films was the use of DHI as the eumelanin precursor in place of commonly used dopa or dopamine, for the following reasons: (1) DHI is soluble in organic solvents and is the ultimate monomer precursor in the pathways of natural and synthetic eumelanins, ensuring the generation of homopolymers rather than copolymers of various intermediates, as in the case of dopa and dopamine melanins[72, 93, 94];

(2) the mode of polymerization of DHI and its dimers and oligomers[95-99], the mechanisms of aggregation underlying particle growth, and the optical and free radical properties of DHI melanin[93-100] have all been clarified in detail;

(3) the electrical properties of DHI melanin suspensions have been characterized using an organic-electrochemical transistor[101];

(4) DHI melanin can be used to prepare thin films by a variety of methodologies, although their morphological properties are not always of high quality[87, 88].

The manifold problems associated with the limited processability of insoluble eumelanins were then overcome by rational development of a procedure, referred to as ammonia induced solid state polymerization (AISSP), which is based on the uniform deposition by spin coating of the soluble DHI monomer as highly homogeneous thin films, followed by solid state polymerization induced by exposure to gaseous ammonia in an air-equilibrated atmosphere. Film fabrication on suitable quartz substrates

allowed to easily follow the polymerization process by UV-vis spectroscopy, observing the spectral evolution with time.

1.7 References

1. P. A. Riley, Melanin. The International Journal of Biochemistry & Cell Biology, 29(11), 1235, 1997. DOI= 10.1016/S1357-2725(97)00013-7
2. G. A. Swan, Structure, chemistry and biosynthesis of the melanins. In Progress in the Chemistry of organic natural products (Springer-Verlag, New York, 1974).
3. G. Prota. Melanins and Melanogenesis (Academic Press, San Diego, 1992).
4. N. Kollias, R. M. Sayer, L. Zeise, and M. R. Chedekel, New trends in photobiology: Photoprotection by melanin. Journal of Photochemistry and Photobiology B Biol 9, 135, 1991. DOI= 10.1016/1011-1344(91)80147-A
5. V. J. Hearing, Biochemical control of melanogenesis and melanosomal organization. Journal of Investigative Dermatology 4, 25, 1999. DOI= 10.1038/sj.jidsp.5640176
6. V. J. Hearing, The regulation of melanin production. In J. J. Norlund, R. E. Boissy, and V. J. Hearing, eds., The Pigmentary System: Physiology and Pathophysiology, pp.423–438 (Oxford University Press, New York, 1998).
7. T. B. Fitzpatrick, A. Z. Eisen, K. Wolf, I. M. Freeberg, and K. F. Austen, Biology of Melanocytes (McGraw-Hill Book Co., Sydney, 1987), 3rd ed.
8. Y. M. Chen, W. Chavin, Radiometric assay of tyrosinase and theoretical considerations of melanin formation. Analytical Biochemistry 13, 234 1965.DOI= 10.1016/0003-2697(65)90194-6
9. M. D'Ischia, G. Prota, Biosynthesis, structure, and function of neuromelanin and its relation to parkinson's disease: A critical update. Pigment Cell Research 10, 370, 1997. DOI= 10.1111/j.1600-0749.1997.tb00694.x
10. B. J. R. Nicolaus, A critical review of the function of neuromelanin and an attempt to provide a unified theory. Medical Hypotheses 65, 791 (2005). DOI= 10.1016/j.mehy.2005.04.011
11. L. Zeise, M. Chedekel, and T. Fitzpatrick, Is melanin photoprotective or photosensitising? (Vladenmar Press, Overland Park, KS, 1995).

12. J. Nofsinger, S. Forest, and J. Simon, Explanation for the disparity among absorption and action spectra of eumelanin. Journal of Physical Chemistry B. 103, 11428, 1999. DOI= 10.1021/jp992640y
13. I. A. Menon and H. F. Haberman, Mechanisms of action of melanins. British Journal of Dermatology 97, 109, 1997. DOI= 10.1111/j.1365-2133.1977.tb15439.x
14. J. Y. Lin and D. E. Fisher, Melanocyte biology and skin pigmentation. Nature 445, 843, 2007. DOI= 10.1038/nature05660
15. C. Kennedy, J. ter Huurne, M. Berkhout, N. Gruis, M. Bastiaens, W. Bergman, R. Willemze, and J. N. B. Bavinck, Melanocortin 1 receptor (mc1r) gene variants are associated with an increased risk for cutaneous melanoma which is largely independent of skin type and hair color. Journal of Investigative Dermatology 117, 294, 2001. DOI= 10.1046/j.0022-202x.2001.01421.x
16. M. C. Scott, K. Wakamatsu, S. Ito, A. L. Kadekaro, N. Kobayashi, J. Groden, R. Kavanagh, T. Takakuwa, V. Virador, V. J. Hearing, and Z. A. Abdel-Malek, Human melanocortin 1 receptor variants, receptor function and melanocyte response to UV radiation. Journal of Cell Science 115, 2349, 2002. PubMed ID: 12006619
17. E. Wenzel, G. P. V. der Schans, L. Roza, R. M. Kolb, A. J. Timmerman, N. P. Smit, S. Pavel, and A. A. Schothorst, (Pheo)melanin photosensitizes UVA-induced DNA damage in cultured human melanocytes. Journal of Investigative Dermatology 111, 678, 1998. DOI= 10.1046/j.1523-1747.1998.00357.x
18. L. A. G. Ries, D. Melbert, M. Krapcho, A. Mariotto, B. A. Miller, E. J. Feuer, L. Clegg, M. J. Horner, N. Howlader, M. P. Eisner, M. Reichman, and B. K. Edwards, SEER cancer statistics review, 1975-2004. National Cancer Institute, 2006.
19. R. Lucas, Global burden of disease of solar ultraviolet radiation, environmental burden of disease series. News release, World Health Organization 13, 2006.
20. G. Prota, M. D'Ischia, A. Napolitano, The chemistry of melanins and related metabolites. In J. J. Norlund, R. E. Boissy, V. J. Hearing, R. A. King, and J. P. Ortonne, eds., The Pigmentary System: Its physiology and Pathophysiology, chap. 24, pp. 307–332 (Oxford University Press, New York, 1998).

21. H. Xie, S. Vucetic, L. I. C. J. Oldfield, A. K. D. Z. Obradovic, and V. N. Uversky, Functional anthology of intrinsic disorder. 3. Ligands, post-translational modifications, and diseases associated with intrinsically disordered proteins. Journal of Proteome Research 6(5), 1917, 2007. DOI= 10.1021/pr060394e
22. K. Shimizu, Y. Muraoka, S. Hirose, K. Tomii, and T. Noguchi, Predicting mostly disordered proteins by using structure-unknown protein data. BMC Bioinformatics 8, 78, 2007. DOI= 10.1186/1471-2105-8-78
23. A. Loettgers, Getting abstract mathematical models in touch with nature. Science in Context 20(1), 97, 2007. DOI= 10.1017/S0269889706001153
24. M. G. Bridelli, A. Ciati, and P. R. Crippa, Binding of chemicals to melanins re-examined: Adsorption of some drugs to the surface of melanin particles. Biophysical Chemistry 119, 137. 2006. DOI= 10.1016/j.bpc.2005.06.004
25. L. Hong, Y. Liu, and J. D. Simon, Binding of metal ions to melanin and their effects on the aerobic reactivity. Photochemistry and Photobiology 80, 477, 2004. DOI= 10.1111/j.1751-1097.2004.tb00117.x
26. A. Samokhvalov, Y. Liu, and J. D. Simon, Characterization of the Fe(III)-binding site in Sepia eumelanin by resonance Raman confocal microspectroscopy. Photochemistry and Photobiology 80, 84, 2004. DOI= 10.1111/j.1751-1097.2004.tb00053.x
27. B. S. Larsson, Interaction between chemicals and melanin. Pigment Cell Research 6, 127, 1993. DOI= 10.1111/j.1600-0749.1993.tb00591.x
28. P. Meredith, T. Sarna, The physical and chemical properties of eumelanin. Pigment Cell Research 19(6), 572, 2006. DOI= 10.1111/j.1600-0749.2006.00345.x
29. P. Meredith, B. J. Powell, J. Riesz, R. Vogel, D. Blake, S. Subianto, G. Will, I. Kartini, Broad band photon-harvesting biomolecules for photovoltaics. In A. Collings and C. Critchley, eds., Artificial Photosynthesis: From Basic Biology to Industrial Application, chap. 3, p. 37, 2005.
30. L. Panzella, A. Pezzella, A. Napolitano, and M. d'Ischia, The first 5,6-dihydroxyindole tetramer by oxidation of 5,5',6,6'-tetrahydroxy-2,4'-biindolyl and an unexpected issue of positional reactivity en route to eumelanin-related polymers. Organic Letters 9(7), 1411-1414, 2007. DOI= 10.1021/ol070268w

31. N. Kollias, R. M. Sayer, L. Zeise, M. R. Chedekel, New trends in photobiology: Photoprotection by melanin. Journal of Photochemistry and Photobiology B Biol 9, 135, 1991. DOI= 10.1016/1011-1344(91)80147-A
32. H. S. Raper, The aerobic oxidases. Physiology Reviews 8, 245, 1928. DOI= 10.1152/physrev.1928.8.2.245
33. S. Ito, A chemist's view of melanogenesis. Pigment Cell Research 16(3), 230, 2003. DOI= 10.1034/j.1600-0749.2003.00037.x
34. A. Pezzella, M. D'Ischia, A. Napolitano, A. Palumbo, G. Prota, An integrated approach to the structure of sepia melanin. Evidence for a high proportion of degraded 5,6-dihydroxyindole-2-carboxylic acid units in the pigment backbone. Tetrahedron 153, 8281, 1997. DOI= 10.1016/S0040-4020(97)00494-8
35. S. Ito, Re-examination of the structure of eumelanin. Biochimica Biophysica Acta 883, 155, 1986. DOI= 10.1016/0304-4165(86)90146-7
36. Y. Liu, V. R. Kempf, J. B. Nofsinger, E. E. Weinert, M. Rudnicki, K. Wakamatsu, S. Ito, J. D. Simon, Comparison of the structural and physical properties of human hair eumelanin following enzymatic or acid/base extraction. Pigment Cell Research 16, 355, 2003. DOI= 10.1034/j.1600-0749.2003.00059.x
37. G. Prota, Progress in the chemistry of melanins and related metabolites. Medical Research Reviews 8, 525, 1988. DOI= 10.1002/med.2610080405
38. M. d'Ischia, A. Napolitano, K. Tsiakas, G. Prota, New intermediates in the oxidative polymerisation of 5,6-dihydroxyindole to melanin promoted by the peroxidase/H2O2 system. Tetrahedron 46, 5789, 1990. DOI= 10.1016/S0040-4020(01)87775-9
39. A. Pezzella, M. Barra, A. Musto, A. Navarra, M. Alfè, P. Manini, S. Parisi, A. Cassinese, V. Criscuolo, M. D'Ischia, Stem cell-compatible eumelanin biointerface fabricated by chemically controlled solid state polymerization. Mater. Horiz., 2, 212, 2015. DOI= 10.1039/c4mh00097h
40. W. L. Cheun, J. D. Simon, S. Ito, The chemical structure of melanin. Pigm. Cell Res., 17, 422 – 424, 2004. DOI= 10.1111/j.1600-0749.2004.00165_1.x

41. S. P. Nighswander-Rempel, J. Riesz, J. Gilmore, P. Meredith, A quantum yield map for synthetic eumelanin. J. Chem. Phys., 123, 194901, 2005. DOI= 10.1063/1.2075147
42. S. P. Nighswander-Rempel, J. Riesz, J. Gilmore, P. Meredith, Quantitative fluorescence excitation spectra of synthetic eumelanin. J. Phys. Chem. B, 109, 20629 – 20635, 2005. DOI= 10.1021/jp053704+
43. J. B. Nofsinger, T. Ye, J. D. Simon, Ultrafast Nonradiative Relaxation Dynamics of Eumelanin. J. Phys. Chem. B, 105, 2864 – 2866, 2001. DOI= 10.1021/jp004045y
44. J. B. Nofsinger, J. D. Simon, Different Molecular Constituents in Pheomelanin are Responsible for
45. Emission, Transient Absorption and Oxygen Photoconsumption. Photochem. Photobiol., 74, 31– 37, 2001. DOI= 10.1111/j.1751-1097.2007.00281.x
46. S. P. Nighswander-Rempel, I. Mahadevan, H. R. Rubinsztein-Dunlop, P. Meredith, Time-resolved and steady-state fluorescence spectroscopy of eumelanin and indolic polymers. Photochem. Photobiol., 83, 1449 – 1454, 2007. DOI= 10.1111/j.1751-1097.2007.00186.x
47. S. A. Centeno, J. Shamir, Surface enhanced Raman scattering (SERS) and FTIR characterization of the sepia melanin pigment used in works of art. J. Mol. Struct., 873, 149 – 159, 2008. DOI= 10.1016/j.molstruc.2007.03.026
48. S. P. Nighswander-Rempel, S. Olsen, I. B. Mahadevan, G. Netchev, B. C. Wilson, S. C. Smith, H. Rubinsztein-Dunlop, P. Meredith, Solvochromic effects in model eumelanin compounds. Photochem. Photobiol., 84, 613 – 619, 2008. DOI= 10.1111/j.1751-1097.2007.00290.x
49. J. Tomkinson, J. Riesz, P. Meredith, S. F. Parker, The vibrational spectrum of indole: An inelastic neutron scattering study. Chem. Phys., 345, 230 – 238, 2008. DOI= 10.1016/j.chemphys.2007.06.007
50. S. Ito, K. Wakamatsu, Quantitative Analysis of Eumelanin and Pheomelanin in Humans, Mice, and Other Animals: a Comparative Review. Pigm. Cell Res., 16, 523 – 531, 2003. DOI= 10.1034/j.1600-0749.2003.00072.x

51. A. Napolitano, M. R. Vincensi, P. Di Donato, G. Monfrecola, G. Prota, Microanalysis of Melanins in Mammalian Hair by Alkaline Hydrogen Peroxide Degradation: Identification of a New Structural Marker of Pheomelanins1. J. Invest. Dermatol., 114, 1141 – 1147, 2000. DOI= 10.1046/j.1523-1747.2000.00977.x
52. G. Prota, Melanins, Melanogenesis and Melanocytes: Looking at Their Functional Significance from the Chemist's Viewpoint. Pigm. Cell Res., 13, 283 – 293, 2000. DOI= 10.1034/j.1600-0749.2000.130412.x
53. M. Irimia-Vladu, ""Green" electronics: biodegradable and biocompatible materials and devices for sustainable future," Chemical Society Reviews, vol. 43, no. 2, pp. 588–610, 2014. DOI= 10.1039/c3cs60235d
54. P. Meredith, C. J. Bettinger, M. Irimia-Vladu, a. B. Mostert, P. E. Schwenn, "Electronic and optoelectronic materials and devices inspired by nature," Reports on Progress in Physics, vol. 76, no. 3, p. 034501, 2013. DOI= 10.1088/0034-4885/76/3/034501
55. C. J. Bettinger, Z. A. Bao, "Biomaterials-based organic electronic devices," Polymer International, vol. 59, no. 5, pp. 563–567, 2010. DOI= 10.1002/pi.2827
56. H. Longuet-Higgins, "On the origin of the free radical property of melanins," Archives of Biochemistry and Biophysics, vol. 86, no. 2, pp. 231–232, 1960. DOI= 10.1016/0003-9861(60)90410-0
57. A. Pullman, B. Pullman, "The band structure of melanin," Biochimica et Biophysica Acta, vol. 54, no. 2, pp. 384–385, 1961. DOI= 10.1016/0006-3002(61)90389-4
58. J. E. McGinness, "Mobility gaps: a mechanism for band gaps in melanins," Science, vol. 177, no. 52, pp. 896–897, 1972. DOI= 10.1126/science.177.4052.896
59. J. McGinness, P. Corry, P. Proctor, "Amorphous semiconductor switching in melanins." Science, vol. 183, no. 127, pp. 853–855, 1974. DOI= 10.1126/science.183.4127.853
60. B. Commoner, J. Townsend, G. E. Pake, "Free radicals in biological materials," Nature, vol. 174, no. 4432, pp. 689–691, 1954. DOI= 10.1038/174689a0\

61. P. Crippa, V. Cristofoletti, N. Romeo, “A band model for melanin deduced from optical absorption and photoconductivity experiments,” Biochimica et Biophysica Acta (BBA) - General Subjects, vol. 538, no. 1, pp. 164–170, 1978. DOI= 10.1016/0304-4165(78)90260-X
62. M. Abbas, F. D’Amico, L. Morresi, N. Pinto, M. Ficcadenti, R. Natali, L. Ottaviano, M. Passacantando, M. Cuccioloni, M. Angeletti, R. Gunnella, “Structural, electrical, electronic and optical properties of melanin films,” European Physical Journal E, vol. 28, no. 3, pp. 285–291, 2009. DOI= 10.1140/epje/i2008-10437-9
63. M. Piacenti da Silva, J. C. Fernandes, N. B. de Figueiredo, M. Congiu, M. Mulato, C. F. de Oliveira Graeff, “Melanin as an active layer in biosensors,” AIP Advances, vol. 4, no. 3, p. 037120, 2014. DOI= 10.1063/1.4869638
64. T. Ligonzo, M. Ambrico, V. Augelli, G. Perna, L. Schiavulli, M. A. Tamma, P. F. Biagi, A. Minafra, V. Capozzi, “Electrical and optical properties of natural and synthetic melanin biopolymer,” Journal of Non-Crystalline Solids, vol. 355, no. 22-23, pp. 1221–1226, 2009. DOI= 10.1016/j.jnoncrysol.2009.05.014
65. C. J. Bettinger, J. P. Bruggeman, A. Misra, J. T. Borenstein, and R. Langer, “Biocompatibility of biodegradable semiconducting melanin films for nerve tissue engineering,” Biomaterials, vol. 30, no. 17, pp. 3050–3057, 2009. DOI= 10.1016/j.biomaterials.2009.02.018
66. M. E. Lynge, R. van der Westen, A. Postma, B. Stadler, “Polydopamine–a nature-inspired polymer coating for biomedical science,” Nanoscale, vol. 3, no. 12, pp. 4916–4928, 2011. DOI= 10.1039/c1nr10969c
67. P. J. Gon¸calves, O. B. Filho, C. F. O. Graeff, “Effects of hydrogen on the electronic properties of synthetic melanin,” Journal of Applied Physics, vol. 99, no. 10, p. 104701, 2006. DOI= 10.1063/1.2201691
68. a) A. B. Mostert, B. J. Powell, F. L. Pratt, G. R. Hanson, T. Sarna, I. R. Gentle, P. Meredith, “Role of semiconductivity and ion transport in the electrical conduction of melanin,” Proceedings of the National Academy of Sciences, vol. 109, no. 23, pp. 8943–8947, 2012. DOI= 10.1073/pnas.1119948109; b) J. Wünsche, Y. Deng, P. Kumar, E. Di Mauro, E. Josberger, J. Sayago, A. Pezzella, F. Soavi, F. Cicoira,

M. Rolandi, C. Santato, Protonic and Electronic Transport in Hydrated Thin Films of the Pigment Eumelanin. Chem. Mater., 27, 436–442, 2015. DOI= 10.1021/cm502939r

69. M. Ambrico, P. F. Ambrico, A. Cardone, T. Ligonzo, S. R. Cicco, R. D. Mundo, V. Augelli, and G. M. Farinola, "Melanin layer on silicon: an attractive structure for a possible exploitation in bio-polymer based metal-insulator-silicon devices," Advanced Materials, vol. 23, no. 29, pp. 3332–3336, 2011. DOI= 10.1002/adma.201101358
70. M. D'Ischia, A. Napolitano, A. Pezzella, P. Meredith, T. Sarna, "Chemical and structural diversity in eumelanins: unexplored bio-optoelectronic materials," Angewandte Chemie (International Edition), vol. 48, no. 22, pp. 3914–3921, 2009. DOI= 10.1002/anie.200803786
71. P. Meredith, T. Sarna, "The physical and chemical properties of eumelanin," Pigment Cell Research, vol. 19, no. 6, pp. 572–594, 2006. DOI= 10.1111/j.1600-0749.2006.00345.x
72. M. D'Ischia, K. Wakamatsu, A. Napolitano, S. Briganti, J.-C. Garcia-Borron, D. Kovacs, P. Meredith, A. Pezzella, M. Picardo, T. Sarna, J. D. Simon, S. Ito, "Melanins and melanogenesis: methods, standards, protocols," Pigment Cell & Melanoma Research, vol. 26, no. 5, pp. 616–633, 2013. DOI= 10.1111/pcmr.12121
73. S. N. Dezidério, C. A. Brunello, M. I. N. da Silva, M. A. Cotta, C. F. O. Graeff, "Thin films of synthetic melanin," Journal of Non-Crystalline Solids, vol. 338-340, pp. 634–638, 2004. DOI= 10.1016/j.jnoncrysol.2004.03.058
74. J. P. Bothma, J. de Boor, U. Divakar, P. E. Schwenn, and P. Meredith, "Device-quality electrically conducting melanin thin films," Advanced Materials, vol. 20, no. 18, pp. 3539–3542, 2008. DOI= 10.1002/adma.200703141
75. A. Pezzella, J. Wunsche, "Eumelanin: an old natural pigment – a new material for ¨ organic electronics. Chemical, physical, and structural properties in relation to potential applications," in Organic Electronics: Emerging Concepts and Technologies, F. Cicoira and C. Santato, Eds. Weinheim, Germany: Wiley-VCH Verlag GmbH & Co. KGaA, 2013. DOI= 10.1002/9783527650965.ch05

76. P. Meredith, K. Tandy, A. B. Mostert, “A hybrid ionic–electronic conductor: melanin, the first organic amorphous semiconductor?” in Organic Electronics: Emerging Concepts and Technologies, F. Cicoira and C. Santato, Eds. Weinheim, Germany: Wiley-VCH Verlag GmbH & Co. KGaA, 2013. DOI= 10.1002/9783527650965.ch04
77. Y. J. Kim, W. Wu, S.-E. Chun, J. F. Whitacre, C. J. Bettinger, “Biologically derived melanin electrodes in aqueous sodium-ion energy storage devices,” Proceedings of the National Academy of Sciences, vol. 110, no. 52, pp. 20 912–20 917, 2013. DOI= 10.1073/pnas.1314345110
78. M. Ambrico, A. Cardone, T. Ligonzo, “Hysteresis-type current–voltage characteristics in Au/eumelanin/ITO/glass structure: Towards melanin based memory devices,” Organic Electronics, vol. 11, no. 11, pp. 1809–1814, 2010. DOI= 10.1016/j.orgel.2010.08.001
79. A. G. Orive, Y. Gimeno, A. Creus, D. Grumelli, C. Vericat, G. Benitez, R. Salvarezza, “Electrochemical preparation of metal–melanin functionalized graphite surfaces,” Electrochimica Acta, vol. 54, no. 5, pp. 1589–1596, 2009. DOI= 10.1016/j.electacta.2008.09.046
80. W. Korytowski, T. Sarna, Bleaching of melanin pigments. Role of copper ions and hydrogen peroxide in autooxidation and photooxidation of synthetic dopa-melanin. J. Biol. Chem., 265, 12410, 1990. PubMed ID: 2165063
81. C. C. Felix, J. S. Hyde, T. Sarna, R. C. Sealy, Melanin photoreactions in aerated media: Electron spin resonance evidence for production of superoxide and hydrogen peroxide. Biochem. Biophys. Res. Commun., 84, 335, 1978. DOI= 10.1016/0006-291X(78)90175-4
82. L. Sangaletti, P. Borghetti, P. Ghosh, S. Pagliara, P. Vilmercati, C. Castellarin-Cudia, L. Floreano, A. Cossaro, A. Verdini, R. Gebauer, and A. Goldoni, Polymerization effects and localized electronic states in condensed-phase eumelanin. Phys. Rev. B, 80, 174203–174209, 2009. DOI= 10.1103/PhysRevB.80.174203

83. M.I.N. da Silva, S.N. Deziderio, J.C. Gonzalez, C.F.O. Graeff, M.A. Cotta, Synthetic melanin thin films: Structural and electrical properties. J. Appl. Phys., 96, 5803, 2004. DOI= 10.1063/1.1803629
84. I. G. Kim, H. J. Nam, H. J. Ahn, D. Y. Jung, Electrochemical growth of synthetic melanin thin films by constant potential methods. Electrochim. Acta, 56, 2954, 2011. DOI= 10.1016/j.electacta.2010.12.095
85. F. Bernsmann, B. Frisch, C. Ringwald, V. Ball, Protein adsorption on dopamine-melanin films: Role of electrostatic interactions inferred from ζ-potential measurements versus chemisorption J. Colloid Interf. Sci., 344, 54, 2010. DOI= 10.1016/j.jcis.2009.12.052
86. M. Abbas , M. Ali , S. K. Shah , F. D'Amico , P. Postorino , S. Mangialardo , M. Cestelli Guidi , A. Cricenti , R. Gunnella, Control of structural, electronic, and optical properties of eumelanin films by electrospray deposition. J. Phys. Chem. B, 115, 11199, 2011. DOI= 10.1021/jp2033577
87. F. Bloisi, and A. Pezzella, M. Barra, F. Chiarella, A. Cassinese, L. Vicari, Matrix assisted pulsed laser deposition of melanin thin films. J. Appl. Phys., 110, 026105–026108, 2011. DOI= 10.1063/1.3602084
88. F. Bloisi, A. Pezzella, M. Barra, M. Alfe, F. Chiarella, A. Cassinese, L. Vicari, Effect of substrate temperature on MAPLE deposition of synthetic eumelanin films. Appl Phys a-Mater, 105, 619-627, 2011. DOI= 10.1007/s00339-011-6603-x
89. P. Diaz, Y. Gimeno, P. Carro, S. Gonzalez, P. L. Schilardi, G. Benitez, R. C. Salvarezza, A. H. Creus, Electrochemical self-assembly of melanin films on gold. Langmuir, 21, 5924, 2005. DOI= 10.1021/la0469755
90. S. Subianto, G. Will, P. Meredith, Electrochemical synthesis of melanin free-standing films. Polymer, 46, 11505, 2005. DOI= 10.1016/j.polymer.2005.10.068
91. H. Lee, S.M. Dellatore, W.M. Miller, P.B. Messersmith, Mussel-inspired surface chemistry for multifunctional coatings. Science, 318, 426, 2007. DOI= 10.1126/science.1147241
92. M. Muller, B. Kessler, Deposition from dopamine solutions at Ge substrates: an in situ ATR-FTIR study. Langmuir, 27, 12499, 2011. DOI= 10.1021/la202908b

93. L. Panzella, G. Gentile, G. D'Errico, N. F. Della Vecchia, M. E. Errico, A. Napolitano, C. Carfagna, M. d'Ischia, Atypical structural and π-electron features of a melanin polymer that lead to superior free-radical-scavenging properties. Angew. Chem., Int. Ed., 52, 12684–12687, 2013. DOI= 10.1002/anie.201305747
94. J. Liebscher, R. Mrowczynski, H. A. Scheidt, C. Filip, N. D. Hadade, R. Turcu, A. Bende, S. Beck, Structure of polydopamine: A never-ending story? Langmuir, 29, 10539–10548, 2013. DOI= 10.1021/la4020288
95. A. Pezzella, O. Crescenzi, L. Panzella, A. Napolitano, E. J. Land, V. Barone, M. d'Ischia, Free radical coupling of o -semiquinones uncovered. J. Am. Chem. Soc., 135, 12142–12149, 2013. DOI= 10.1021/ja4067332
96. A. Pezzella, L. Panzella, A. Natangelo, M. Arzillo, A. Napolitano, M. d'Ischia, 5,6-Dihydroxyindole tetramers with "anomalous" interunit bonding patterns by oxidative coupling of 5,5′,6,6′-tetrahydroxy-2,7′- biindolyl: Emerging complexities on the way toward an improved model of eumelanin buildup. J. Org. Chem., 72, 9225–9230, 2007. DOI= 10.1021/jo701652y
97. A. Pezzella, L. Panzella, O. Crescenzi, A. Napolitano, S. Navaratman, R. Edge, E. J. Land, V. Barone, M. d'Ischia, Short-lived quinonoid species from 5,6-dihydroxyindole dimers en route to eumelanin polymers: Integrated chemical, pulse radiolytic, and quantum mechanical investigation. J. Am. Chem. Soc., 128, 15490–15498, 2006. DOI= 10.1021/ja0650246
98. M. D'Ischia, A. Napolitano, A. Pezzella, E. J. Land, C. A. Ramsden, P. A. Riley, 5,6-Dihydroxyindoles and indole-5,6-diones. Adv. Heterocycl. Chem., 89, 1–63, 2005. DOI= 10.1016/S0065-2725(05)89001-4
99. S. Reale, M. Crucianelli, A. Pezzella, M. d'Ischia, F. De Angelis, Exploring the frontiers of synthetic eumelanin polymers by high-resolution matrix-assisted laser/desorption ionization mass spectrometry. J. Mass Spectrom., 47, 49–53, 2012. DOI= 10.1002/jms.2025
100 L. Ascione, A. Pezzella, V. Ambrogi, C. Carfagna, M. d'Ischia, Intermolecular π-electron perturbations generate extrinsic visible contributions to eumelanin black chromophore in model polymers with interrupted interring conjugation. Photochem. Photobiol., 89, 314–318, 2013. DOI= 10.1111/php.12003

101. G.Tarabella, A. Pezzella, A. Romeo, P. D'Angelo, N. Coppede, M. Calicchio, M. d'Ischia, R. Mosca, S. Iannotta, Irreversible evolution of eumelanin redox states detected by an organic electrochemical transistor: En route to bioelectronics and biosensing. J. Mater. Chem. B, 1, 3843–3849, 2013. DOI= 10.1039/c3tb20639d

2. Integration of Eumelanin within Conductive Polymers

2.1 Introduction

Since the initial discovery of conducting polymers (CPs) in the 1970s[1], the field of organic electronics has seen significant development. The application of CPs at the interface with biology is an exciting new topic in the field of organic electronics[2]. The term organic bioelectronics[3] refers to the coupling of CP (and conducting small molecule)- based devices with biological systems, in an effort to bridge the biotic/abiotic interface. Applications to date include (but are not limited to) biosensing, diagnostics, tissue engineering, and neural interfacing. The field of organic electronics has progressed a great deal in the past[4] years Here will be shown the advantage of the unique functionalities associated with CPs, as opposed to traditional biomaterials and electronic materials. Due to the versatility of polymer synthesis, there is a large catalog of CPs and small molecules, with champion materials optimized for the various applications. Some common CPs

used for biological applications are shown in Figure 2.1. The conjugated bonding structure of the polymers shown in Figure 2.1 gives rise to their metal-like, semiconducting properties. However, dopants are necessary to raise the room-temperature electrical conductivity to practical levels (100 S/cm and above). For p-type doping, in which the material is oxidized into a more conductive state, the dopant can be any form of anion. When in close proximity with the conjugated polymer, the negative charge will be compensated with a mobile hole along the conjugated polymer backbone. Such is the case for polypyrrole (PPy) an poly(3,4-ethylenedioxythiophene) (PEDOT), which are both considered hole conductors. Figure 2.1b shows how a polaron on the backbone of a CP chain neutralizes the SO_3^- on the PSS molecule, a common macromolecular dopant. A common small-molecule dopant is the anion of p-toluenesulfonic acid (pTS), sometimes referred to as tosylate (TOS).

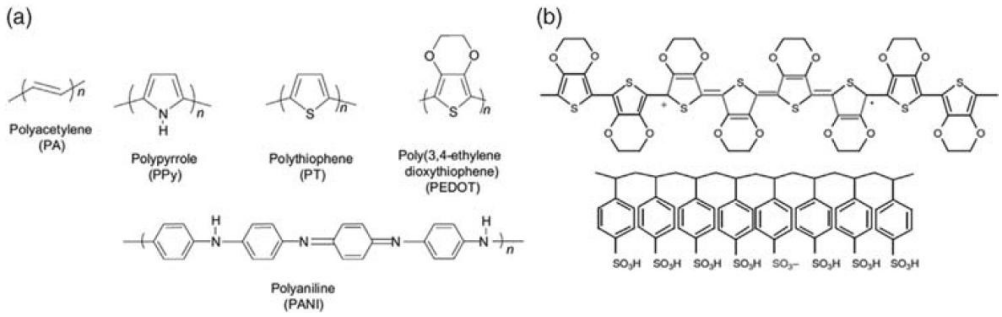

Figure 2.1 (a) Chemical structures of common conducting polymers used in biological applications: polypyrrole, polythiophene, poly (3,4-ethylenedioxythiophene), and polyaniline. (b) Chemical structure of PEDOT doped with PSS, showing a delocalized hole in the form of a positive polaron. The anion on the PSS chain acts as the dopant (acceptor)**.**

Conducting polymers serve as the active layer in a variety of different applications. The attributes of CPs that make these materials uniquely suited for interfacing with biological systems include soft mechanical properties: the soft mechanical properties allow for compatibility with flexible substrates and good mechanical matching with delicate biological tissue. In applications for neuroprobes or functional substrates for cell growth, these materials better mimic in vivo environments compared to their inorganic counterparts.

Mixed conduction and ideal interfaces: The unique ability of organic electronic materials to conduct ions, in addition to electrons and holes, facilitates their communication with biological systems, which rely heavily on ion fluxes.

Freedom in chemical modification: The nature of polymer synthesis allows for a level of chemical variation not achievable with inorganic materials. Various moieties can be covalently added to a polymer chain for the purpose of increased biological functionality. In situ polymerization enables physical entrapment of desired molecules, including large polyanions and bulky proteins. Overall, the extensive catalog of available chemistries is extremely useful in optimizing materials for various applications.

Ease of processing: Along with the advantages unique to bioelectronics, the benefits of organic electronics as seen in other fields are maintained. Namely, commercially available CP inks and monomers are extremely adaptable to a wide

range of processing techniques based on solution- and vapor-phase deposition methods. The ease of processing facilitates deposition on a variety of substrates with unique mechanical properties and form factors, including extreme aspect ratios[4].

Moreover, easily scaled-up processing techniques, such as spray coating and other roll-to-roll compatible techniques, lower the cost of the final product. In developing single-use devices for point-of-care diagnostics, low cost remains extremely important.

In this chapter will be discussed the integration of PEDOT:PSS as conductive material within eumelanin, in order to investigate the electrical properties and the structural organization of this blend in the way to create a merge between the unique properties of both of these two polymers.

2.2 Pigment functionalization: tailoring Eumelanin conductivity properties by hybrid buildup

The growing interest toward biocompatible and bioinspired materials is boosting the investigation and the engineering of natural products as active components in electronic devices. Capitalizing on a recently developed protocol to prepare high quality eumelanin coatings, herein will be discribed the design and the integration of standard commercial poly(3,4-ethylenedioxythiophene) with the poly(styrenesulfonate) (PEDOT:PSS) with eumelanin pigment.

The growing advancements of organic (bio)electronics[3, 5] together with a number of concurrent needs[6], such as processability, and issues[7], as the scarcity of the indium[8], a critical raw material[9], are spurring the search for an alternative to replace the indium tin oxide (ITO) in organic electronic devices[10]. To date, other transparent conductors cannot compete with the ITO, particularly on its transparency, conductivity, and electronic properties, and on the performances of the devices basing on it. A number of different solutions are under investigation, including metal nanowires[7, 11], graphene and/or graphene oxide[12], conductive polymers[13], carbon nanotubes[14], and fullerenes[15], each one of these carrying pros and cons. The applications in bioelectronics have particularly fuelled the

investigation on conjugated polymers, especially as they can play a key role in bridging the electrodes with the living systems[16], by combining high electronic and ionic conductivity together with suitable mechanical properties, including flexibility[10b]. In the realm of conducting polymers, the blend of poly(3,4-ethylenedioxythiophene) with the poly(styrenesulfonate) (PEDOT:PSS, Figure 2.1) is a very promising candidate for the next generation of transparent electrodes materials[17], because of its good processability, mechanical flexibility, optical properties, and dispersibility in water and in some polar organic solvents[18]. Large area high-quality PEDOT:PSS films can be easily prepared using low-cost solution processing techniques, such as coating and printing[19]. Furthermore, PEDOT:PSS thin films are quite transparent in the visible range and highly mechanically flexible[18, 20, 21]. Beyond this picture, PEDOT:PSS does exhibit some limitations[22], including the relatively low adhesion[23] particularly on inorganic substrates[24] and low stability to water[25]. Indeed, improving the mechanical properties of PEDOT coatings appears mandatory to the achievement of true water stable organic electrodes featuring a limited cracking and delamination of the coatings from substrates[10, 23a] and possibly the long term performance required for interfacing applications[25, 26].

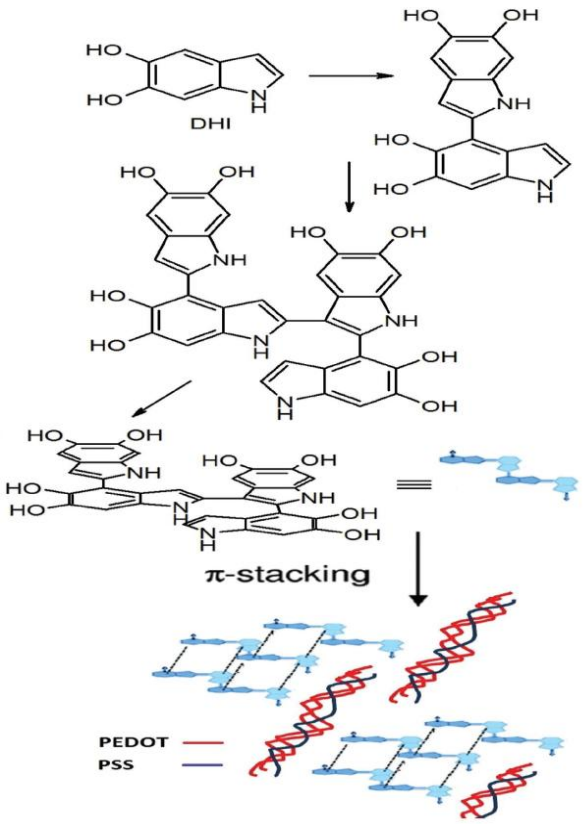

Figure 2.2. Schematic view of eumelanin build up (after DHI oxidative polymerization and π stacking of oligomeric species) and possible organization of the Eu–PH blend. It has to be highlighted that literature evidences have been reported in support of organization of sole eumelanin constituents[32], while the spatial arrangement reported in the picture for PEDOT, PSS, and eumelanin is actually speculative.

At the same time, the increasing interest toward biocompatible[25, 26] and bioinspired[27] materials is boosting the investigation and the engineering of natural products as active components in electronic devices[28]. Indeed, a number of

materials of natural origin are recently emerging as highly valuable sources for the fabrication of biocompatible[23b] and bioinspired devices[28, 29], thanks to their capability to merge multiple functionalities and mechanical performances[30]. The human pigment melanin, and particularly its subgroup composed by the eumelanin, the black-brown pigments derived from the oxidative polymerization of L-3,4-dihydroxyiphenylalanine L-DOPA via 5,6-dihydroxy-indole (DHI) intermediates[31], are increasingly emerging as valuable candidates for organic (bio)electronics applications[11, 12a, 12b, 28a].

2.3 Eumelanin integration within PEDOT:PSS conductive polymer and structural organization

Charge transport properties in conducting polymers feature a marked dependence over the structural organization at the molecular level[33] which in turn is largely dictated by the processing protocols[34]. Also post processing treatments can produce a main impact over the conductivity properties, as widely reported for the most studied PEDOT[35] and the PEDOT:PSS blend[36]. Indeed, the extensive work addressing the investigation on conductivity properties of PEDOT:PSS[37-40] has led to the definition of a supramolecular model of the two interacting polymers envisaging a sort of micellar organization featuring a more or less produced segregation of PEDOT and PSS with a varying degree of crystallinity[33, 41] Since the pioneer work by Kim et al.[42], methods have been reported, involving the addition of dimethyl sulfoxide (DMSO) or dimethylformamide (DMF) into the PEDOT:PSS aqueous solutions[43], to enhance significantly the conductivity of PEDOT:PSS thanks to a PSS rich phase segregation[41, 44, 35b]. Indeed the effects of PSS weight fraction on the conductivity of PEDOT:PSS blends was investigated, disclosing the presence of a conductivity threshold at the PEDOT:PSS ratio 1:6 where the PSS component is regarded as the not conducting one[45].

Other approaches for the improvement[42]. also involved the search for ternary blends where the PEDOT:PSS is paired with a third component, including a conductive carbon material[46] or natural products[47].

Integration of the mammal pigment eumelanin into PEDOT:PSS was recently proposed as a strategy to gain improvements of adhesion on inorganic substrates

and enhanced stability to water[48]. The new blend (EUPH) proved to possess appropriate merit figure to allow its use as anode of OLED (Organic Light Emitting Device) devices despite the very low conductivity of eumelanins with respect to PEDOT (as will be shown in the next section). Indeed, the dependence of EUPH conductivity on the eumelanin content proved to follow a plot significantly different from the one observed for PSS in spite of the low intrinsic conductivity of eumelanin. In particular, the conductivity of EUPH featuring a PEDOT percent content of 24% is comparable to the one in PEDOT:PSS with a PEDOT content of 28.57%. This finding has relevance not only for its possible role in expanding the scope of eumelanin based PEDOT blends, but also with respect to possible insights it can provide in the PEDOT doping. Here is reported a systematic investigation of structural motifs associated to the eumelanin introduction in PEDOT:PSS and the conductivity of the ternary blend.

Eu-PH thin films were prepared at different eumelanin content starting from mixtures (DHI:PEDOT:PSS w/w ratio of X:1:2.5), obtained combining two mother solutions: a) DHI in isopropyl alcohol and b) PEDOT:PSS in water (a Clevios™ PH 1000 commercial product)[49]. Blank films of sole eumelanin and PH-1000 were also prepared and film thicknesses were in the 800-2000 nm range. Films were fabricated on glass substrates by drop casting with the appropriate DHI containing mixture and subsequently inducing eumelanin formation by AISSP protocol (ammonia induced solid state polymerization)[50].

Conductivity measurements were carried out via four probes equipment and conductivity values are reported (Figure. 2.3) on logarithmic scale in function of PEDOT weight content within the Eu-PH blend. The plot presents a double sigmoid profile and is reminiscent of the profile observed in the case of sole PEDOT:PSS at different PEDOT:PSS ratios[51]. Indeed, conductivity of

PEDOT:PSS was reported to feature a sigmoid decay with PSS content increase featuring a marked decay of the recorded conductivity at the weight fraction of 1:6. This behavior was accounted for by considering percolation between conducting PEDOT:PSS domains embedded in a poorly conducting PSS matrix[45].

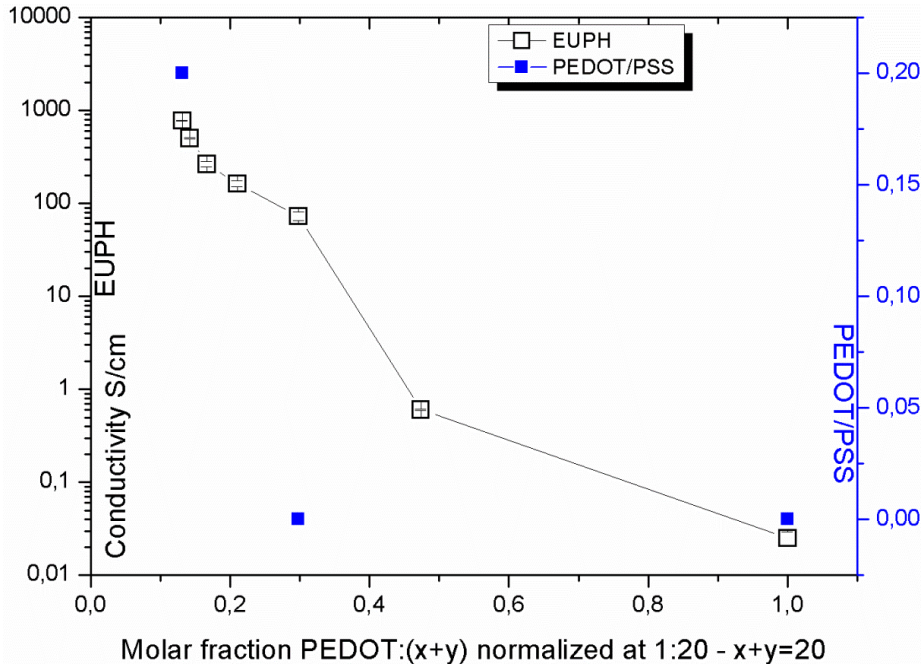

Figure 2.3. Electrical conductivity (▫) of PEDOT:(PSS + eumelanin) and (▪) PEDOT:PSS[52] as a function of the normalized PEDOT content (relative PEDOT = 0.05)

In the operating condition of this study eumelanin can be considered as poorly conducting as PSS and thus a conductivity dependence on the ratio of PEDOT to PSS plus eumelanin might be expected to resemble the one in the case of sole PSS as PEDOT pairing material.

On the contrary, this was not the case and not only the conductivity profiles appeared different, but also decay amounts proved different. When normalizing conductivity to the value measured for PEDOT:PSS 1:2.5 ratio we observe a 90 % decay after dropping to the PEDOT:(PSS+ Eumelanin) 1:7 ratio. In comparison, moving from PEDOT:PPS 1:2.5 to 1:7 is reported[52] to produce a 99.9 % decay. There are few PEDOT based ternary blends in literature[53-55] and even fewer addressing the effect on conductivity of a third polymer in the blend[56], and there is limited knowledge concerning the relationship between the conductivity dependence in PEDOT based ternary blends.

Because of the low conductivity of eumelanin, its introduction into the PEDOT containing blend was expected to produce a conductivity decay of the blend which, in light of literature[50], could be produced by a modification of PEDOT packing.

The effect of eumelanin on conductivity was thus related to structural features in Wide Angle X-ray Scattering (WAXS) and diffraction (XRD) patterns of films with different eumelanin content and fixed PEDOT:PSS ratio. Analysis of free-standing films in transmission geometry (WAXS) allows to get rid of substrate scattering contribution, and mainly probe crystallographic directions parallel to the film plane. On the other hand, reflection geometry (XRD, GIWAXS) allows probing structural order in both directions, in and out of the film plane, and can be used for the as prepared films, laying on glass substrates, to better relate structural and electrical properties.

Typical diffraction patterns collected from free-standing films of the blends with and without Eu inclusions are reported in Figures 2.4a and 2.5. Eumelanin

diffraction pattern features an amorphous-like broad band (Fig. 2.5, bottom curve), the pigment being expected to consist of a disordered mixture of several oligomeric species. The presence of PEDOT:PSS in the blend is associated to the appearance of bands at q = 0.24 $Å^{-1}$, q = 1.2 $Å^{-1}$ and q = 1.8 $Å^{-1}$ (Figures 2.5 and 2.4a). These correspond to the lamellar packing of PEDOT chains along the *a* axis, and to the π-π stacking distance in PSS and PEDOT, respectively[35b, 56].

The patterns in Figure 2.5 were collected at a smaller sample-to-detector distance (28mm) allowing the access to larger q-values for a better definition of the q = 1.8 $Å^{-1}$ peak, ascribed to the π-π stacking (*b* axis) of the PEDOT orthorhombic structure[57, 35b], and to highlight the additive and broadening effect of the diffracting Eu on the latter peak.

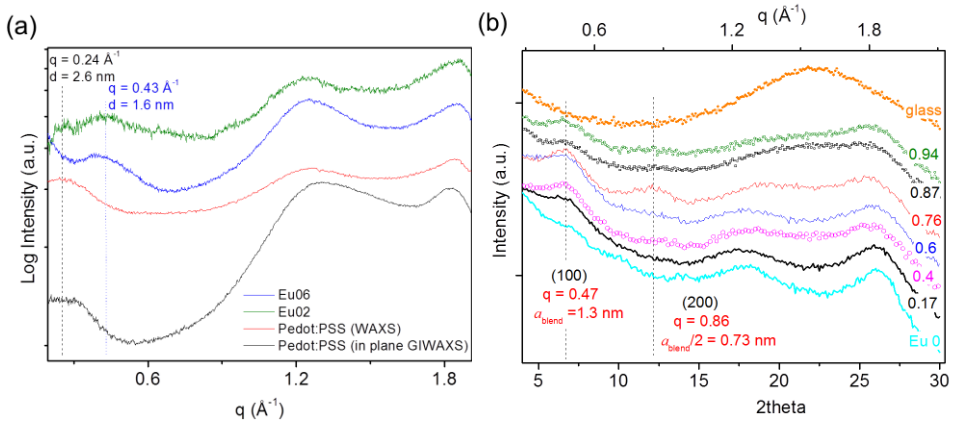

Figure 2.4 . (a) 1D-folded WAXS patterns (radial profiles) for 0, 0.2 and 0.6 Eu fractions. The in plane radial cut from the GIWAXS pattern in Fig. 2.10 is also shown to be consistent. (b) XRD patterns collected in detector scan mode, at 1° incidence angle. In figure 2.4b the numbers on the right are referred to Eu fraction of 0, 0.17, 0.4, 0.6, 0.76, 0.87, 0.94.

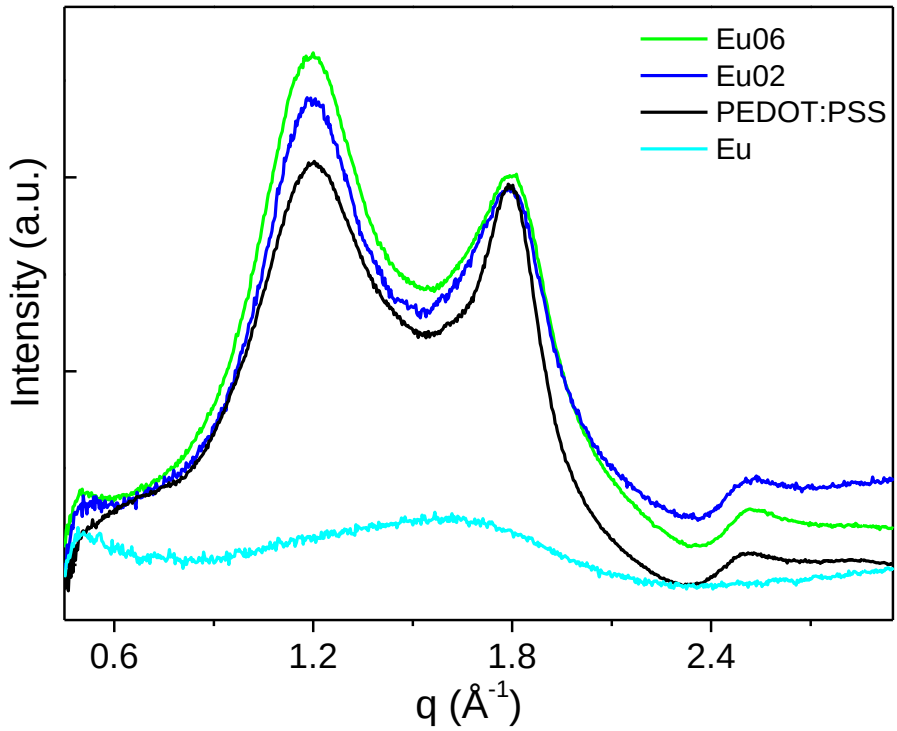

Figure 2.5. Integrated radial Wide Angle X-ray Scattering (WAXS) patterns from PEDOT:PSS blends, with and without embedded eumelanin, and bare eumelanin film as a blank, collected at 28 mm sample-detector distance.

A similar effect is seen in reflection geometry, in GIWAXS in and out of plane cuts in Figures 2.6 and 2.7, and even more evidently in the detector scans in Figure 2.4b, where also scattering from the substrate is no more negligible as long as the Eu fraction increases and film thickness decreases, leading to a convolution of PEDOT and PSS peaks. Substrate scattering contribution increases indeed with both the incidence (compare Figures 2.6 and 2.7) and scattering angles, and with decreasing film thickness (Figure 2.4b); so that in-plane cuts in Figure 2.6a better

account for the Eu diffraction contribution, whereas out of plane cuts in Figure 2.6b and detector scans in Figure 2.4b better show the substrate contribution, both occurring in the same angular/q range.

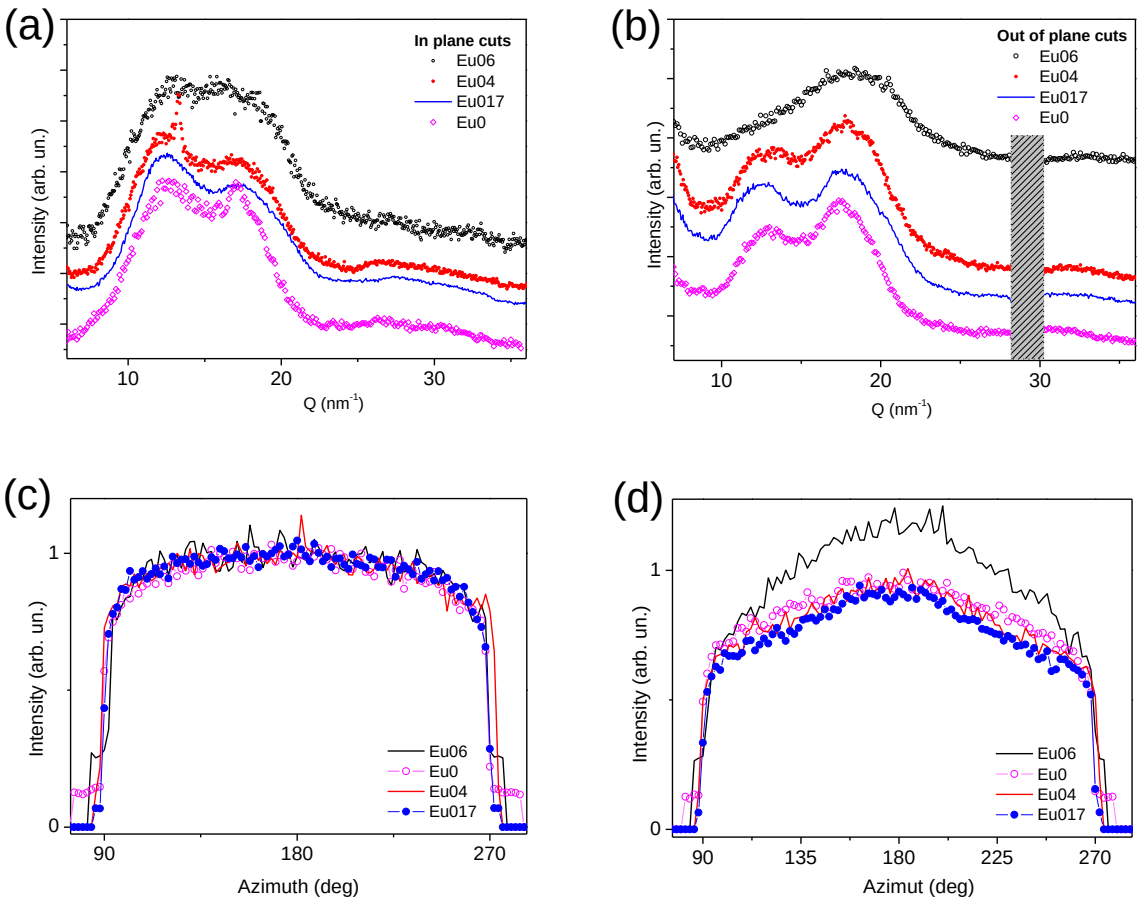

Figure 2.6. GIWAXS patterns collected at 0.2° incidence angle, in vacuum. Linear cuts of the in (d) and out of (e) plane from EUPH 2D GIWAXS patterns of PEDOT:PSS blends with Eu fractions 0, 0.17, 0.4, 0.6; azimuthal profiles for the q = 1.2 $Å^{-1}$ (PSS) and the q = 1.8 $Å^{-1}$ (PEDOT) diffraction rings, respectively (f, g).

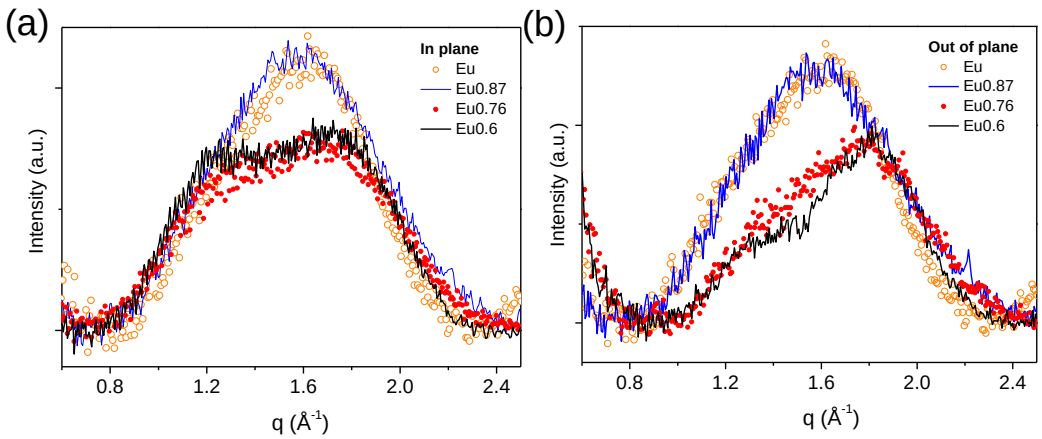

Figure 2.7. GIWAXS patterns collected at 0.5° incidence angle, at room pressure. Linear cuts of the in (a) and out of (b) plane from EUPH 2D GIWAXS patterns of PEDOT:PSS blends with Eu fractions 0.6, 0.76, 0.87.The pattern of the bare Eu film is also replicated from Figure 2.5 and scaled for comparison.

On the other hand, the patterns in Figure 2.4a were collected at a larger sample-to-detector distance (about 20 cm), allowing to improve the definition of the $q = 0.24 \pm 0.02$ Å^{-1} peak and disclosing the structural effect of Eu inclusion on the PEDOT in-plane lattice parameter a (100). The last resulted equal to $a_0 = 2.6 \pm 2$ nm in the bare PEDOT:PSS blend (the same value resulted from the out of plane GIWAXS profile, Fig. 2.4c), and was found to decrease to blend = 1.6 ± 2 nm ($q = 0.4$ Å^{-1}) when Eu is included in the blend, for any concentration (Figures 2.4a, and Figure 2.4b). In particular, the XRD patterns reported in Figure 2.4b, collected in detector (2θ) scan mode, accurately show the unaltered blend value as a function of Eu concentration, while the degree of order (domain size) along a is seen improving

based on the increased visibility of the 100 peak and the appearance of the second order (200) diffraction peak. Figure 2.4b also confirms that no significant changes occur in the PSS and PEDOT π-π stacking distance (the apparent peak broadening is ascribed to the decreasing film thickness with increasing Eu concentration, and consequent increasing scattering from both Eu and the substrate). The [100] crystallographic direction is thus the only affected by Eu inclusion, both in molecular packing distance (a parameter) and orientation. Indeed, the intensity plot along the azimuth (Figure 2.8) for the q = 0.24 $Å^{-1}$ diffraction ring shows a mild modulation with about 180° period in the case of the PEDOT:PSS sample, indicating a partial orientation of PEDOT chains within the film plane; whereas no such modulation results when Eu is included in the blend.

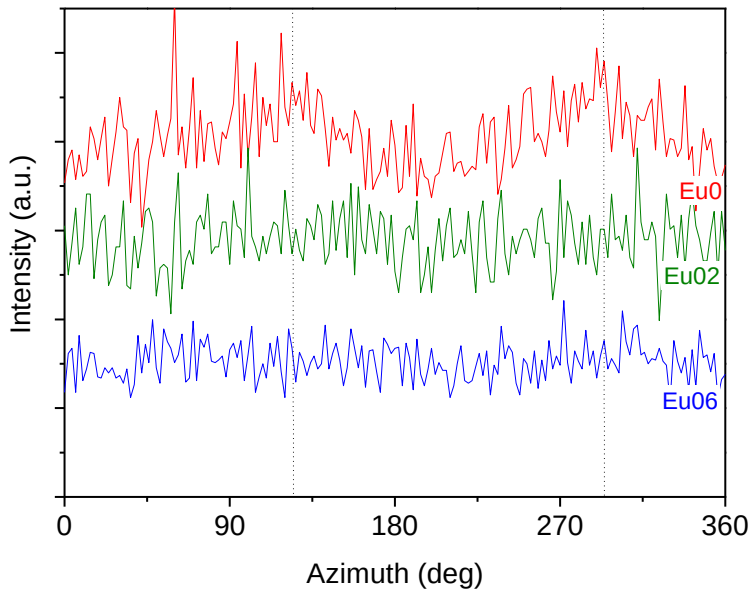

Figure 2.8. Azimuthal profiles of the first ring of diffraction (q = 0.24 $Å^{-1}$ peak in Fig. 2.4a).

Diffraction data therefore indicate that Eu somehow affects the arrangement of PEDOT/PSS molecules towards in-plane randomization, while making them approach each other. Since the a lattice parameter is expected to be related to the lamellar stacking of intercalated PEDOT and PSS[35b], the observed decrease of periodicity distance along a could be ascribed to Eu molecules partially substituting PSS ones intercalating with PEDOT, as observed with other additives such as dimethyl sulphoxide (DMSO) or ethylene glycol (EG)[53].

In Figure 2.9 the 2D patterns for films with Eu fraction of 0.17, 0.4, 0.6 (a,b,c) are reported, respectively, and in Figure 2.6 the corresponding in (d) and out of (e) plane linear cuts, and the azimuthal profiles for the PSS (f) and the PEDOT (g) rings are reported.

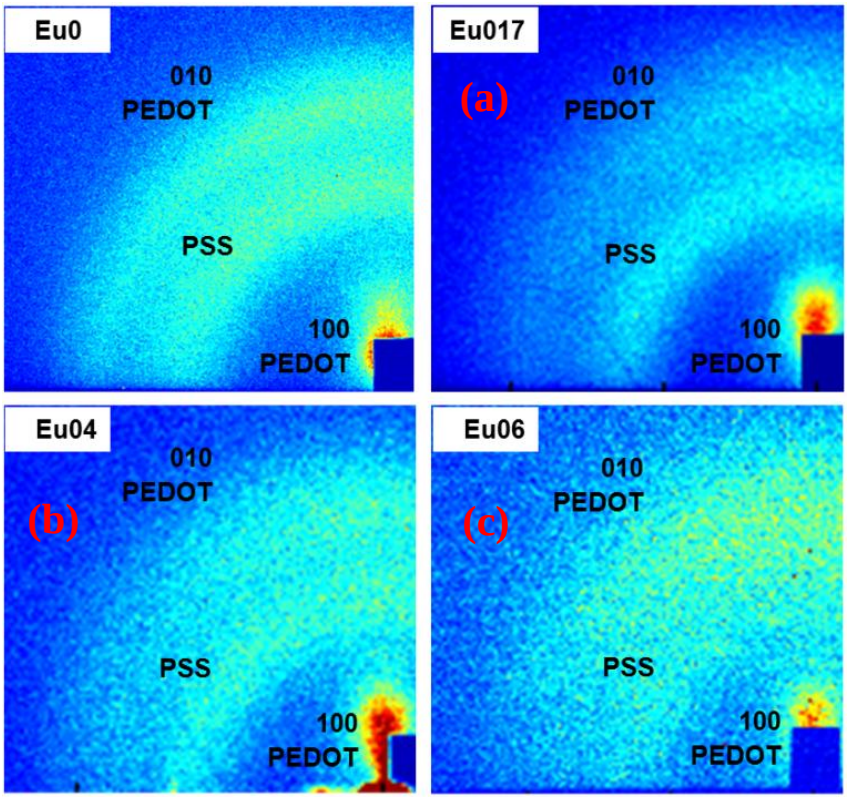

Figure 2.9. GIWAXS 2D patterns of EUPH: Eu fraction of 0, a) 0.17, b) 0.4, c) 0.6 .

Direct evidence of film texture (orientation of crystalline domains) comes from 2D GIWAXS patterns: the intensity distribution along the diffraction rings in Figure 2.9 indicates a random orientation of PSS molecules on average (isotropic intensity of the q = 1.2 $Å^{-1}$ ring) and a preferred out of plane orientation of PEDOT molecules, mainly in domains with the a axis [100] oriented perpendicular to the film plane (high intensity anisotropy of the q = 0.4 $Å^{-1}$ ring), and to a less extent in domains with the b axis [010] oriented perpendicular to the film plane (slight intensity anisotropy of the q = 1.8 $Å^{-1}$ ring). On the contrary, no preferred orientation of the PSS molecules is detected (similar diffraction intensity in both the in and out of plane cuts), likely because most part of the PSS is not bound to PEDOT and is randomly oriented, while only the small fraction of PSS intercalated with PEDOT is expected to be oriented giving rise to a negligible anisotropic scattering. On the other hand, the partial preferred orientation of PEDOT domains with the b axis perpendicular to the film plane is quantitatively visible in the 1D patterns (linear cuts in Figures 2.6 and 2.7), by comparing the intensity ratio of the PEDOT to the PSS ring, featuring opposite trends in the in and out of plane cuts, respectively. As a further check, in Figure 2.6c,d the raw azimuthal profiles are reported, where only a scale factor has been applied in order to normalize all of them to the PSS diffraction intensity, for an easy comparison. It is indeed clearly recognized a basically identical intensity distribution in the PSS ring for all samples (Figure 2.6c,d. GIWAXS), whereas intensity differences are found in the PEDOT ring intensity (Figure 2.6c) , which are in particular related to its overall (normalized) level rather than to its distribution along the azimuth. The similar intensity spread indicates a similar degree of orientation of PEDOT molecules along the b axis; on the other hand, different intensity levels (as for Eu06 in Fig. 2.6d) would suggest increasing fractions of ordered molecules of (crystalline) PEDOT with increasing Eu content, but such trend is expected to be also affected by the increasing scattering from the substrate, besides the additive Eu scattering

contribution close to the PEDOT angular region, as previously discussed, so that such different contributions are hardly discriminated.

It is worth noting that the film without Eu features a significantly lower diffraction intensity of the PEDOT:PSS 100 peak in Fig. 2.4b and 2.9a, compared to the films embedding Eu. The reason is explained in Fig. 2.10, showing the GIWAXS pattern of the PEDOT:PSS film collected at a larger distance from the sample, allowing the 100 and 200 to show up as spots and confirming the out of plane orientation of the a axis, with 2.4 nm periodicity (as in Fig. 2.4a). Thus the texture of the PEDOT:PSS blend does not change qualitatively upon Eu addition, yet it changes quantitatively, due to the increasing degree of orientational and crystalline order (Fig. 2.4b); moreover, a structural variation occurs, with a decrease of the a lattice parameter (Fig. 2.4a)

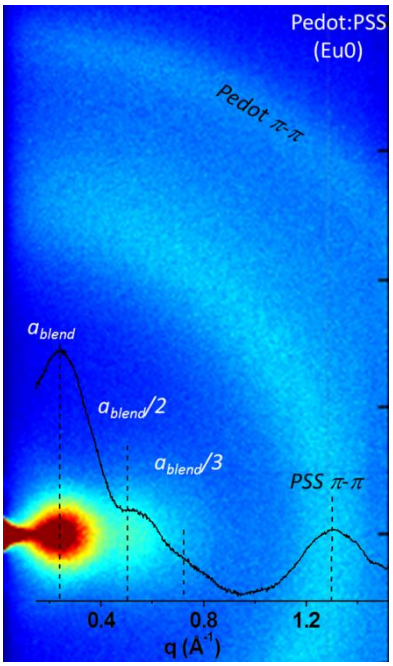

Figure 2.10 . GIWAXS pattern from the bare PEDOT:PSS film, collected at 19 cm distance from the sample, clearly showing the out of plane orientation of the a axis [100] with 0.25 Å^{-1} periodicity.

On the other hand, the evolution of the 010-oriented minority domains with Eu concentration is not clear, because of the simultaneuous scattering increase from Eu and the substrate. Indeed, at larger Eu concentrations and incidence angle 0.5°, Eu and substrate scattering signals enlarge and overwhelm the PSS and PEDOT ones which finally disappear for a 0.87 Eu concentration, where both in- and out-of-plane GIWAXS cuts become similar to the amorphous-like WAXS pattern (transmission geometry) of the bare Eu film (Figure 2.5). As a result, X-ray

diffraction data suggest an increasing ordering and approaching of PEDOT molecules with Eu content up to a fraction of 0.76. For larger Eu concentrations, diffraction from PSS and PEDOT becomes negligible, so that details about their structure are progressively hidden, although the net decrease of the PEDOT 100 and 200 reflection visibility (Figure 2.4b) suggests an increasing disorder of PEDOT chains for Eu fractions larger than 0.76.

The Eu–PH blends were prepared starting from a mixture DHI-PEDOT:PSS (w/w ratios of 0:1:2.5, 0.2:1:2.5, 0.7:1:2.5, 1.5:1:2.5, 3.2:1:2.5, 6.5:1:2.5), obtained by two mother solutions: (a) DHI in isopropyl alcohol and (b) PEDOT: PSS in water (a Clevios PH1000 commercial product). In order to enhance the conductivity of the pristine PEDOT:PSS, 5% DMSO was added to the PH1000. The two solutions were mixed for 5 min in a vial placed on a shaking plate under inert atmosphere, in order to give a homogeneous solution. The DHI-PEDOT:PSS blend was filtered through a 0.20 μm PTFE membrane, deposited by drop casting on glass substrates and then annealed at 110°C for 20 min on a hot plate, to evaporate the residual water. The Eu–PH thin films were thus obtained by exposing the DHI-PEDOT:PSS films for 1 h to air-equilibrated gaseous ammonia, from an ammonia solution (28% in water) inside a sealed chamber at 1 atm pressure and at controlled temperature (25 ÷ 40 ◦C). For reference purposes, films by sole Eumelanin and sole PH1000 were also prepared, using the same experimental conditions.

Wide Angle X-ray Scattering data were collected from both free-standing films in transmission geometry (WAXS), and from as prepared films deposited on glass substrates in Grazing Incidence reflection geometry (GIWAXS). A Fr-E+ SuperBright rotating anode microsource (CuKa, λ=0.154 nm) was employed, equipped to a three-pinhole camera (Rigaku SMAX-3000) through a multilayer focusing optics (Confocal Max-Flux; CMF 15–105). An image plate (IP) detector with 100 mm pixel size was placed at about 28 mm or 20 cm, and 8.7 or 19 cm far

from the sample for WAXS and GIWAXS measurements, respectively. Diffraction patterns were calibrated by using LaB6 or Ag Behenate standard reference materials, for 28 mm and larger sample-to-detector distances, respectively. The diameter of the primary X-ray beam was approximately 200 μm. The incidence angle in GIWAXS experiments was 0.2 or 0.5°.

X-ray diffraction (XRD) data in detector scan mode were collected from the as prepared films deposited on glass substrates, by a Bruker D8 Discover (CuKa, λ = 0.154 nm), equipped with a Göbel mirror, an Eulerian cradle, and a scintillation point detector.

The effect of eumelanin integration within PEDOT:PSS layers was investigated in terms of the changes in the hierarchical structure of PEDOT:PSS films. The results of the X-ray scattering characterization clearly demonstrate that the presence of eumelanin affects the PEDOT component of the blend molecules inducing an overall increase of crystalline order at low eumelanin contents. This effect is associated with the approaching of the PEDOT chains and the overall result appears to be a less steep decay of the blend conductivity, when eumelanin percent content increases, than the one expected on the basis of data reported on conductivity of PEDOT ternary mixtures. At the same time, the introduction of eumelanin confers noteworthy properties to the EUPH blend, including a strong adhesion on inorganic substrates, and water stability, which opens to efficient exploitation of EUPH as conductive coatings within biointerfaces for application in bioelectronics.

2.4 Exploitation of Eumelanin-PEDOT:PSS as polymeric anode for the design and fabrication of ITO-free OLED

In light of the approach[58] explained in the previous section, the new blend has made it possible to obtain water stable transparent thin films, capable to operate as electrodes for organic devices, complementing the PEDOT:PSS electronic conductivity with the peculiar eumelanin properties, including adhesion, water stability, and ionic–electronic conductivity.

As a proof of concept, an unprecedented ITO-free organic light emitting diode (OLED) implementing an eumelanin – PEDOT:PSS layer as the anode was fabricated and characterized. To the best of our knowledge this is the first evidence of an optoelectronic device based on an anode layer integrating eumelanin[59]. To integrate eumelanin and PEDOT:PSS, a protocol involving in situ eumelanin generation was designed. This approach has made it possible not only to circumvent the actual insolubility of eumelanin in any solvent[60, 61], but also to gain over the PEDOT:PSS molecular organization[62]. The rationale supporting this is rooted in the chemistry of DHI, in particular the control over the eumelanin fabrication via solid state polymerization of DHI and the known hydrophobic organization of the eumelanin supramolecular constituents (Figure 2.11) driven by

the π–π stacking interaction, which proved to allow efficient blending with conducting carbon-based systems[32].Indeed, in previous studies, the complementing of the conducting graphene-like systems with the eumelanin concrete proved to result in a blend featuring higher conductivity than the one expected on the basis of the conductivities of the starting materials and their weight ratio[62].

On this basis, it was expected a significant control over the structural, mechanical, and chemical characteristics of the eumelanin–PEDOT:PSS (Eu–PH) films, without a parallel detrimental decay of the conductivity. The target was to obtain a material featuring good conductivity (not less than 300 $S*cm^{-1}$, for a small voltage decay) and a work function at least comparable with the ITO (whose commonly reported values are around 4.4 ÷ 4.7 eV[63] or larger for an efficient hole injection, to be effectively used as the anodic material in organic electronic devices.

The Eu–PH blend was prepared starting from a mixture DHI-PEDOT:PSS (w/w ratio of 0.7:1:2.5), obtained by two mother solutions: (a) DHI in isopropyl alcohol and (b) PEDOT:PSS in water (a Clevios PH1000 commercial product). In order to enhance the conductivity of the pristine PEDOT:PSS, 5% DMSO was added to the PH1000. The two solutions were mixed for 5 min in a vial placed on a shaking plate under oxygen free atmosphere, in order to give a homogeneous solution. The DHI-PEDOT:PSS blend was filtered through a 0.45 μm nylon membrane, deposited by spin coating on glass substrates and then annealed at 80 °C for 30 min on a hot plate, to evaporate the residual water (Figure 2.11).

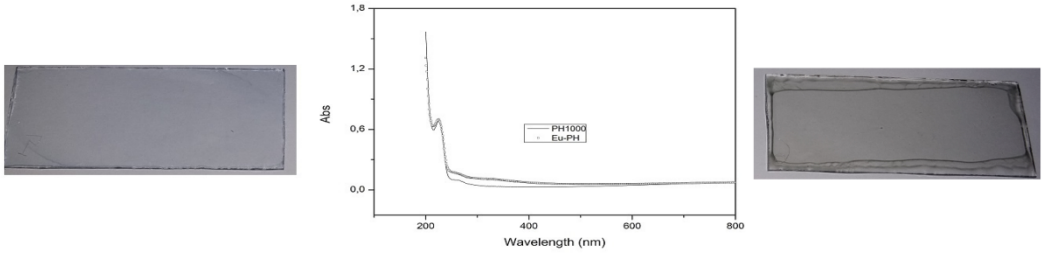

Figure 2.11. UV –vis plots of PH1000 and Eu-PH (60 min AISSP time) films on glass substrates are showed with the corresponding substrate picture: PH1000, left and Eu-PH: right

Evaluation of the water content within the films before, and after the annealing, was obtained by thermogravimetric analysis (TGA) (Figure 2.12) which proved the actual complete removal of water after thermal treatment of the films.

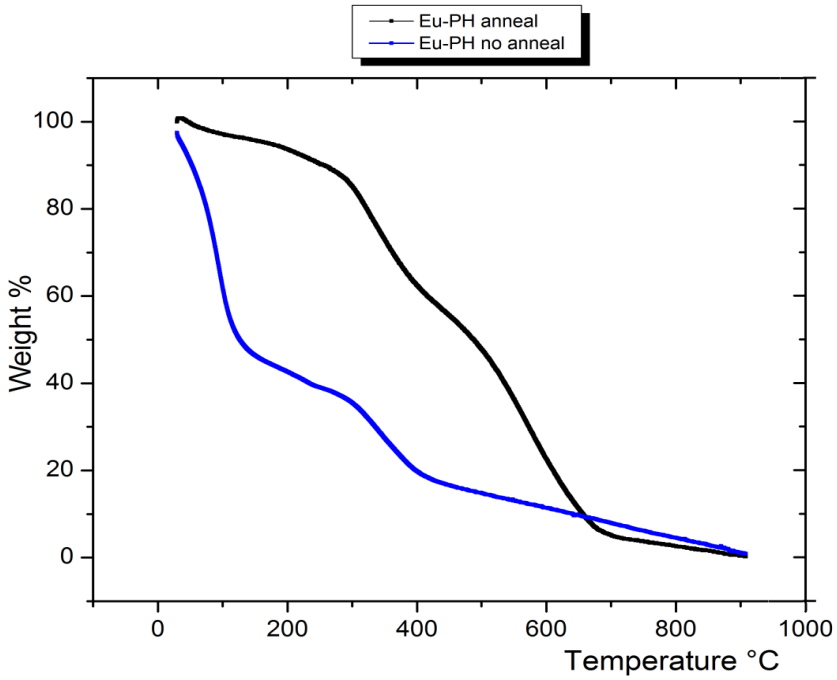

Figure 2.12. TGA profiles Eu-PH before (blue) and after (black) thin layer annealing (80 °C, 30 min)

The Eu–PH thin films were thus obtained by exposing the DHI-PEDOT:PSS films for 1 h to air-equilibrated gaseous ammonia, from an ammonia solution (28% in water) inside a sealed chamber at 1 atm pressure and at controlled temperature (25 ÷ 40 °C). Film inspection by optical surface profiling (Figure 2.13) revealed a thickness in the range of 120–130 nm and an average roughness of about 9 nm, so confirming the thin film quality and the ability to overcome the many problems associated with the limited processability of the insoluble eumelanins.

ITO

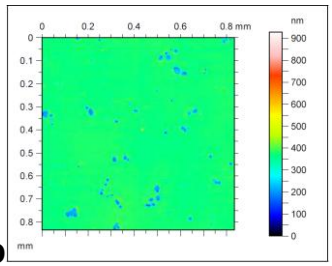

ISO 25178		
Height Parameters		
Sq	23.1	nm
Ssk	-5.67	
Sku	50.1	

PH1000)

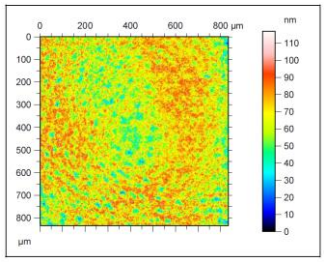

ISO 25178		
Height Parameters		
Sq	13.2	nm
Ssk	-0.232	
Sku	3.07	

Eu-PH)

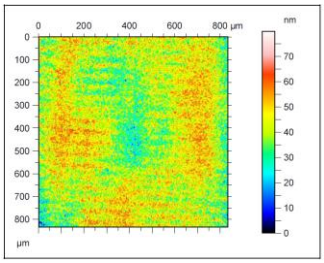

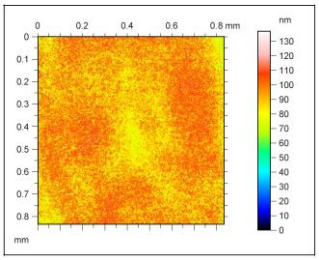

before

ISO 25178		
Height Parameters		
Sq	8.96	nm
Ssk	-0.096	
Sku	2.99	

and after 24h in water)

ISO 25178		
Height Parameters		
Sq	8.47	nm
Ssk	-0.0899	
Sku	3.34	

Eumelanin)

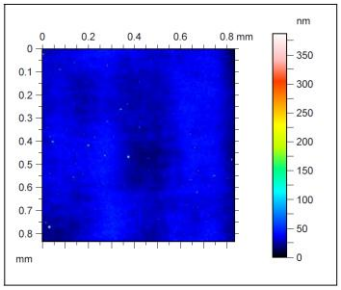

ISO 25178		
Height Parameters		
Sq	6.76	nm
Ssk	3.99	
Sku	160	

Figure 2.13. (A) Surface analysis pictures of ITO, PH1000, Eu-PH (before and after immersion in water) and DHI melanin thin films on glass. The Eu-PH film has been characterized before and after the immersion in water to test the stability of the film

Material	Roughness (nm)	H_2O contact angle (°)	CH_2I_2 contact angle (°)
PH1000 (+ 5% DMSO)	11.0	---	53.9
Eu-PH	8.7	57.9	48.1
Eumelanin	6.6	50.5	28.1

Table 2.1. Values of roughness and contact angle for the investigated materials. Errors are in the limit of 2% for each datum

For reference purposes, films by sole DHI and sole PH1000 were also prepared, using the same experimental conditions. The optical transmittance of thin films of ITO as well as eumelanin, PH1000 and Eu–PH were measured for comparison (Figure 2.14). Films of PH1000 and Eu–PH are both quite transparent in the visible range featuring a transmittance of nearly 80%–90% in the range 400–600 nm. Further insights into the Eu–PH chemistry were obtained from the Fourier Transform Infrared Spectroscopy (FTIR) spectra of Eu–PH in comparison with the spectra of sole eumelanin and PH1000 films (Figure 2.15). All the spectra showed a composite absorption profile in the 1100–1800 cm^{-1} region (CC, CO, and CN bonds) and large signals at 1600–1700 cm^{-1}, typical of aromatic systems. Although the complexity of the polymer constituents prevents a more detailed signal identification, it is worth of note the clear evidence of the C-S bond stretching in the thiophene ring at 982 and 840 cm^{-1} . Also, the bands appearing at 1520 and 1380 cm^{-1} have to be ascribed to the C=C stretching of the quinonoid structures present in both eumelanin and PH1000.

Overall the comparison of the profiles witness the retaining of the chemical composition of both the constituents (eumelanin and PH1000) demonstrating no appreciable degradation occurs, following the film fabrication steps.

The electrical conductivity of the films was evaluated by sheet-resistance measurements, performed with a four-point probe system. The sheet resistance values of the PH1000 and Eu–PH films were 1.02×10^2 and 1.98×10^2 Ω sq^{-1}, respectively. The eumelanin conductivity was estimated according to a reported protocol[32]. In Table 1, the values of the various parameters for the tested materials are reported, including a sample of commercial ITO (Delta Technologies, Ltd. on Corning Eagle XG glass (substrate thickness 1.1 mm)), routinely used as anodic material, and here used as a further reference material. Data in Table 2.1 also demonstrate the critical role of DMSO in improving electrical properties of the films. Addition of 5 % of DMSO to the starting solutions allowed to get up to a value around 800 S cm^{-1} for the PH1000 and of 370 S cm^{-1} for the Eu–PH blend, a value well fitting in the range required for a conducting layer of a device. Relevant information concerning the stability of Eu–PH films to water and organic solvents were also acquired and H_2O and CH_2I_2 contact angles were determined, to better understand the wettability of these surfaces and the possibility to use other solvents for the deposition of subsequent polymeric layers in view to fabricate a device based on Eu–PH film as the anode. Relevant data and film surface characterization are reported in the Table 2.2 and Figure 2.13.

It is worth to note that EU–PH films did exhibit marked stability to water and retention of the adhesion over the substrates, even after 24 h of film immersion in water, with roughness actually unchanged and film thickness decreased of about 3%. PH1000 films partially dissolved and detached from the substrate within 1 h after water immersion. Indeed, after 24 h of water exposition PH1000 films appeared completely ruined. The electrical and optical characteristics of Eu–PH thin film did suggest its actual exploitation as the device anode instead of ITO. To verify this conjecture, three model OLED devices were fabricated differing only for the anode materials: the Eu–PH and, as reference devices, ITO and PH1000. To get the devices layout, each anodic material was shaped by mechanical/chemical removal of the exceeding material. The ITO layer profile was obtained by photolithography and wet chemical etching, followed by a UV-ozone treatment to remove organic residues and activate the ITO surface. In the case of PH1000 and Eu–PH, the exceeding zones were mechanically removed before the annealing step.

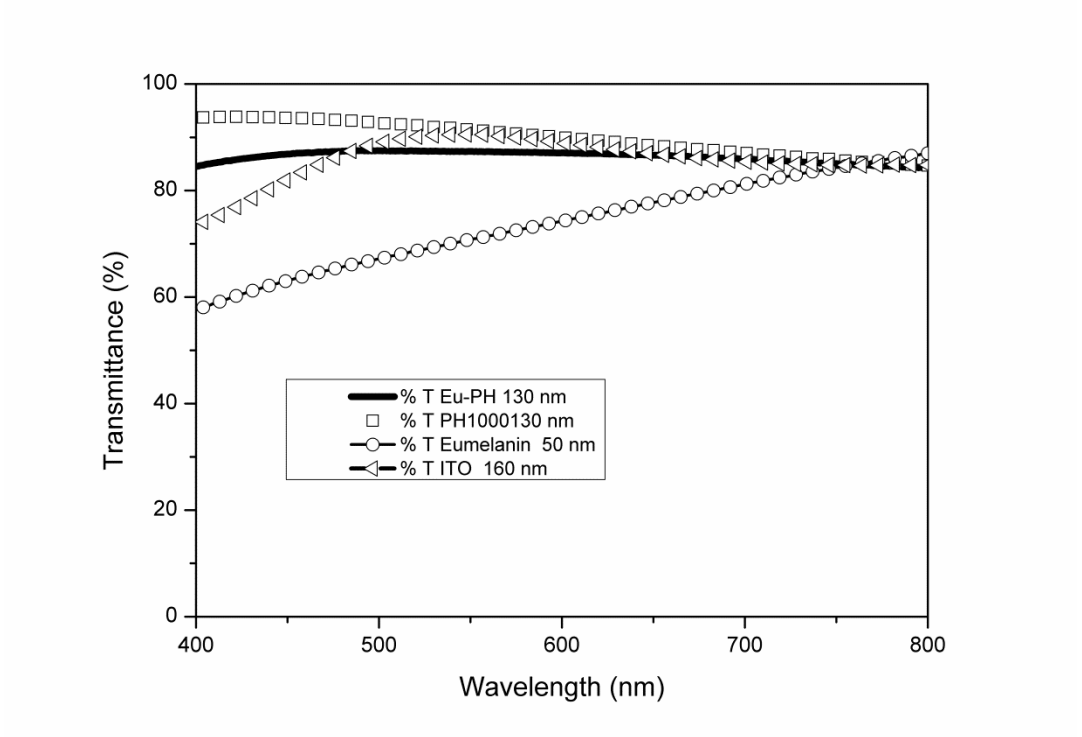

Figure 2.14. UV–vis transmittance spectra of thin films of: Eu–PH, —; Eumelanin, O; Clevios PH 1000, □; ITO, Δ.

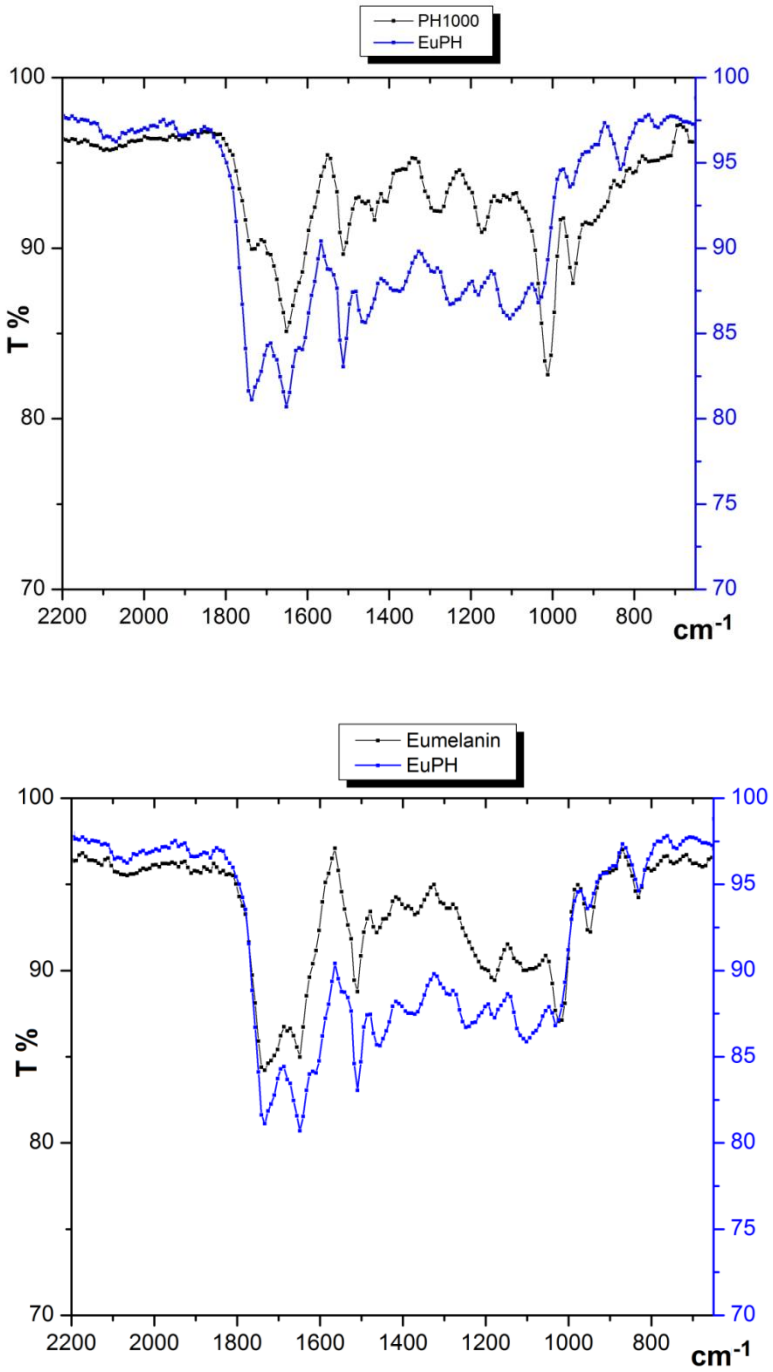

Figure 2.15. FTIR spectra of Eu-PH before (blue) and after (black) thin layer annealing (80 °C, 30 min)

Material[a)]	Thickness [nm]	Optical transmittance [%, 555nm]	Sheet Resistance [Ω sq^{-1}]	Conductivity [S cm^{-1}]
ITO	160	90.0	8 ÷ 12	5200
PH1000	130	91.2	1.02×10^2	780
Eu-PH	130	87.3	1.98×10^2	370
Eumelanin	50	71.1	2.0×10^7	4.0×10^{-7}

a) Data reported are the average of triplicate measures. Errors are in the limit of 0.5% for each datum

Table 2.2 Values of the valuable parameters for the investigated materials.

The Eu–PH layer was obtained by spin coating of the mother solution comprising DHI and PH1000, the layer was then subjected to the ammonia-induced solid state polymerization (AISSP) protocol[51] to finally obtain the integrated Eu–PH thin film. As the oxidative polymerization process is carried out in solid phase, at the supramolecular scale it is expected that the layer retain the homogeneity of the starting solution. Indeed, although in view of future development a more detailed analysis of the layer buildup is required, this hypothesis is consistent with the reaction to AISSP of the surface profile of the film, which appeared virtually unchanged before and after the treatment. The other functional layers of the OLEDs were all identically fabricated for the three OLED typologies. A hole injection layer (HIL), CLEVIOS PEDOT:PSS PVP Al 4083, used as-is, was deposited via dip-coating (Figure 2.16).

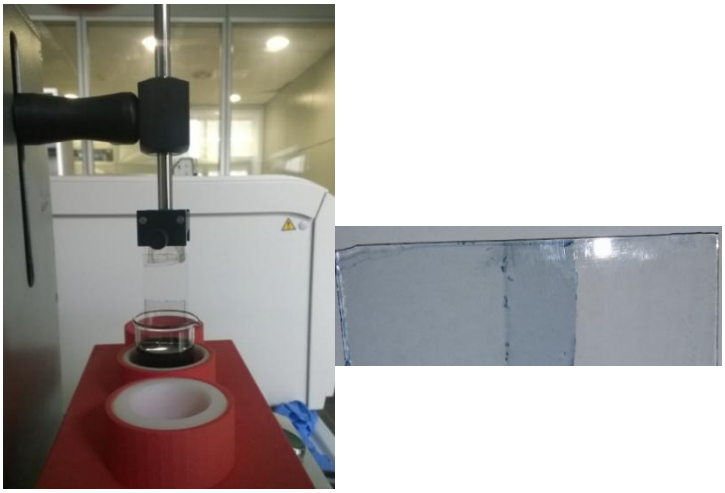

Figure 2.16. Image of HIL (PEDOT:PSS PVP Al 4083) deposition via dip-coating.

Final steps of the OLEDs fabrication were carried out under controlled atmosphere. All the substrates were loaded into a glove box system (N_2 atmosphere, O_2 < 1 ppm, H_2O < 1 ppm), and transferred into an in-line evaporation chamber. Functional organic layers and cathode materials were deposited by thermal evaporation, at rates below 1 Å s^{-1}, through shadow masks to define the devices layout. The active area of the devices is 7×10^{-6} m^2. Since the devices were not encapsulated, they were kept inside the glove box to be characterized. The final OLED architecture (Figure 2.17) includes: the glass substrate; the anode (ITO; CLEVIOS PH1000; Eu–PH); the HIL; the HTL; the ETL-EML and the cathode.

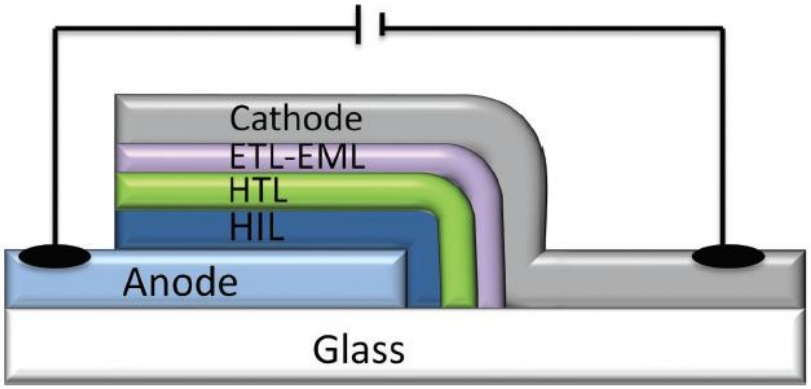

Figure 2.17. Schematic section of the OLED device here adopted, organic layers are: N,N′-di-1-naphthaleyl-N,N′-diphenyl-1,1′-biphenyl-4,4′-diamine (α-NPD) as the hole transport layer (HTL, thickness 40 nm), and tris- 8-hydroxyquinoline aluminum salt (Alq_3), which acts as the electron transport layer (ETL) and the emitting layer (EML, thickness 60 nm). Cathode is a bilayer made of calcium (Ca) (20 nm) and aluminum (Al) (80 nm).

The electro-optical characterization of the OLEDs was performed in triplicate for those devices featuring organic anodes and a comparison measure was taken in the case of the ITO anode, all device typologies featured the same emission spectra (Figure 2.18), a picture of the emitting devices is also reported in Figure 2.19. The current density and the luminance vs. the applied tension are reported in Figure 2.20.

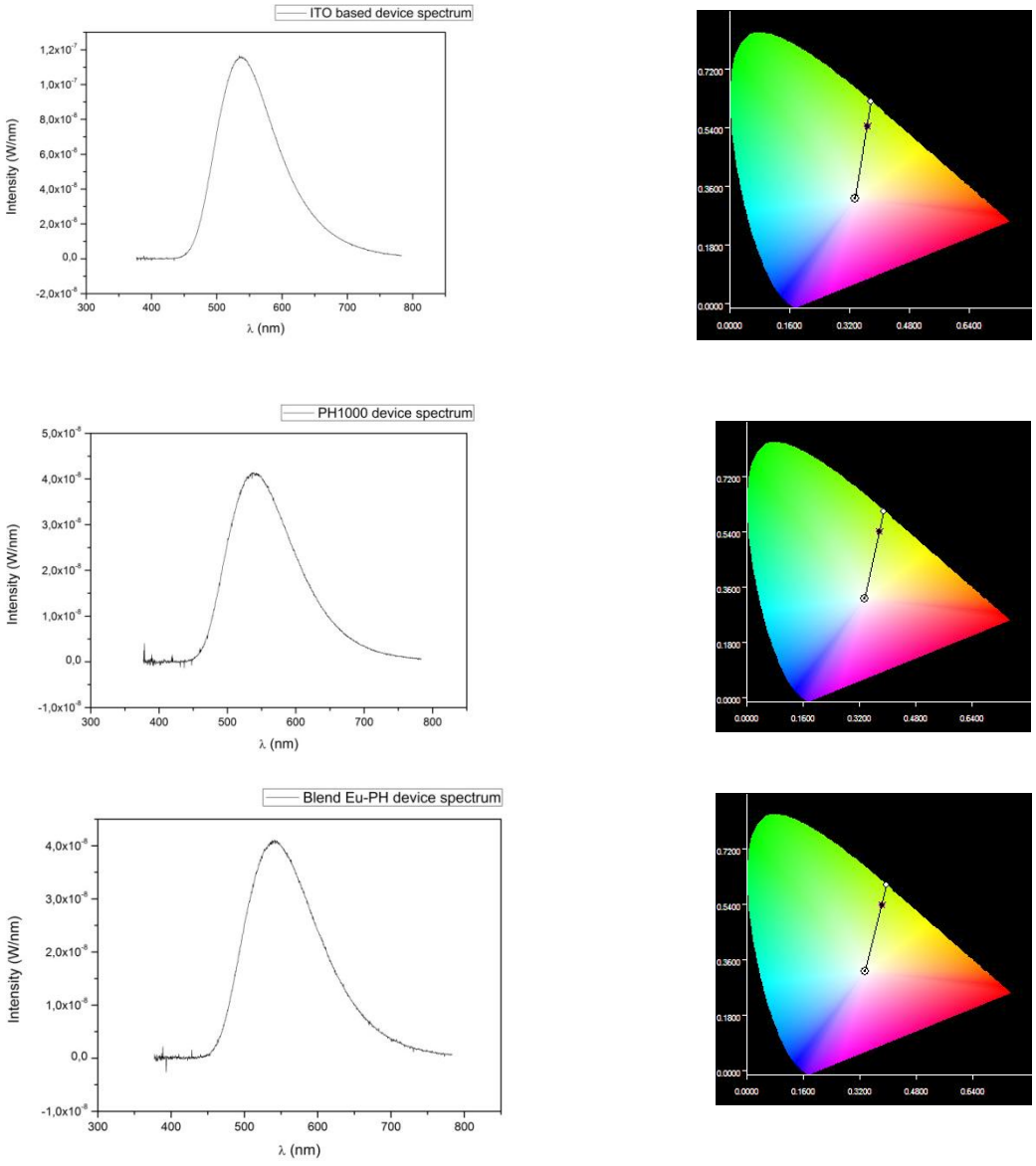

Figure 2.18: Spectra of ITO, PH1000 and Eu-PH based devices and CIE coordinates

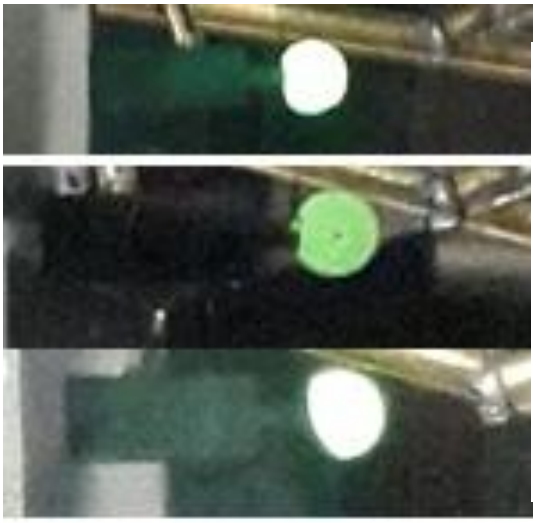

Figure 2.19: Pictures of OLEDs equipped with anodes of: **ITO (a), PH1000 (b), Eu-PH (c).** (a) and (c) appear white because the light emitted has saturated the sensitivity of the camera.

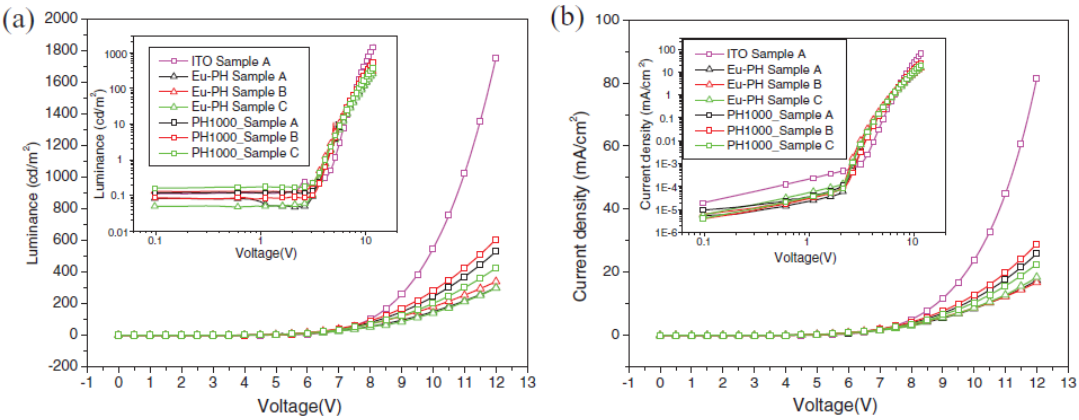

Figure 2.20. a) Luminance and b) current density measured for the OLEDs equipped with the different anodes. -□-, cyan: ITO; -Δ-, green, red, black: Eu–PH; -□- green, red, black: PH1000.

The performances of the Eu–PH OLEDs are characterized by a turn-on voltage of 2.5 V and a luminance of 300 cd*m^{-2} at 12 V. These performances are very near to the ones of the PH1000 devices and, moreover, even to those of the ITO OLED when looking at the efficiency plots (Figure 2.21)

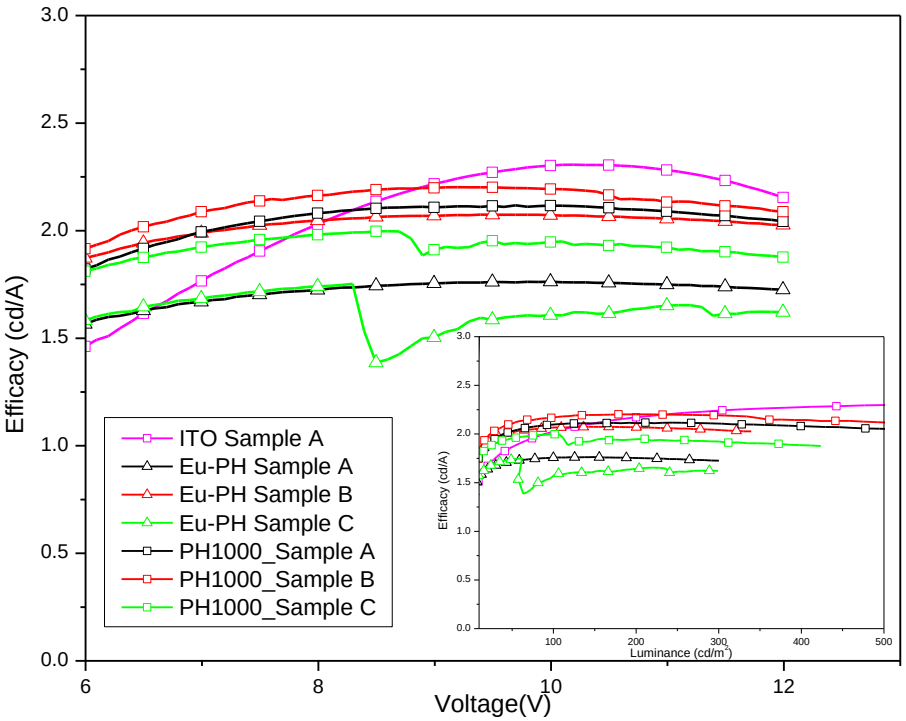

Figure 2.21: Efficiency-voltage and efficiency-luminance (inset) characteristics of the three different OLED fabricated.

witnessing the little impact of the lower transmittance of the Eu–PH film with respect to the ITO film. Organic OLEDs featured a lower turn on voltage than the ITO device possibly as consequence of a better charge injection also associated to the smoother surfaces of organic anode layers. Moreover, PH1000 and Eu–PH

present similar behaviors, with the performances of the Eu–PH OLEDs just a few below the first ones. Some performance decrease was expected, because of the lower conductivity and smaller transmittance of the eumelanin with respect to PH1000, which induces a reduction of these parameters for the mixture.

Although a more in-depth investigation is required to fully address the eumelanin–PEDOT integration, these data do demonstrate that the two materials interaction within the blend allows to get an efficiently working anode. It may be speculated that a contribution from the large scale homogeneity of the layer, warranted by the solid state fabrication protocol and associated with a better connection between uniformly distributed PEDOT chains, is at the origin of possible percolating paths inside the Eu–PH layer.

In summary, a blend of the mammalian eumelanin pigment and the PEDOT:PSS, is devised and prepared featuring good conductivity and thus suitable to be employed as the anodic material for organic devices.

A new method has been designed and exploited to prepare the eumelanin-PEDOT blend and fabricate thin films of it, starting from the solutions of the eumelanin precursor DHI and of the water soluble polymer mixture PEDOT:PSS, and applying the AISSP procedure to get in situ polymerization of the DHI in the solid state. This approach allowed to meet the needs required by the processing of the insoluble eumelanin and those of expedient PEDOT thin film deposition. Thanks to the formation of the eumelanin crosslinked eumelanin matrix, the Eu–PH material proved to be resistant to water, retaining the actual surface smoothness after

immersion in water for 24 h. Moreover, it showed to be highly adhesive, stable to solvent treatment and capable to maintain its electrical performances over weeks.

The final demonstration of the potentialities of this approach was obtained by the actual exploitation of the Eu–PH as the anode within ITO-free organic light emitting devices, presenting performances comparable to reference ITO-free devices. Because of the versatility of the coating technique and the chemical and mechanical properties of the Eu–PH these findings are as well applicable for other electronic devices featuring different architectures, including organic electrochemical transistors and photoelectrochemical cells. Overall, the results here presented appear highly promising in view of the eumelanin applications in organic (bio)electronics and biocompatible interface fabrication and pave the way for innovative ITO-free electrodes susceptible of eumelanin-based tuning of the electrical and electrochemical properties.

2.5 References

1. A.G. Macdiarmid, et al., Electrically conducting covalent polymers – halogen derivatives of (Sn)X and (Ch)X. J. Electrochem. Soc., 124, C304–C304, 1977.
2. R.M. Owens, G.G. Malliaras, Organic electronics at the interface with biology. MRS Bull., 35, 449–456, 2010. DOI= 10.1557/mrs2010.583
3. M Berggren, A. Richter-Dahlfors, Organic bioelectronics. Adv. Mater., 19, 3201–3213, 2007. DOI= 10.1002/adma.200700419
4. M. Gao, L. Dai, G.G. Wallace, Biosensors based on aligned carbon nanotubes coated with inherently conducting polymers. Electroanalysis, 15, 1089–1094, 2003. DOI= 10.1002/elan.200390131
5. a) A. Pron, P. Gawrys, M. Zagorska, D. Djurado, R. Demadrille, Electroactive materials for organic electronics: Preparation strategies, structural aspects and characterization techniques. Chem. Soc. Rev., 39, 2577, 2010. DOI= 10.1039/b907999h; b) C. Liao, M. Zhang, M. Y. Yao, T. Hua, L. Li, F. Yan, Flexible Organic Electronics in Biology: Materials and Devices. Adv. Mater., 27, 7493, 2015. DOI= 10.1002/adma.201402625; c) G. G. Malliaras, Organic bioelectronics: A new era for organic electronics. Biochim. Biophys. Acta, Gen. Subj., 1830, 4286, 2013. DOI= 10.1016/j.bbagen.2012.10.007
6. N. Espinosa, A. Laurent, G. A. d. R. Benatto, M. Hosel, F. C. Krebs, Which Electrode Materials to Select for More Environmentally Friendly Organic Photovoltaics. Adv. Eng. Mater., 18, 490, 2016. DOI= 10.1002/adem.201500509
7. J.-Y. Lee, S. T. Connor, Y. Cui, P. Peumans, Solution-processed metal nanowire mesh transparent electrodes. Nano Lett., 8, 689, 2008. DOI= 10.1021/nl073296g
8. U.S. Department of the Interior – U.S. Geological Survey, Mineral commodity summaries, http://dx.doi.org/10.3133/70140094 (accessed: July 2016).
9. European Commission Report on Critical Raw Materials for the EU, http://www.actu environnement.com/media/pdf/news-23426-report-criticam-rax-materials-2014.pdf (accessed: May 2014).

10. a) A. Kumar, C. Zhou, The Race To Replace Tin-Doped Indium Oxide: Which Material Will Win, ACS Nano, 4, 11, 2010. DOI= 10.1021/nn901903b; b) D. C. Martin, G. G. Malliaras, Interfacing Electronic and Ionic Charge Transport in Bioelectronics. ChemElectroChem, 3, 686, 2016. DOI= 10.1002/celc.201500555
11. C. J. Bettinger, J. P. Bruggeman, A. Misra, J. T. Borenstein, R. Langer, Biocompatibility of biodegradable semiconducting melanin films for nerve tissue engineering. Biomaterials, 17, 3050, 2009. DOI= 10.1016/j.biomaterials.2009.02.018 a) M. R. Abidian, K. A. Ludwig, T. C. Marzullo, D. C. Martin, D. R. Kipke, Interfacing conducting polymer nanotubes with the central nervous system: chronic neural recording using poly(3,4-ethylenedioxythiophene) nanotubes. Adv. Mater., 21, 3764, 2009. DOI= 10.1002/adma.200900887; b) G. Zotti, G. Schiavon, S. Zecchin, L. Groenendaal, Conductive and magnetic properties of 3,4-dimethoxy- and 3,4-ethylenedioxy-capped polypyrrole and polythiophene. Chem. Mater., 10, 2996, 2000. DOI= 10.1021/cm000400l
12. a) J. Wu, H. A. Becerril, Z. Bao, Z. Liu, Y. Chen, P. Peumans, Organic solar cells with solution-processed graphene transparent electrodes. Appl. Phys. Lett., 92, 263302, 2008. DOI= 10.1063/1.2924771; b) J. P. Bothma, J. De Boor, U. Divakar, P. E. Schwenn, P. Meredith, Device-Quality Electrically Conducting Melanin Thin Films. Adv. Mater., 20, 3539, 2008; DOI= 10.1002/adma.200703141
13. L. K. Povlich, J. Le, J. Kim, D. C. Martin, Poly(5,6-dimethoxyindole-2-carboxylic acid) (PDMICA): A melanin-like polymer with unique electrochromic and structural properties. Macromolecules, 43, 3770, 2010. DOI= 10.1021/ma9023558
14. a) Y. H. Kim, C. Sachse, M. L. Machala, C. May, L. Mueller-Meskamp, K. Leo, Highly Conductive PEDOT:PSS Electrode with Optimized Solvent and Thermal Post-Treatment for ITO-Free Organic Solar Cells. Adv. Funct. Mater., 21, 1076, 2011. DOI= 10.1002/adfm.201002290; b) M. Vosgueritchian, D. J. Lipomi, Z. Bao, Highly Conductive and Transparent

PEDOT:PSS Films with a Fluorosurfactant for Stretchable and Flexible Transparent Electrodes. Adv. Funct. Mater., 22, 421, 2012. DOI= 10.1002/adfm.201101775

15. a) D. Simien, J. A. Fagan, W. Luo, J. F. Douglas, K. Migler, J. Obrzut, Influence of nanotube length on the optical and conductivity properties of thin single-wall carbon nanotube networks. ACS Nano, 2, 1879, 2008. DOI= 10.1021/nn800376x; b) A. A. Green, M. C. Hersam, Colored Semitransparent Conductive Coatings Consisting of Monodisperse Metallic Single-Walled Carbon Nanotubes. Nano Lett., 8, 1417, 2008. DOI= 10.1021/nl080302f
16. C. J. Brabec, S. Gowrisanker, J. J. M. Halls, D. Laird, S. Jia, S. P. Williams, Polymer-fullerene bulk-heterojunction solar cells. Adv. Mater., 22, 3839, 2010. DOI= 10.1002/adma.200903697
17. K. C. Larsson, P. Kjall, A. Richter-Dahlfors, Biochim. Biophys. Acta, Organic bioelectronics for electronic-to-chemical translation in modulation of neuronal signaling and machine-to-brain interfacing. Gen. Subj., 1830, 4334, 2013. DOI= 10.1016/j.bbagen.2012.11.024
18. a) B. L. Groenendaal, F. Jonas, D. Freitag, H. Pielartzik, J. R. Reynolds, Poly(3,4-ethylenedioxythiophene) and Its Derivatives: Past, Present, and Future. Adv. Mater., 12, 481, 2000. DOI= 10.1002/(SICI)1521-4095(200004)12:7<481::AID-ADMA481>3.0.CO;2-C; b) Q. B. Pei, G. Zuccarello, M. Ahlskog, O. Inganas, Electrochromic and highly stable poly(3,4-ethylenedioxythiophene) switches between opaque blue-black and transparent sky blue. Polymer, 35, 1347, 1994. DOI= 10.1016/0032-3861(94)90332-8; c) J. Ouyang, ‘‘Secondary doping’’ methods to significantly enhance the conductivity4 of PEDOT:PSS for its application as transparent electrode of optoelectronic devices. Displays, 34, 423, 2013. DOI= 10.1016/j.displa.2013.08.007
19. Z. Yu, Y. Xia, D. Du, J. Ouyang, Higher PEDOT Molecular Weight Giving Rise to Higher Thermoelectric Property of PEDOT:PSS: A Comparative Study of Clevios P and Clevios PH1000. ACS Appl. Mater. Interfaces, 8, 11629, 2016. DOI= : 10.1021/acsami.6b15158

20. S. Khan, L. Lorenzelli, R. S. Dahiya, Technologies for printing sensors and electronics over large flexible substrates: A review. IEEE Sens. J., 15, 3164, 2015. DOI= 10.1109/JSEN.2014.2375203
21. J. Y. Kim, J. H. Jung, D. E. Lee, J. Joo, Enhancement of electrical conductivity of poly(3,4-ethylenedioxythiophene)/poly(4-styrenesulfonate) by a change of solvents. Synth. Met., 126, 311, 2002. DOI= 10.1016/S0379-6779(01)00576-8
22. T. R. Chou, S. H. Chen, Y. T. Chiang, Y. T. Lin, C. Y. Chao, Highly Conductive PEDOT:PSS Film by Post-Treatment with Dimethyl Sulfoxide for ITO-Free Liquid Crystal Display. Mol. Cryst. Liq. Cryst., 612, 201, 2015. DOI= 10.1080/15421406.2015.1031581
23. a) M. R. Abidian, K. A. Ludwig, T. C. Marzullo, D. C. Martin, D. R. Kipke, Interfacing Conducting Polymer Nanotubes with the Central Nervous System: Chronic Neural Recording using Poly(3,4-ethylenedioxythiophene) Nanotubes. Adv. Mater., 21, 3764, 2009. DOI= 10.1002/adma.200900887; b) G. Zotti, G. Schiavon, S. Zecchin, L. Groenendaal, Conductive and magnetic properties of 3,4-dimethoxy- and 3,4-ethylenedioxy-capped polypyrrole and polythiophene. Chem. Mater., 10, 2996, 2000. DOI= 10.1021/cm000400l
24. a) L. Ouyang, C. C. Kuo, B. Farrell, S. Pathak, B. Wei, J. Qu, D. C. Martin, Poly[3,4-ethylene dioxythiophene (EDOT) -co- 1,3,5-tri[2-(3,4-ethylene dioxythienyl)]-benzene (EPh)] copolymers (PEDOT-co-EPh): optical, electrochemical and mechanical properties. J. Mater. Chem. B, 3, 5010, 2015. DOI= 10.1039/C5TB00053J; b) K. A. Ludwig, J. D. Uram, J. Yang, D. C. Martin, D. R. Kipke, Chronic neural recordings using silicon microelectrode arrays electrochemically deposited with a poly(3,4-ethylenedioxythiophene) (PEDOT) film. J. Neural Eng., 3, 59, 2006. DOI= 10.1088/1741-2560/3/1/007
25. a) F. S. Marrikar, M. Brumbach, D. H. Evans, A. Lebron-Paler, J. E. Pemberton, R. J. Wysocki, N. R. Armstrong, Modification of indium-tin oxide electrodes with thiophene copolymer thin films: optimizing electron transfer to solution probe molecules. Langmuir, 23, 1530, 2007. DOI= 10.1021/la061840f; b) B. Wei, J. Liu, L. Ouyang, C.-C. Kuo, D. C. Martin, Significant Enhancement of PEDOT Thin Film Adhesion to Inorganic Solid

Substrates with EDOT-Acid. ACS Appl. Mater. Interfaces, 7, 15388, 2015. DOI= 10.1021/acsami.5b03350

26. S. Zhang, E. Hubis, C. Girard, P. Kumar, J. DeFranco, F. Cicoira, Water stability and orthogonal patterning of flexible micro-electrochemical transistors on plastic. J. Mater. Chem. C, 4, 1382, 2016. DOI= 10.1039/C5TC03664J
27. M. Jorfi, J. L. Skousen, C. Weder, J. R. Capadona, Progress towards biocompatible intracortical microelectrodes for neural interfacing applications. J. Neural Eng., 12011001, 2015. DOI= 10.1088/1741-2560/12/1/011001
28. a) D. H. Yoon, S. H. Yoon, K.-S. Ryu, Y. J. Park, PEDOT:PSS as multi-functional composite material for enhanced Li-air-battery air electrodes. Sci. Rep., 6, 19962, 2016. DOI= 10.1038/srep19962; b) M. Irimia-Vladu, N. S. Sariciftci, S. Bauer, Exotic materials for bio-organic electronics. J. Mater. Chem., 21, 1350, 2011. DOI= 10.1039/C0JM02444A
29. a) M. Ambrico, P. F. Ambrico, T. Ligonzo, A. Cardone, S. R. Cicco, M. D'Ischia, G. M. Farinola, From commercial tyrosine polymers to a tailored polydopamine platform: concepts, issues and challenges en route to melanin-based bioelectronics. J. Mater. Chem. C, 3, 6413, 2015. DOI= 10.1039/C5TC00570A; b) M. d'Ischia, K. Wakamatsu, F. Cicoira, E. Di Mauro, J. C. Garcia-Borron, S. Commo, I. Galván, G. Ghanem, K. Kenzo, P. Meredith, A. Pezzella, C. Santato, T. Sarna, J. D. Simon, L. Zecca, F. A. Zucca, A. Napolitano, S. Ito, Melanins and melanogenesis: from pigment cells to human health and technological applications. Pigm. Cell Melanoma Res., 28, 520, 2015. DOI= 10.1111/pcmr.12393\
30. B. Wei, J. Liu, L. Ouyang, C. C. Kuo, D. C. Martin, Significant Enhancement of PEDOT Thin Film Adhesion to Inorganic Solid Substrates with EDOT-Acid. ACS Appl. Mater. Interfaces, 7, 15388, 2015. DOI= 10.1021/acsami.5b03350
31. a) H. Lee, S. M. Dellatore, W. M. Miller, P. B. Messersmith, Mussel-inspired surface chemistry for multifunctional coatings. Science, 318, 426, 2007. DOI= 10.1126/science.1147241; b) J. Jin, D. Lee, H. G. Im, Y. C. Han, E. G. Jeong,

M. Rolandi, K. C. Choi, B. S. Bae, Chitin Nanofiber Transparent Paper for Flexible Green Electronics. Adv. Mater., 28, 5169, 2016. DOI= 10.1002/adma.201600336

32. S. Ito, K. Wakamatsu, M. d'ischia, A. Napolitano, A. Pezzella, in Melanins and Melanosomes: Biosynthesis, Biogenesis, Physiological, and Pathological Functions (Eds.: Jan Borovansky, Patrick A. Riley), Wiley-VCH, Weinheim, Germany 2011, Ch.6. ISBN: 978-3-527-32892-5

33. J. Rivnay, S. Inal, B. A. Collins, M. Sessolo, E. Stavrinidou, X. Strakosas, C. Tassone, D. M. Delongchamp, G. G. Malliaras, Structural control of mixed ionic and electronic transport in conducting polymers. Nature communications, 7, 11287, 2016. DOI= 10.1038/ncomms11287
34. J. Rivnay, Organic electronics: Efficiency through dilution. Nat. Mater., 15, 594-595, 2016. DOI= 10.1038/nmat4632
35. a) S. Kirchmeyer, K. Reuter, Scientific importance, properties and growing applications of poly(3,4-ethylenedioxythiophene). J. Mater. Chem., 15, 2077-2088, 2005. DOI= 10.1039/B417803N; b) N. Massonnet, A. Carella, A. de Geyer, J. Faure-Vincent, J. P. Simonato, Metallic behaviour of acid doped highly conductive polymers. Chem Sci, 6, 412-417, 2015. DOI= 10.1039/c4sc02463j
36. Y. H. Kim, C. Sachse, M. L. MacHala, C. May, L. Müller-Meskamp, K. Leo, Highly Conductive PEDOT:PSS Electrode with Optimized Solvent and Thermal Post-Treatment for ITO-Free Organic Solar Cells. Adv. Funct. Mater., 21, 1076-1081, 2011. DOI= 10.1002/adfm.201002290
37. A. M. Nardes, M. Kemerink, R. A. J. Janssen, J. A. M. Bastiaansen, N. M. M. Kiggen, B. M. W. Langeveld, A. J. J. M. Van Breemen, M. M. De Kok, Microscopic understanding of the anisotropic conductivity of PEDOT:PSS thin films. Adv. Mater., 19, 1196-1200, 2007. DOI= 10.1002/adma.200602575
38. U. Lang, E. Muller, N. Naujoks, J. Dual, Microscopical Investigations of PEDOT:PSS Thin Films. Adv. Funct. Mater., 19, 1215-1220, 2009. DOI= 10.1002/adfm.200801258

39. X. Crispin, F. L. E. Jakobsson, A. Crispin, P. C. M. Grim, P. Andersson, A. Volodin, C. Van Haesendonck, M. Van Der Auweraer, W. R. Salaneck, M. Berggren, The Origin of the High Conductivity of Poly(3,4-ethylenedioxythiophene)−Poly(styrenesulfonate) (PEDOT−PSS) Plastic Electrodes. Chem. Mater., 18, 4354-4360, 2006. DOI= 10.1021/cm061032+
40. S. Inal, J. Rivnay, A. I. Hofmann, I. Uguz, M. Mumtaz, D. Katsigiannopoulos, C. Brochon, E. Cloutet, G. Hadziioannou, G. G. Malliaras, Organic Electrochemical Transistors Based on PEDOT
41. with Different Anionic Polyelectrolyte Dopants. Journal of Polymer Science, Part B: Polymer Physics, 54, 147-151, 2016. DOI= 10.1002/polb.23938
42. T. Takano, H. Masunaga, A. Fujiwara, H. Okuzaki, T. Sasaki, PEDOT Nanocrystal in Highly Conductive PEDOT:PSS Polymer Films. Macromolecules, 45, 3859-3865, 2012. DOI= 10.1021/ma300120g
43. J. Y. Kim, J. H. Jung, D. E. Lee, J. Joo, Enhancement of electrical conductivity of poly(3,4-ethylenedioxythiophene)/poly(4-styrenesulfonate) by a change of solvents. Synth. Met., 126, 311, 2002. DOI= 10.1016/S0379-6779(01)00576-8
44. T. R. Chou, S. H. Chen, Y. T. Chiang, Y. T. Lin, C. Y. Chao, Highly Conductive PEDOT:PSS Film by Post-Treatment with Dimethyl Sulfoxide for ITO-Free Liquid Crystal Display. Molecular Crystals and Liquid Crystals, 612, 201-210, 2015. DOI= 10.1080/15421406.2015.1031581
45. V. Andrei, K. Bethke, F. Madzharova, S. Beeg, A. Knop-Gericke, J. Kneipp, K. Rademann, Size Dependence of Electrical Conductivity and Thermoelectric Enhancements in Spin-Coated PEDOT:PSS Single and Multiple Layers. Adv. Electron. Mater., 3, 2017. DOI= 10.1002/aelm.201600473
46. T. Stocker, A. Kohler, R. Moos, Why does the electrical conductivity in PEDOT:PSS decrease with PSS content? A study combining thermoelectric measurements with impedance spectroscopy. J Polym Sci Pol Phys, 50, 976-983, 2012. DOI= 10.1002/polb.23089
47. H. T. Ham, Y. S. Choi, M. G. Chee, M. H. Cha, I. J. Chung, PEDOT-PSS/singlewall carbon nanotubes composites. Polym. Eng. Sci., 48, 1-10, 2008. DOI= 10.1002/pen.20805

48. Z. Yi, Y. Zhao, P. Li, K. Ho, N. Blozowski, G. Walker, S. Jaffer, J. Tjong, M. Sain, Z. Lu, The effect of tannic acids on the electrical conductivity of PEDOT:PSS Films. Appl. Surf. Sci. 2018. DOI= 10.1016/j.apsusc.2018.04.168
49. L. Migliaccio, S. Aprano, L. Iannuzzi, M. G. Maglione, P. Tassini, C. Minarini, P. Manini, A. Pezzella, Eumelanin–PEDOT:PSS Complementing En Route to Mammalian-Pigment-Based Electrodes: Design and Fabrication of an ITO-Free Organic Light-Emitting Device. Adv. Electron. Mater., 3, 2017. DOI= 10.1002/aelm.201600342
50. Y. Xia, J. Ouyang, Significant different conductivities of the two grades of poly(3,4-ethylenedioxythiophene):Poly(styrenesulfonate), Clevios P and clevios PH1000, arising from different molecular weights. ACS Applied Materials and Interfaces, 4, 4131-4140, 2012. DOI= 10.1021/am300881m
51. A. Pezzella, M. Barra, A. Musto, A. Navarra, M. Alfè, P. Manini, S. Parisi, A. Cassinese, V. Criscuolo, M. d'Ischia, Stem cell-compatible eumelanin biointerface fabricated by chemically controlled solid state polymerization. Mater. Horiz., 2, 212-220, 2015. DOI= 10.1039/c4mh00097h
52. T. Stocker, A. Kohler, R. Moos, Why does the electrical conductivity in PEDOT:PSS decrease with PSS content? A study combining thermoelectric measurements with impedance spectroscopy. J Polym Sci Pol Phys, 50, 976-983, 2012. DOI= 10.1002/polb.23089
53. M. Petrosino, P. Vacca, R. Miscioscia, G. Nenna, C. Minarini, A. Rubino, Effect of PEDOT:PSS ratio on the electrical and optical properties of OLEDs, in Microtechnologies for the New Millennium, Vol. 6593, SPIE, , p. 9, 2007. DOI= 10.1117/12.722022
54. E. J. Lee, J. P. Han, S. E. Jung, M. H. Choi, D. K. Moon, Improvement in half-life of organic solar cells by using a blended hole extraction layer consisting of PEDOT:PSS and conjugated polymer electrolyte. ACS Applied Materials and Interfaces, 8, 31791-31798, 2016. DOI= 10.1021/acsami.6b09846
55. N. S. Liu, G. J. Fang, J. W. Wan, H. Zhou, H. Long, X. Z. Zhao, Electrospun PEDOT:PSS–PVA nanofiber based ultrahigh-strain sensors with controllable

electrical conductivity. J. Mater. Chem., 21, 18962-18966, 2011. DOI= 10.1039/C1JM14491J

56. W. Cho, J. K. Hong, J. J. Lee, S. Kim, S. Im, D. Yoo, J. H. Kim, Multi-purpose overcoating layers based on PVA/silane hybrid composites for highly transparent, flexible, and durable AgNW/PEDOT:PSS films. RSC Advances, 6, 63296-63303, 2016. DOI= 10.1039/c5ra27311k
57. M. N. Gueye, A. Carella, N. Massonnet, E. Yvenou, S. Brenet, J. Faure-Vincent, S. Pouget, F. Rieutord, H. Okuno, A. Benayad, R. Demadrille, J. P. Simonato, Structure and Dopant Engineering in PEDOT Thin Films: Practical Tools for a Dramatic Conductivity Enhancement. Chem. Mater., 28, 3462-3468, 2016. DOI= 10.1021/acs.chemmater.6b01035
58. M. D'Ischia, K. Wakamatsu, A. Napolitano, S. Briganti, J. C. Garcia-Borron, D. Kovacs, P. Meredith, A. Pezzella, M. Picardo, T. Sarna, J. D. Simon, S. Ito, Melanins and melanogenesis: methods, standards, protocols. Pigment Cell and Melanoma Research, *26*, 616, 2013. DOI= 10.1111/pcmr.12121
59. C. H. Chen, J. C. LaRue, R. D. Nelson, L. Kulinsky, M. J. Madou, Electrical conductivity of polymer blends of poly(3,4- ethylenedioxythiophene): Poly(styrenesulfonate): N-methyl-2-pyrrolidinone and polyvinyl alcohol. J. Appl. Polym. Sci., *125*, 3134, 2012; b) P. Li, K. Sun, J. Ouyang, ACS Applied Materials and Interfaces, 7, 18415, 2015. DOI= 10.1002/app.36474
60. Y. J. Kim, W. Wu, S. E. Chun, J. F. Whitacre, C. J. Bettinger, Biologically derived melanin electrodes in aqueous sodium-ion energy storage devices. PNAS, 110, 20912, 2013. DOI= 10.1073/pnas.1314345110
61. V. Gargiulo, M. Alfè, R. D. Capua, A. R. Togna, V. Cammisotto, S. Fiorito, A. Musto, A. Navarra, S. Parisi, A. Pezzella, Supplementing π-systems: eumelanin and graphene-like integration towards highly conductive materials for the mammalian cell culture bio-interface. J. Mater. Chem. B, 3, 5070, 2015. DOI= 10.1039/C5TB00343A
62. K. Sun, H. Zhang, J. Ouyang, Indium tin oxide modified with sodium compounds as cathode of inverted polymer solar cells. J. Mater. Chem., 21, 18339, 2011. DOI= 10.1039/C1JM12281A

63. Y. Xia, J. Ouyang, Significant different conductivities of the two grades of poly(3,4-ethylenedioxythiophene):Poly(styrenesulfonate), Clevios P and clevios PH1000, arising from different molecular weights. ACS Applied Materials and Interfaces, 4, 4131-4140, 2012. DOI= 10.1021/am300881m
64. Y. M. Xiao, J. Y. Lin, S. Y. Tai, S. W. Chou, G. T. Yue, J. H. Wu, Pulse electropolymerization of high performance PEDOT/MWCNT counter electrodes for Pt-free dye-sensitized solar cells. J. Mater. Chem., 22, 19919, 2012. DOI= 10.1039/c2jm34425d

3 Enhancement of electrical conductivity of Eumelanin through vacuum processes

3.1 Introduction on high vacuum annealed DHI Eumelanin

To date, eumelanin conductivity is reported in the range[1, 2] 10^{-13}-10^{-5} S/cm, largely depending on the measuring conditions, and especially on the presence of humidity in the measuring environment[3]. For valuable applications, higher conductivity values are needed yet, thus several studies explored the integration of the eumelanin with other more conductive materials[4-6], but strongly affecting its chemistry, or exploiting severe modifications of eumelanin-like materials to gain a graphene-like material, as for example by pyrolytic treatment of polydopamine under hydrogen or argon atmosphere[7, 8].

Although the mechanisms of charge transport in eumelanin are still not fully clear, several evidences are concurring to sustain its hybrid ionic-electronic behaviour[9, 10], where the electronic contribution depends on the presence, extent and the redox properties[9] of the delocalized aromatic systems, while the ionic part is largely dictated by the hydration level of the material[10] (i.e. the humidity in the measuring environment).

Basing on the concurring evidences disclosing the correlation between the chemical-physical properties of the eumelanin and the polyindole π-system stacking, as well as the packing of molecular constituents within the material[11, 12], we speculated about the modulation of the electronic conductivity[13, 14] by acting on the polyindole packing in eumelanin thin films. This is bringing us, here, for the first time in our knowledge, to report the preparation and characterization of eumelanin thin films showing the highest conductivity values of this material up to 318 S/cm. Conductive eumelanin films were prepared via the preliminary oxidative polymerization of the solid state form of the 5,6-dihydroxyindole (DHI, the ultimate monomer precursor in the formation pathways of natural and synthetic eumelanin[15]), and then by thermal annealing of the material films, at temperatures no higher than 600°C and under high vacuum conditions. We name the obtained material as High Vacuum Annealed Eumelanin, HVAE.

3.2 High vacuum annealing of DHI Eumelanin thin films: synthesis and characterization

The samples were prepared on quartz substrates (dimensions 15 mm X 6 mm X 1.2 mm), cleaned by sonication in a solution of detergent Borer Chemie AG Deconex 12PA® in deionized water (18 MΩ·cm) at 70°C for 30 min, and rinsed in acetone and then in isopropanol for 15 min each sequentially. A concentrated solution of DHI in methanol-ethyl acetate (1:1 v/v) (50 mg/mL) was prepared, filtered through a 0.2 μm Whatman membrane before deposition; on each sample, 15 μL of this solution were applied. Thin films were obtained by spin coating, using a Laurell WS-650MZ23NPP/LITE coater, with the spinning recipe acceleration 2000 rpm/s, speed 3500 rpm, duration 30 s; the samples were then dried at 90°C for 30 min in oven in air, the thicknesses of the resulting films were 230 nm ± 10 nm, measured using a stylus profilometer KLA Tencor P-10.

The eumelanin formation was obtained by the oxidation of the DHI films thanks to the Ammonia-Induced Solid State Polymerization (AISSP) method, a recently developed solid state protocol[15, 16]: each sample was exposed for 12 hours to an oxidizing atmosphere made of oxygen and ammonia vapours at controlled temperature (25°C), produced by the equilibrium of the air with an ammonia

solution (5% NH_3 in H_2O) in a sealed chamber at 1 bar pressure. The thicknesses of the resulting films were 260 nm ± 6 nm. Films showed the typical dark brown colour of the eumelanin, presenting flat surfaces (Figure 3.1, Figure 3.2, surfaces roughness images were taken using a Taylor Hobson® CCI-HD noncontact 3D Optical Profilometer with thin & thick film measurement capability; films' roughness was estimated as a Root Mean Square (RMS) value from several scans on each sample). This material is here named DHI-eumelanin, to distinguish it from the starting DHI, and from the final HVAE.

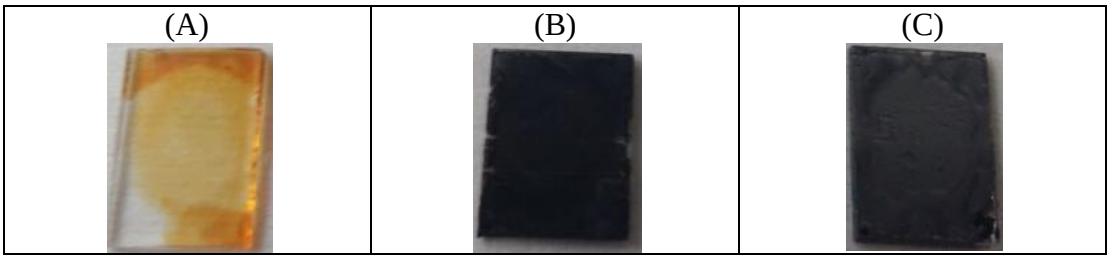

Figure 3.1. Images of some samples of the main materials prepared in this work: (A) DHI, before AISSP and no high vacuum thermal annealing; (B) DHI-eumelanin, after AISSP and before annealing; (C) High Vacuum Annealed Eumelanin (HVAE), after AISSP and after high vacuum thermal annealing (here performed at 600°C, 10^{-6} mbar, 2 h). The DHI-eumelanin film shows the typical dark brown colour of this material.

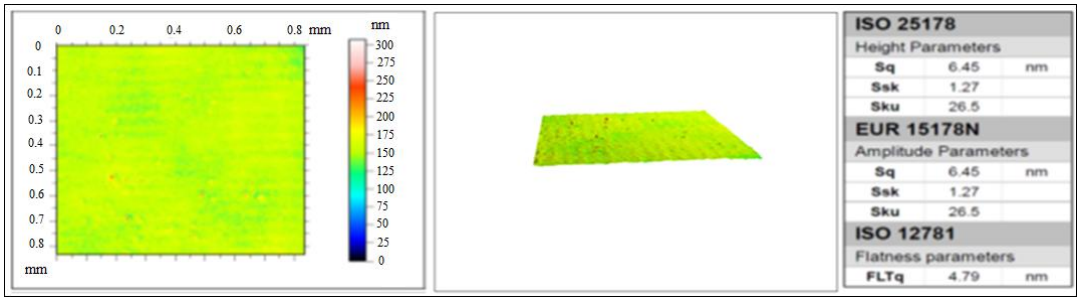

(A)

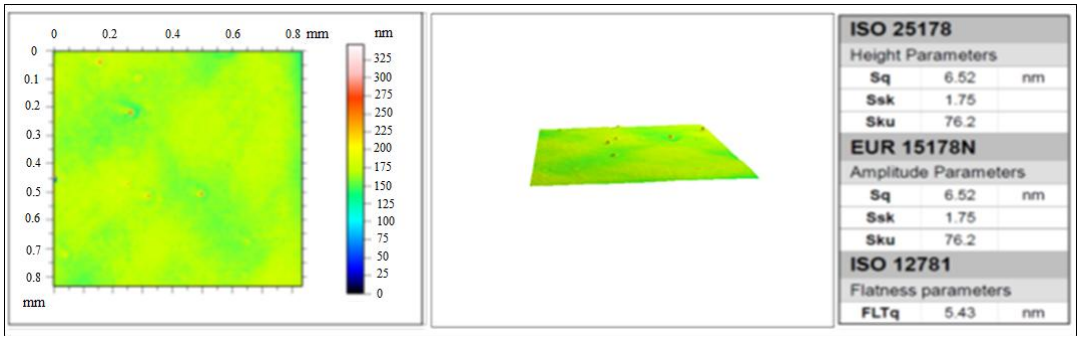

(B)

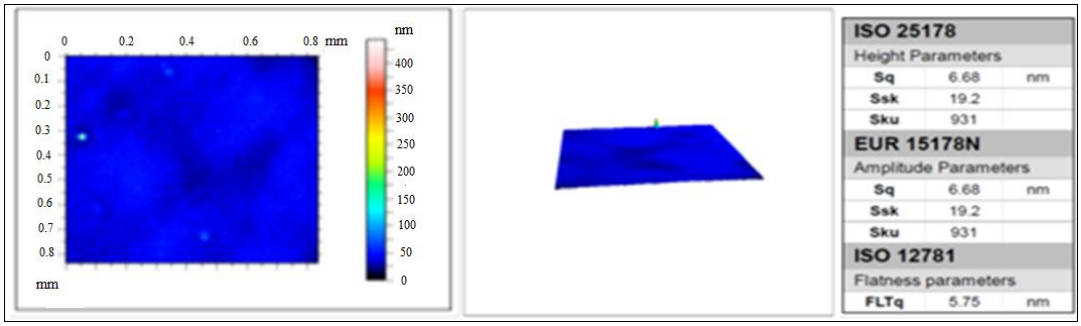

(C)

Figure 3.2. Surface profilometer characterizations of the samples of Figure 3.1: (A) DHI surface; (B) DHI-eumelanin surface; (C) HVAE surface. All the samples present low roughness values (Sq defines the roughness following the standard law ISO 25178; DHI roughness = 6.45nm; DHI Eumelanin roughness = 6.52nm; HAVE roughness = 6.58nm).

The eumelanin films were then annealed at different controlled temperatures (230°C, 300°C, 450°C and 600°C, ± 1°C for each value) in high vacuum conditions (10^{-6} mbar); some samples were annealed at various time lengths (from 30 min up to 6 hours). The processes were performed in a dedicated high vacuum chamber using a turbomolecular pump, and doing preliminary leak detection and samples temperature verifications. The mean thicknesses of the HVAE films were dependent on the annealing conditions, with the smallest value down to 110 nm ± 2 nm for the processes at 600°C for more than 1 hour (Figure 3.3).

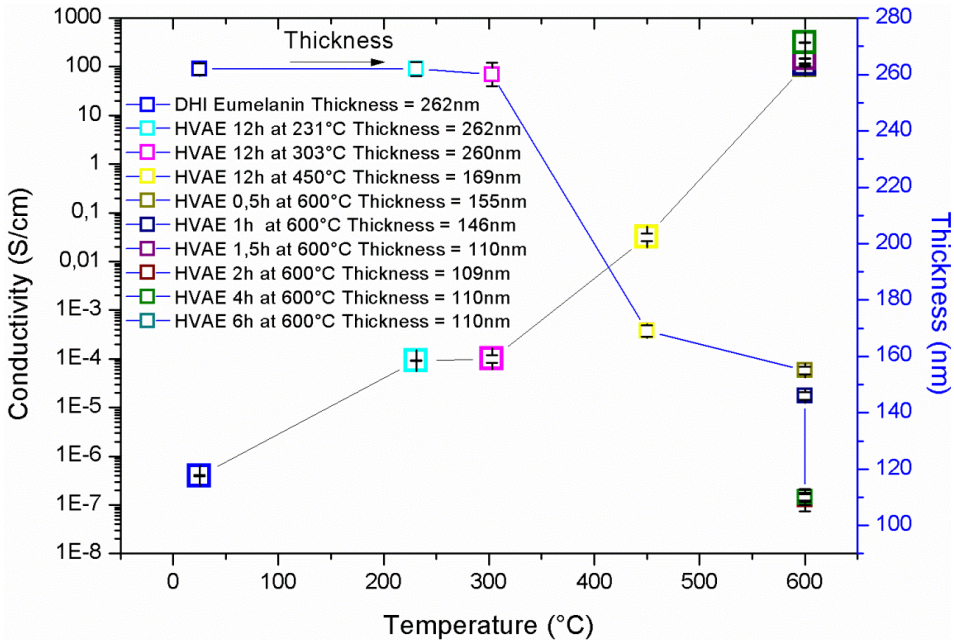

Figure 3.3. Conductivity (open squares) and Thickness (filled squares) vs. the Annealing Temperature of the HVAE films.

The chosen annealing temperatures are well below the values reported as the starting temperature for the degradation[17] and/or the carbonization processes in similar materials[18], but includes a significant part of the eumelanin mass loss region, as shown by thermogravimetric analysis (TGA) performed under not oxidizing atmosphere (Figure3.4), using a Perkin–Elmer Pyris 1 thermogravimetric analyser. Moreover, applied temperatures include the complete loss of both weakly and strongly bound water[1, 17, 19], as well as the loss of CO_2 from carboxyl groups in DHI-melanin (thermal decarboxylation)[20]. Indeed, TGA data under not oxidizing conditions indicate that mass loss is nearly completed at 800°C, suggesting that little or no modification of the molecular backbone occurs at 600°C. Instead, a complete different picture is obtained in presence of oxygen, which critically affects the stability of the material (Figure 3.4).

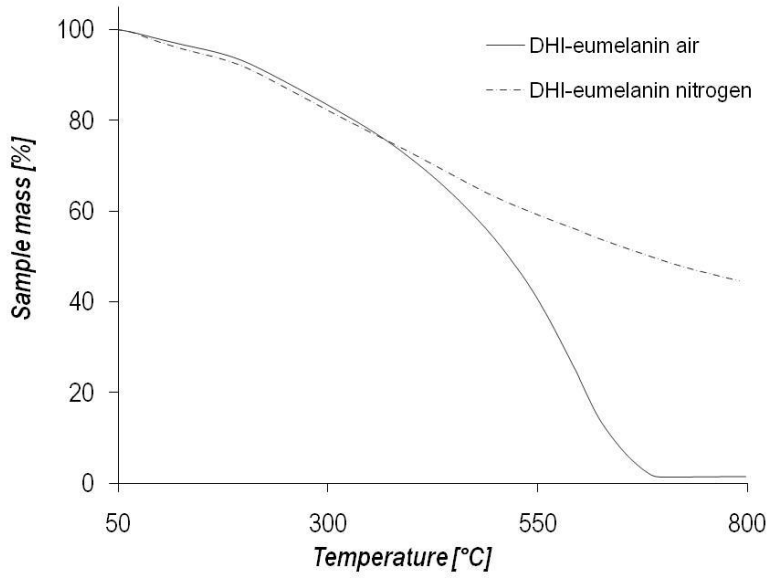

(A)

(B)

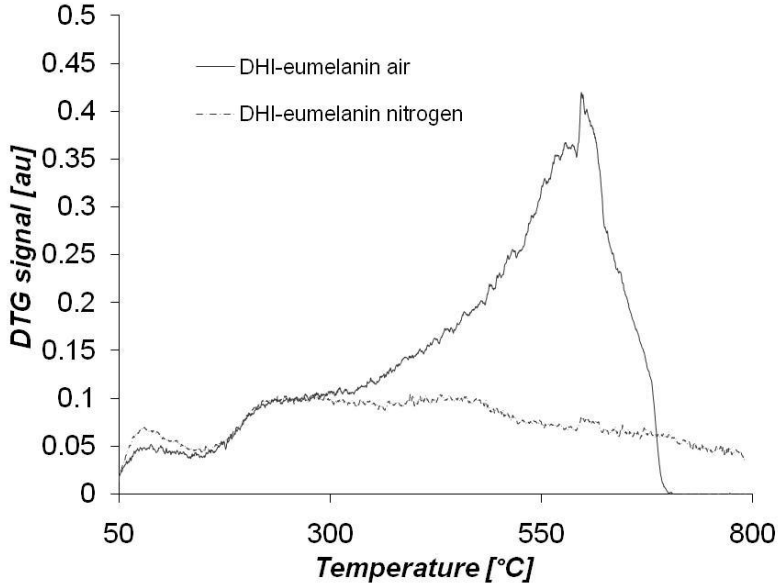

Figure 3.4. (A) Mass loss vs. Temperature, and (B) TGA plots for DHI-eumelanin films in air and in nitrogen. An inert environment preserves the material from a complete degradation.

Morphology and surface analysis of the materials at the different stages of the process revealed a nearly unmodified roughness, passing from the starting DHI films to the HVAE films (Figure 3.2), while, as said, the thicknesses suffered a significant decrease in function of the annealing temperature (Figure3.3). This was expected because of the known tendency of the eumelanin to loss labile carboxylic groups[15, 17, 20] and on the possible loss of low molecular weight components embedded in the material layers.

Scanning electronic microscopy (SEM) inspection (using a SEM Zeiss Leo 1530 Gemini) confirmed the retaining of the high quality morphology in the HVAE films (Figure 3.5), showing an uniform surface of this material. Data from the microanalysis inspection are coherent with the polyindolic nature of the HVAE.

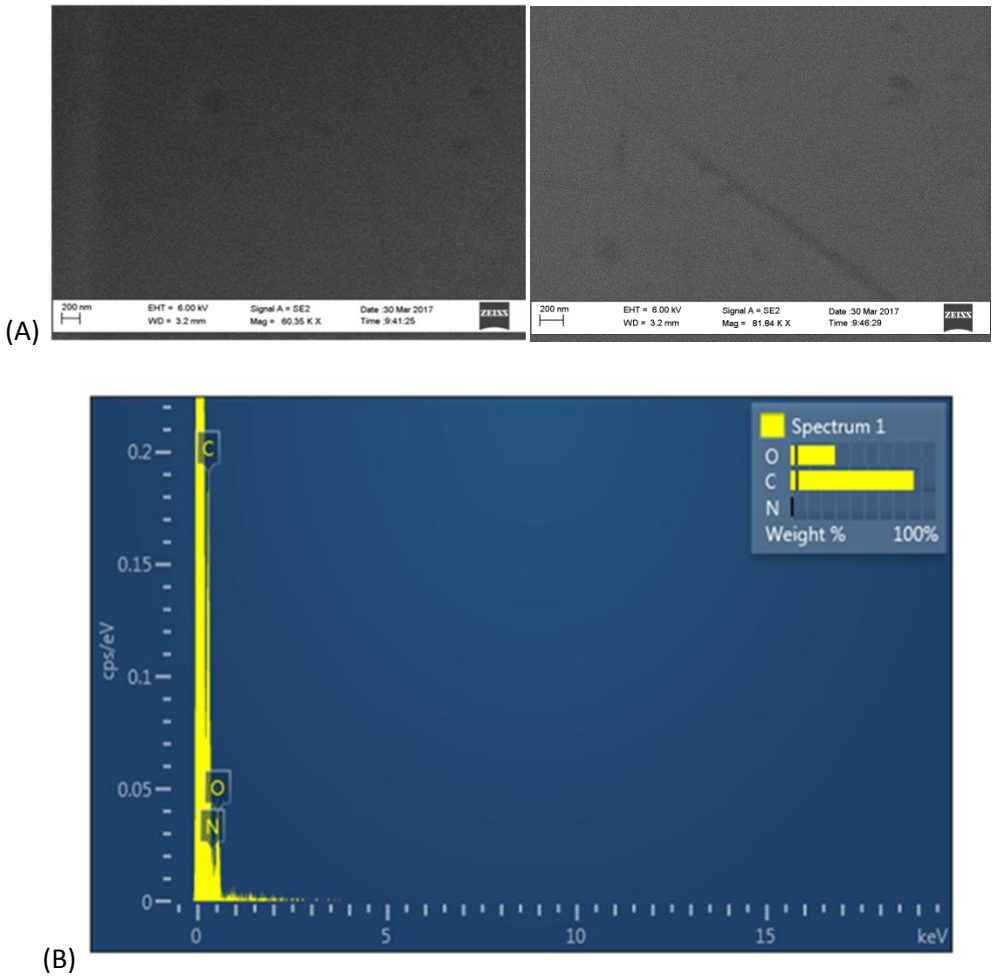

Figure 3.5. (A) SEM images (two different section of the same sample; the scratch was made to measure the thickness of the film) and (B) microanalysis of the HVAE treated at 600°C, 10^{-6} mbar, 2 h. All the materials' films showed an uniform surface, while microanalysis indicated that HVAE had still a polyindolic nature.

UV-Vis inspection was carried out using a Perkin-Elmer Lambda 900 spectrophotometer. Samples were observed at the different process steps (Figure 3.6) to record the spectra. It can be seen an evident increase in the absorption coefficients in nearly the entire UV-Vis range, passing from the DHI to the DHI-eumelanin and to the HVAE. This phenomenon is associated to the increase of both the delocalization of the aromatic systems and their π-stacking interactions[11, 12], that suggest the actual increase of the extension and of the filling factor[12, 19] for the delocalized aromatic systems of the material backbone, in particular happening after the thermal annealing in vacuum, i.e. this reorganization results in an overlap of the π-electronic density of the adjacent packed chains and the delocalization of their electronic wave-functions[21].

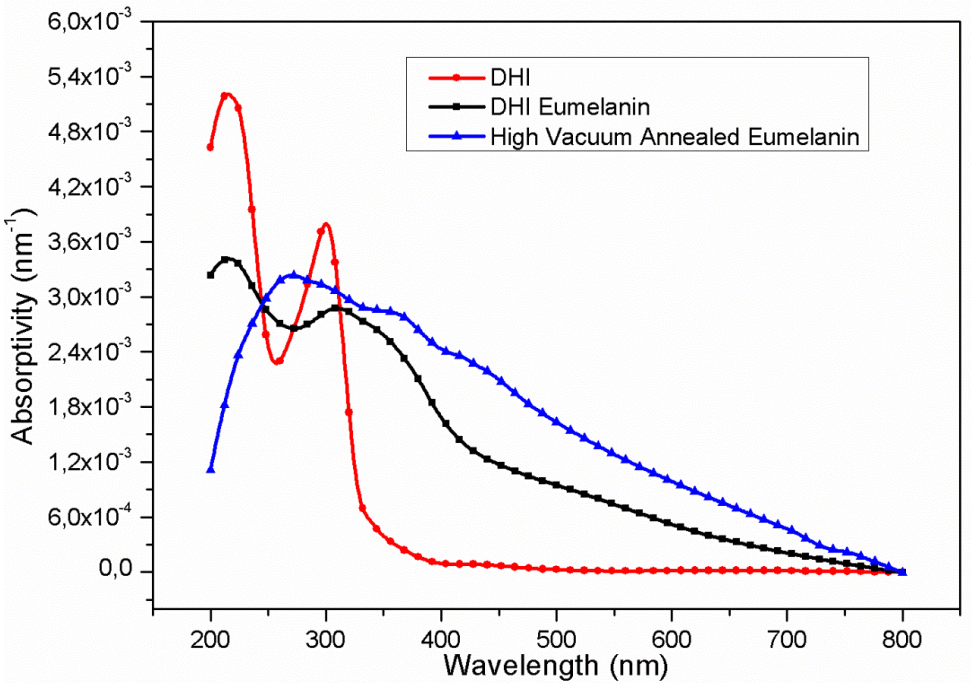

Figure 3.6. UV-Vis absorptivity (percent absorbance / film thickness) of the films at the different process stages: (red, circles) DHI thin film; (black, squares) eumelanin film after AISSP; (blue, triangles) HVAE film after thermal annealing in vacuum (600°C; 2 h; 10^{-6} mbar).

Strong supports to the picture of a structural reorganization and an enhanced packing order[22-24] of the molecular constituents within the eumelanin films (made possible by the concomitant loss of labile and low molecular weight components[20] and the clustering of the longer polyindole chains (a graphic representation of these mechanisms is shown in Figure 3.7)), were further given by the retaining, in the annealed films, of the typical eumelanin signature observed in the electron paramagnetic resonance (EPR) spectrum[1, 15] (measured using an X-band (9 GHz)

Bruker Elexys E-500 spectrometer, equipped with a superhigh sensitivity probe head), in the FTIR analysis[25] (using a Thermo Fischer Scientific Nicolet 6700 FTIR to determine the attenuated total reflectance (ATR) spectra of the samples, with a resolution of 4 cm^{-1} and 16 scans averaged for each spectrum in a range between 4000 – 650 cm^{-1}), in the Raman spectroscopy[17, 26] (Renishaw inVia 2 Raman microscope (532 nm), which uses a microscope to focus a laser source onto specific areas of a sample, then the light scattered off the surface of the sample is collected and directed to a Raman spectrometer), and in the MALDI-MS[16] analysis (positive reflectron MALDI and LDI spectra were recorded on a Sciex 4800 MALDI ToF/ToF instrument) (Figures 3.8 to 3.11).

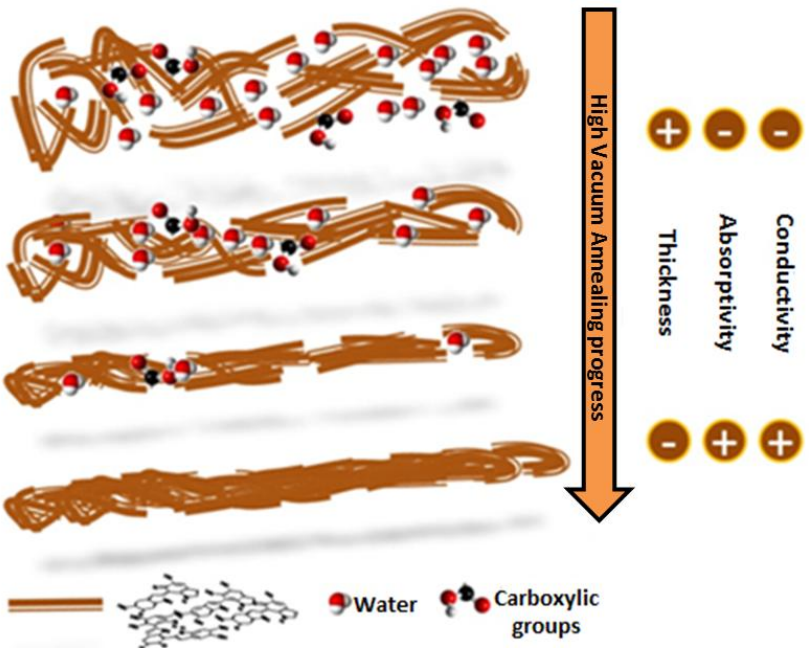

Figure 3.7. Pictorial model of the polyindole packing evolution during high vacuum annealing. Water molecules and carboxylic groups are evidenced, to show their reduction in the material as the process temperature increases.

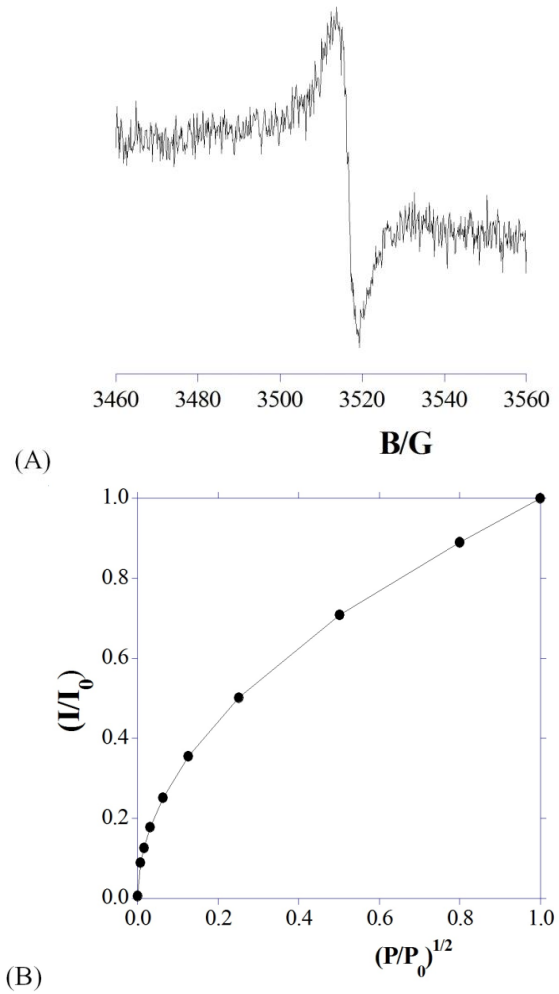

Figure 3.8. (A) EPR spectrum and (B) power saturation profile of HVAE (600°C, 10^{-6} mbar, 2 h). Data were recorded on thoroughly desiccated samples. Measurement conditions: T = 25.8°C, microbridge power = 0.6 mW.

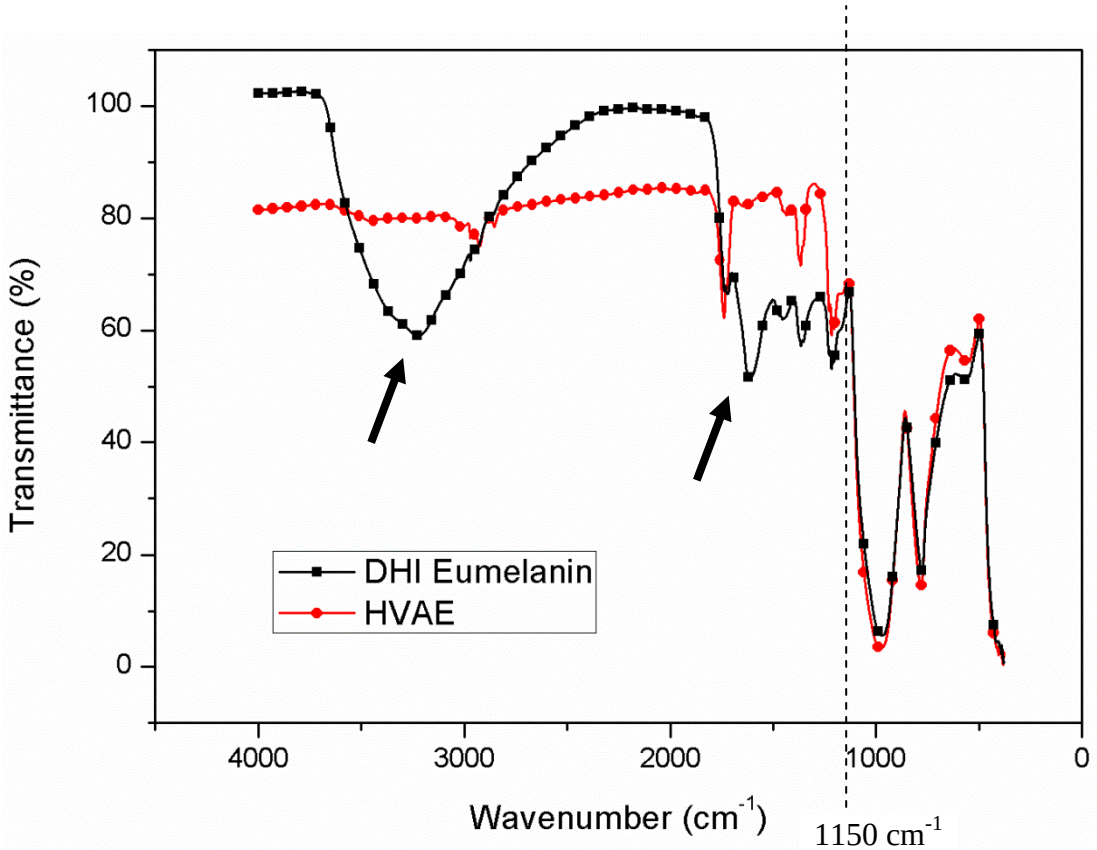

Figure 3.9. FTIR spectra of DHI Eumelanin (black, squares) and of HVAE (red, circles). Arrows denote signals associated to water (3200 cm^{-1}), hydrogen bonds and carboxyl groups (1620 cm^{-1}). The region with wavenumber smaller than 1150 cm^{-1} (the dotted line) is dominated by the quartz substrate signal.

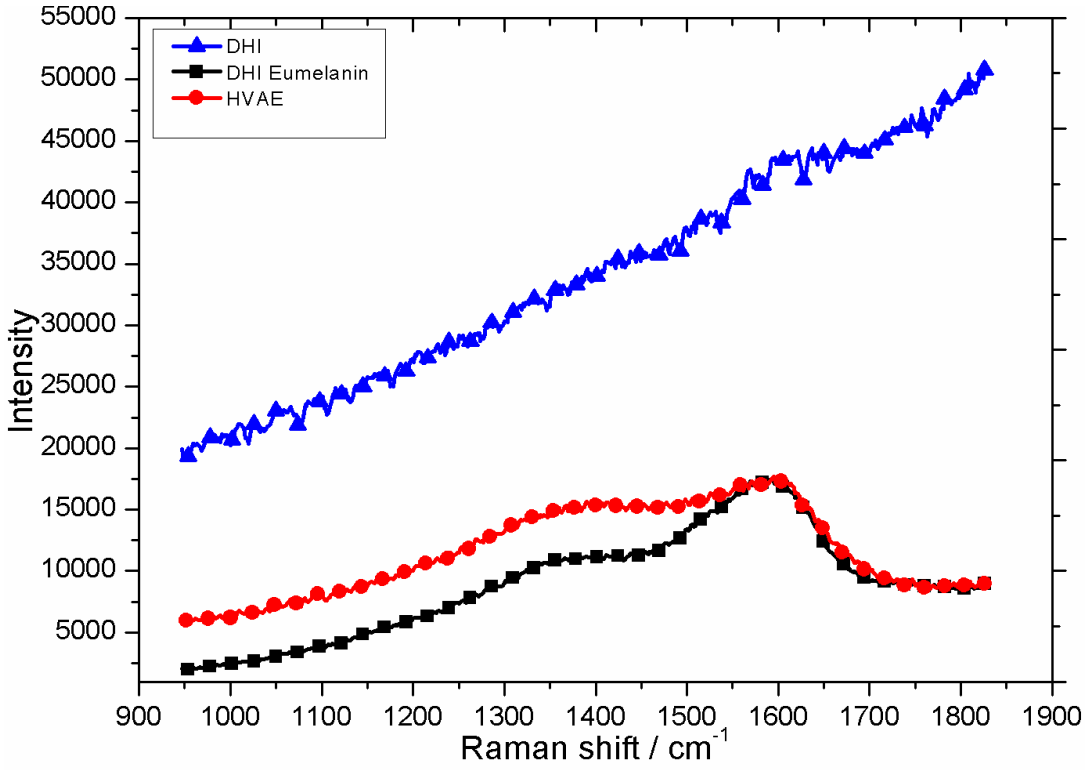

Figure 3.10. Comparison of Raman spectra of films of pristine DHI-eumelanin (black, squares), HVAE (600°C, 10^{-6} mbar, 2 h) (red, circles), and DHI as is before oxidative polymerization (blue, triangles).

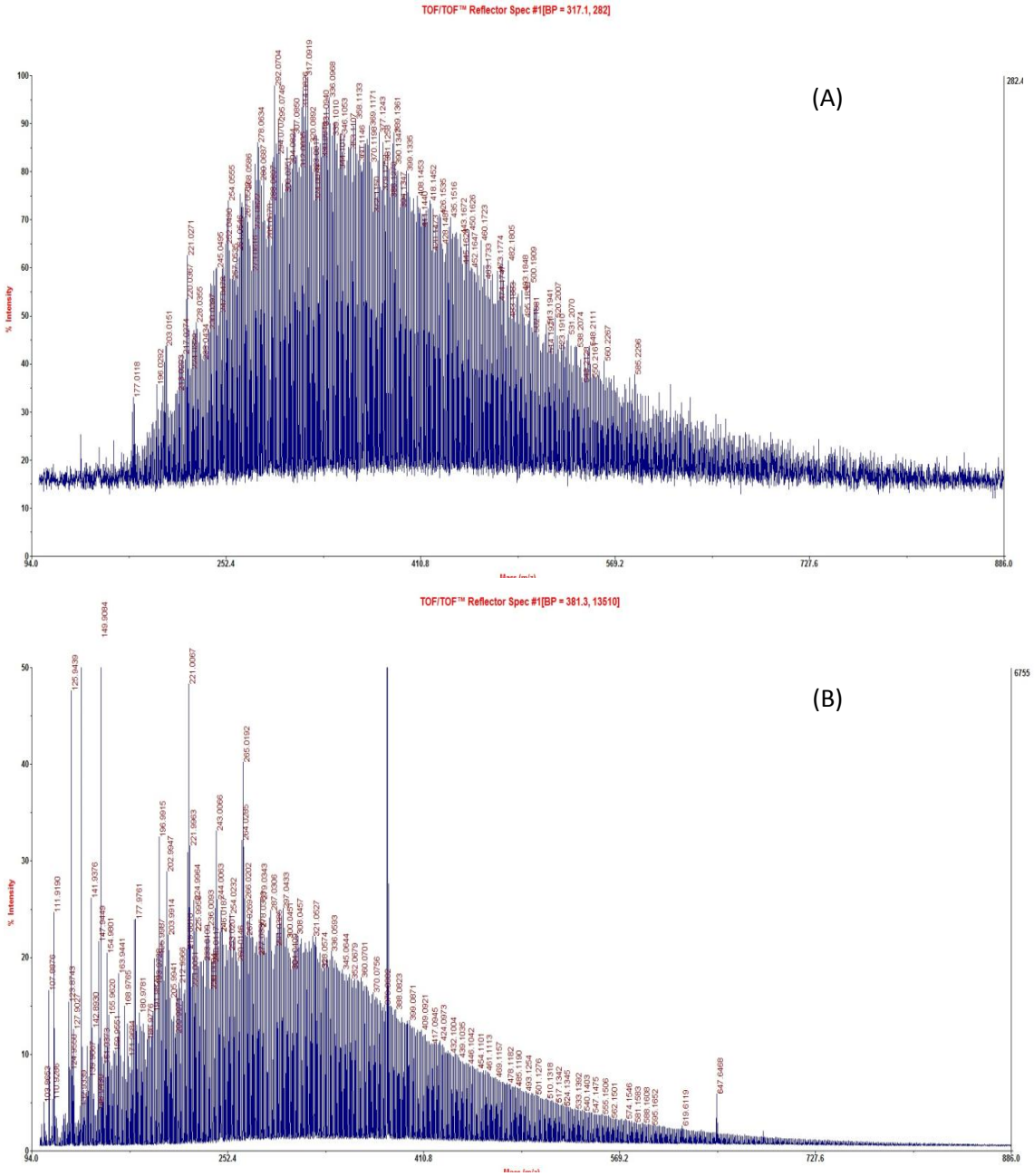

Figure 3.11. MALDI-MS spectra of DHI-eumelanin, (A) before and (B) after high vacuum annealing. The recurring profile of masses of general formula *DHI oligomer* $+ rnO_2 - nCO_2$ are recognizable in both spectra for low molecular weights[27].

Without entering into the details of the Raman spectra (Figure 3.10), it is worth to note here how the comparison of the profiles before and after the annealing reveals, in agreement with the loss of carboxylic groups and possible pyrrolic acids, a relative reduction of the G band (the range of 1600 cm^{-1}) following the reduction of O and N contribution.

Consistent information is provided by the FTIR spectra of eumelanin and HVAE films (Figure 3.9) too, highlighting in particular the drastic decrease of signals associated to C=O stretching (1620 cm^{-1}) and to the water (3200 cm^{-1})[25].

Finally, direct support to the packing evolution hypothesis comes from 2D GIWAXS patterns, as the anisotropic intensity distribution along the diffraction rings in Figure 3.12 indicates an increased orientation degree after the vacuum thermal treatment is operated. In particular, the HVAE film (Figure 3.12A) features a diffraction intensity definitely concentrated along the Q_z axis, i.e. perpendicular to the sample surface, denoting a preferred orientation of the diffracting planes parallel to the film surface. On the other hand the Eumelanin film (Figure 3.12B) features a weak diffraction intensity evenly distributed along the azimuth of a broad diffraction ring, indicating low crystallinity and random orientation of the molecules. The 1D radial cuts extracted from the GIWAXS maps along the out of plane (Figure 3.12C) and in plane (Figure 3.12D) directions show indeed a clear difference between the two directions in the case of the HVAE film, with a peak asymmetry in the out of plane direction revealing a diffraction contribution of the

oriented molecules appearing as a shoulder at q = 1.85 Å of the main peak at q = 1.56 Å ascribed to the substrate which gives in turn the only scattering contribution in the in plane cut. On the contrary, no difference between the two directions is recognized in the case of the Eumelanin film (so that a 5.5 additional scale factor has been applied in Figure 3.12C for the sake of clarity in the comparison).

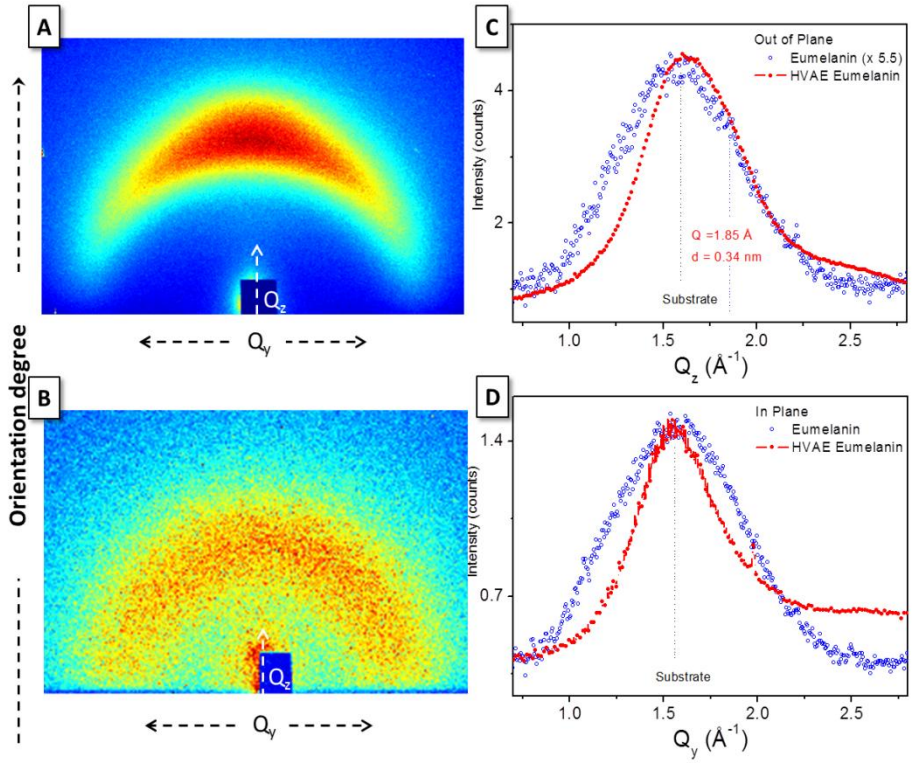

Figure 3.12. GIWAXS 2D patterns of HVAE films processed at (A) 600°C (2h treatment) and (B) eumelanin thin films; 1D out of plane (C) and in plane (D) radial cuts from the 2D maps in A,B.

The electrical properties of the various materials was measured using a four probes system[28] Napson RESISTAGE RG-80 and a power supply source meter Keithley 2410 for the different ranges of conductivity, working in air at room temperature. The samples conductivity vs. the annealing temperature and vs. the duration of the processes are shown in Figure 3.13. After the vacuum annealing, the conductivity of the eumelanin films featured a remarkable increase, up to over 9 orders of magnitude, passing from around 10^{-7} S/cm for the DHI and DHI-eumelanin films, up to an unprecedented value of 318 S/cm for the material processed at 600°C for 2 hours, and anyway obtaining values larger than 10^{2} S/cm for all the samples processed at 600°C (Figure 3.13 inset).

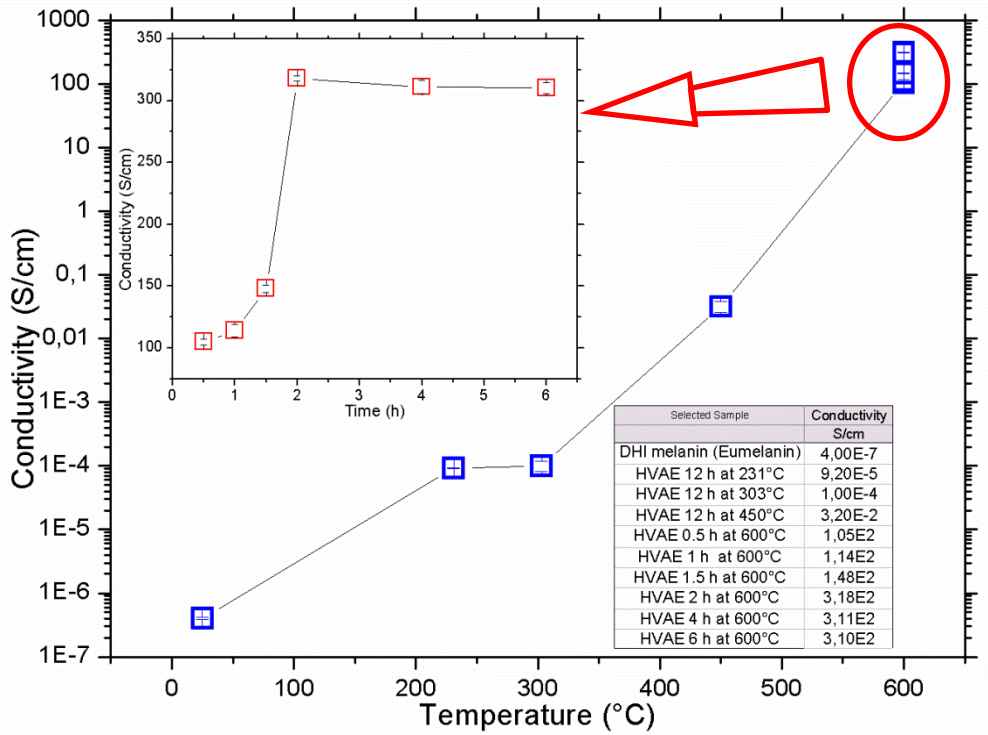

Figure 3.13. Conductivity of vacuum annealed eumelanin thin films, vs. the annealing temperature and (inset) vs. the annealing time at 600°C temperature. Data are listed in the table. All the measurements were performed in air at room temperature. Errors of each point are indicated inside the plots symbols.

This record result is not a humidity response effect, as the data acquisitions were performed in few tens of seconds for each sample, with no variation of the ambient relative humidity, so suggesting that actual nature of the involved charge carriers is electronic.

Current-voltage measurements performed before and after the exposition of the films to water or acidic conditions conclusively ruled out any conductivity increase with the water content of the film.

Immersion of the films in deionised water results in a marked decrease of the conductivity, also associated to a deterioration of the surface smoothness (Figure 3.14 and Table 3.1).

(A)

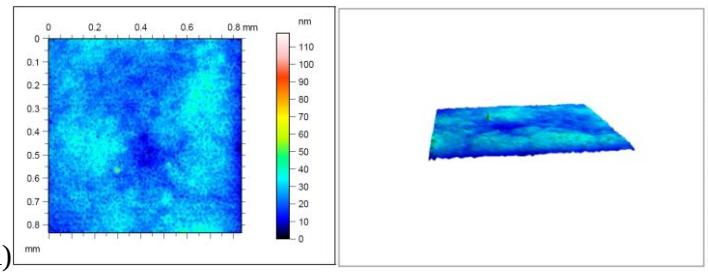

ISO 25178		
Height Parameters		
Sq	5.68	nm
Ssk	-0.0187	
Sku	5.37	
EUR 15178N		
Amplitude Parameters		
Sq	5.68	nm
Ssk	-0.0187	
Sku	5.37	
ISO 12781		
Flatness parameters		
FLTq	4.84	nm

(B)

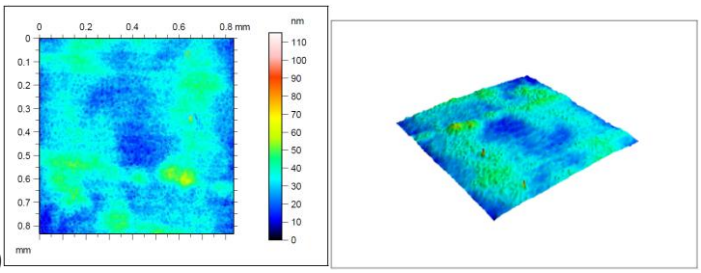

ISO 25178		
Height Parameters		
Sq	7.25	nm
Ssk	0.181	
Sku	3.95	
EUR 15178N		
Amplitude Parameters		
Sq	7.25	nm
Ssk	0.181	
Sku	3.95	
ISO 12781		
Flatness parameters		
FLTq	6.64	nm

Figure 3.14. Optical profilometer surface analysis of HVAE: (A) before and (B) after 2 h immersion in deionized water (18 MΩ*cm) at room temperature. All the roughness values increase after the immersion.

HVAE (600°C, 2 h)	Before 2 h water immersion	After 2 h DI water immersion	After three weeks at standard humidity and temperature conditions	After climatic chamber treatment: *RH* = 85% *T* = 65°C time = 90 h	After annealing on hot plate: in air *T* = 115°C time = 5 h
Thickness (nm)	96.8	96.8	105.4	109.2	103.7
Sheet resistance (Ω/□)	415	540	1670	1850	1441
Normalized Conductivity (%)	100	76.4	22.80	19.80	26.80

Table 3.1. Thickness, Sheet Resistance and Normalized Conductivity values of one of the HVAE samples (600°C, 2 hours annealing), measured before and after water immersion and after different treatment conditions. Errors are in the limit of 2% for each datum.

Reduction of the conductivity is even more pronounced when films are exposed to acidic solutions[15] (Figure 3.15 and Table 3.2).

(A)

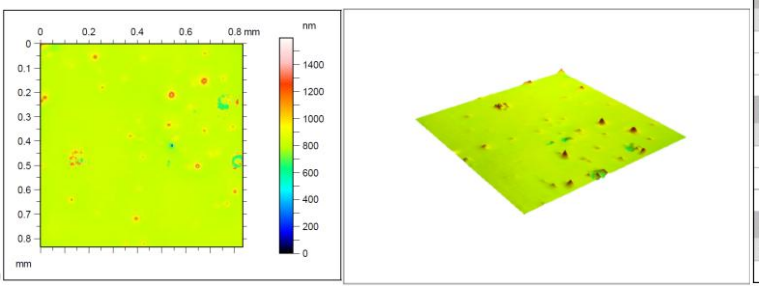

ISO 25178		
Height Parameters		
Sq	37.2	nm
Ssk	6.33	
Sku	93.1	
EUR 15178N		
Amplitude Parameters		
Sq	37.2	nm
Ssk	6.33	
Sku	93.1	
ISO 12781		
Flatness parameters		
FLTq	30.0	nm

(B)

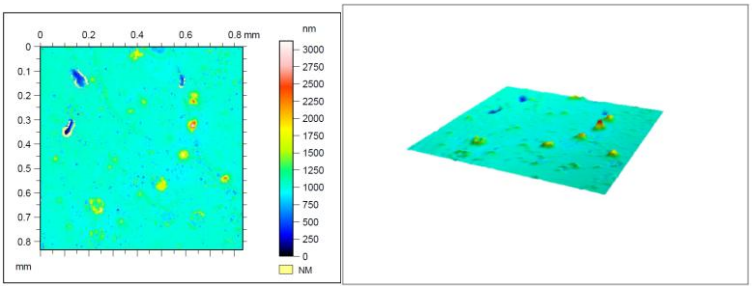

ISO 25178		
Height Parameters		
Sq	121	nm
Ssk	3.51	
Sku	43.8	
EUR 15178N		
Amplitude Parameters		
Sq	121	nm
Ssk	3.51	
Sku	43.8	
ISO 12781		
Flatness parameters		
FLTq	101	nm

Figure 3.15. Optical profilometer surface analysis of HVAE: (A) before and (B) after immersion in a sulfuric acid solution (96 w/w%) for 2 hours at room temperature.

HVAE (600°C, 2 h)	Before H_2SO_4 treatment for 2 h	After H_2SO_4 (96 w/w% in DI water) treatment for 2 h
Thickness (nm)	120	161
Sheet resistance (Ω/□)	342	404
Normalized Conductivity (%)	100	63.1

Table 3.2. Thickness, Sheet Resistance and Normalized Conductivity values of one of the HVAE samples (600°C, 2 hours annealing), measured before and after sulfuric acid treatment. Errors are in the limit of 2% for each datum.

Notably, the films appear moderately stable under accelerated ageing (Table 3.3), but stability is lost if the film were previously immersed in water (Table 3.1).

HVAE (600°C, 6 h)	After preparation process	After three weeks at standard humidity and temperature conditions	After climatic chamber treatment: *RH* = 85% *T* = 65°C time = 90 h	After annealing on hot plate: in air *T* = 115°C time = 5 h
Thickness (nm)	95.5	115.7	121.2	118.1
Sheet resistance (Ω/□)	340	440	528	527
Normalized Conductivity (%)	100	62.07	49.67	51.93

Table 3.3. Thickness, Sheet Resistance and Normalized Conductivity values of one of the HVAE samples (600°C, 6 hours annealing), measured immediately after the preparation process and after different treatments or storage conditions. Errors are in the limit of 2% for each datum.

HVAE (600°C, 2 h)	Before 2 h water immersion	After 2 h DI water immersion	After three weeks at standard humidity and temperature conditions	After climatic chamber treatment: *RH* = 85% *T* = 65°C time = 90 h	After annealing on hot plate: in air *T* = 115°C time = 5 h
Thickness (nm)	96.8	96.8	105.4	109.2	103.7
Sheet resistance (Ω/□)	415	540	1670	1850	1441
Normalized Conductivity (%)	100	76.4	22.80	19.80	26.80

Table 3.4. Thickness, Sheet Resistance and Normalized Conductivity values of one of the HVAE samples (600°C, 2 hours annealing), measured before and after water immersion and after different treatment conditions. Errors are in the limit of 2% for each datum.

In light of known literature[10, 29], this behaviour clearly suggests that contribution of the ionic effects in the charge transport can be considered negligible in HVAE. Moreover, the drastic effects induced by the exposition to soaking[30] water or acidic solutions witness the key role of packing of the aromatic polyindole systems in determining electrical properties of the films[13, 14, 31].

The here observed increases in the conductivity cannot be ascribed to the formation of films akin to dense carbon black materials[32, 33], because the processes producing these materials operate at much higher temperature (1000°C or more) when applied to eumelanin-like materials[7, 8], or anyway using temperatures above 600°C to

obtain good conductivity values when applied to polypeptides rich in eumelanin precursors (phenylalanine)[34]. Instead, in this study we observed a conductivity increase from 3 to 5 order of magnitude even after annealing in the 200°C-450°C range. This strongly suggests that conductivity rise has not to be ascribed to carbonization processes. Indeed, elemental analysis data (Table 3.5) do confirm the material does not present C/X ratios expectable for carbon black materials[34].

Sample	%C	%H	%N	%O	C/O	C/N	N/O	(C+N)/O
DHI	63.81	4.01	8.14	24.02	3.54	9.14	0.38	2.28
Eumelanin	50.53	2.28	5.87	41.3	1.63	10.02	0.16	1.04
HVAE (231°C, 12 h)	59.65	2.01	7.12	31.22	2.54	9.77	0.26	1.63
HVAE (600°C, 6 h)	57.34	2.98	9.13	30.55	2.50	7.32	0.34	1.67

Table 3.5. Elemental analysis, estimated by a Perkin–Elmer 2400 CHNSO elemental analyzer, of the various samples prepared . Elemental composition wt% (average of duplicate measures) and element ratios of: DHI, DHI-eumelanin as prepared, and HVAE samples. Errors are in the limit of 2% for each datum. It is worth of note how the relative oxygen content increases after the DHI oxidative polymerization and decreases with thermal treatment. The relative ratios of the elements may be interpreted as a consequence of the loss of water and CO_2. The values obtained after the more extensive treatment does not match the ones of ordinary carbon black materials[35].

Measurements of electrical resistance vs. temperature were also performed (Figure 3.16), using two terminals devices.

Nonetheless, at fixed temperature the conductivity appears pretty stable with time (Figure 3.16), allowing the material to sustain a constant current with a very low increase in the applied voltage along the time, as it can be expected for electronic conductive organics[36].

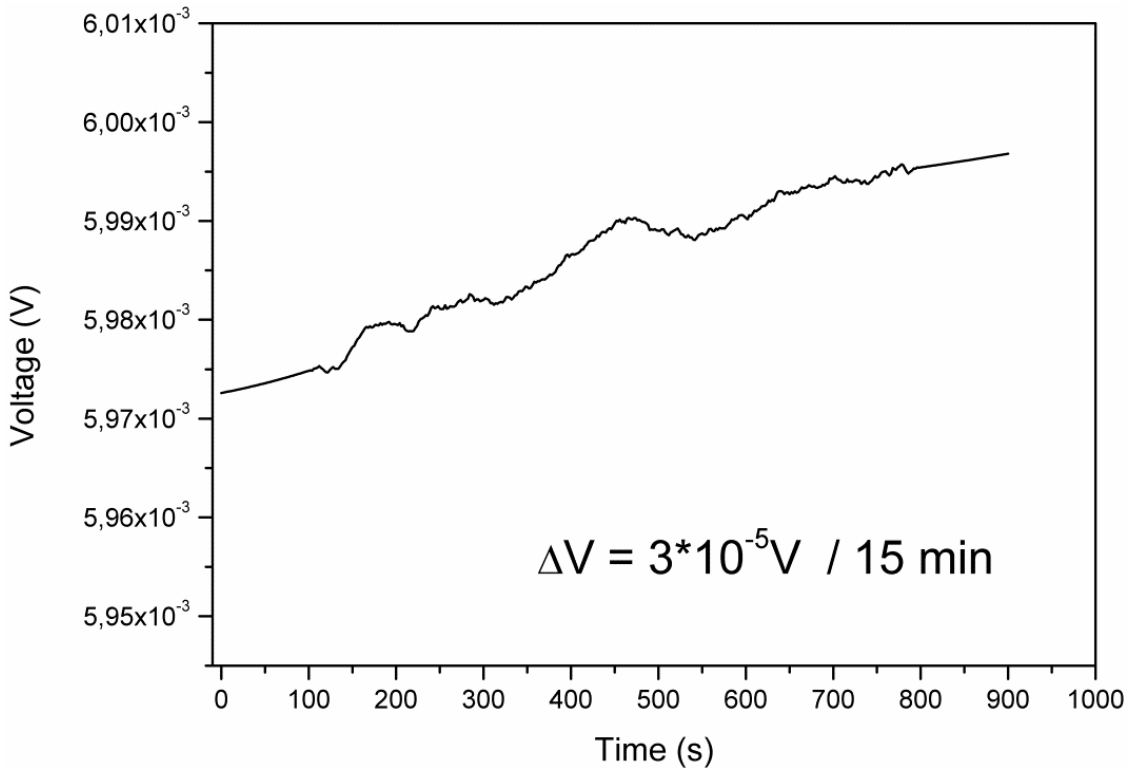

Figure 3.16. Voltage vs. Time in HVAE layers (annealing conditions: 600°C, 2 h, 10^{-6} mbar). This plot shows the trend of the voltage required to sustain a fixed current (100 μA) in a HVAE thin film (thickness = 109 nm), using two probes with 1 mm spacing, measured at room temperature in air.

Results here reported indicate a radical modification of the actual picture of the eumelanin charge transport properties, reversing the paradigm according to which eumelanin conductivity increases with the water content of the material. Indeed, if the eumelanin films are rearranged into conductive layers, thanks to a simple thermal annealing in vacuum which succeeds in inducing a structural reorganization of their molecular constituents and the removal of low molecular weight components embedded in the pigment layer. A potential aspect behind the conductivity increases can also be chemical changes to the eumelanin in the form of further condensation of the eumelanin heterocyclic components with each other. The contribution of the electronic current is here demonstrated to be largely preeminent with respect to the ionic one, allowing to obtain unprecedented high conductivity values, up to 318 S/cm in this work, and the mammalian pigment can be considered as an actual conductor.

The conductivity values achieved and their fine tuning allowed by the control of the process conditions, open to possible tailoring of ad-hoc eumelanin-based active layers for a wide range of applications in organic electronics and bioelectronics, deserving further extensive investigations to get a conclusive picture about the conductor vs. semiconductor behaviour of the eumelanin and insights about the mobility of charge carriers.

3.3 References

1. P. Meredith, T. Sarna, The physical and chemical properties of eumelanin. Pigm. Cell Res. 19, 572-594, 2006. DOI= 10.1111/j.1600-0749.2006.00345.x

2. W. Osak, K. Tkacz, H. Czternastek, J. SłAwiński, I – V characteristics and electrical conductivity of synthetic melanin. Biopolymers 28, 1885-1890, 1989. DOI= 10.1002/bip.360281105

3. M. M. Jastrzebska, H. Isotalo, J. Paloheimo, H. Stubb, Electrical conductivity of synthetic DOPA-melanin polymer for different hydration states and temperatures. J. Biomater. Sci., Polym. Ed. 7, 577-586, 1995. DOI= 10.1163/156856295X00490

4. I. Mihai, F. Addiégo, D. Del Frari, J. Bour, V. Ball, Associating oriented polyaniline and eumelanin in a reactive layer-by-layer manner: Composites with high electrical conductivity. Colloids Surf., A 434, 118-125, 2013. DOI= 10.1016/j.colsurfa.2013.05.028

5. V. Gargiulo, M. Alfè, R. Di Capua, A. R. Togna, V. Cammisotto, S. Fiorito, A. Musto, A. Navarra, S. Parisi, A. Pezzella, Supplementing π-systems: eumelanin and graphene-like integration towards highly conductive materials for the mammalian cell culture bio-interface. J. Mater. Chem. B 3, 5070-5079, 2015. DOI= 10.1039/C5TB00343A

6. L. Migliaccio, S. Aprano, L. Iannuzzi, M. G. Maglione, P. Tassini, C. Minarini, P. Manini, and A. Pezzella, Eumelanin-PEDOT:PSS Complementing En Route to Mammalian-Pigment-Based Electrodes: Design and Fabrication of an ITO-Free Organic Light-Emitting Device. Adv. Electron. Mater., 2017. DOI= 10.1002/aelm.201600342

7. R. Li, K. Parvez, F. Hinkel, X. Feng, K. Müllen, Bioinspired wafer-scale production of highly stretchable carbon films for transparent conductive electrodes. Angew. Chem., Int. Ed. 52, 5535-5538, 2013. DOI= 10.1002/anie.201300312

8. J. Kong, W. A. Yee, L. Yang, Y. Wei, S. L. Phua, H. G. Ong, J. M. Ang, X. Lic, X. Lu, Highly electrically conductive layered carbon derived from polydopamine and its functions in SnO2-based lithium ion battery anodes. Chem. Commun. 48, 10316-10318, 2012. DOI: 10.1039/C2CC35284B

9. A. B. Mostert, B. J. Powell, F. L. Pratt, G. R. Hanson, T. Sarna, I. R. Gentle, P. Meredith, Role of semiconductivity and ion transport in the electrical conduction of melanin. Proc. Natl. Acad. Sci. U. S. A. 109, 8943-8947, 2012. DOI: 10.1073/pnas.1119948109

10. J. Wünsche, Y. Deng, P. Kumar, E. Di Mauro, E. Josberger, J. Sayago, A. Pezzella, F. Soavi, F. Cicoira, M. Rolandi, C. Santato, Protonic and electronic transport in hydrated

thin films of the pigment eumelanin. Chem. Mater. 27, 436-442, 2015. DOI: 10.1021/cm502939r

11. A. Pezzella, A. Iadonisi, S. Valerio, L. Panzella, A. Napolitano, M. Adinolfi, M. d'Ischia, Disentangling Eumelanin "black chromophore": Visible absorption changes as signatures of oxidation state- and aggregation-dependent dynamic interactions in a model water-soluble 5,6-dihydroxyindole polymer. J. Am. Chem. Soc. 131, 15270-15275, 2009. DOI= 10.1021/ja905162s

12. C. Bonavolontà, C. de Lisio, M. d'Ischia, P. Maddalena, P. Manini, A. Pezzella, M. Valentino, Anomalous evolution of broadband optical absorption reveals dynamic solid state reorganization during eumelanin build-up in thin films. Sci. Rep. 7, 2017. DOI= 10.1038/s41598-017-00597-8

13. R. Noriega, J. Rivnay, K. Vandewal, F.P. Koch, N. Stingelin, P. Smith, M.F. Toney, A. Salleo, A general relationship between disorder, aggregation and charge transport in conjugated polymers. Nat. Mater. 12, 1038-1044, 2013. DOI: 10.1038/nmat3722.

14. C. Liu, K. Huang, W.T. Park, M. Li, T. Yang, X. Liu, L. Liang, T. Minaric, Y.Y. Noh, A unified understanding of charge transport in organic semiconductors: the importance of attenuated delocalization for the carriers. Mater. Horiz., 2017. DOI= 10.1039/C7MH00091J

15. M. d'Ischia, K. Wakamatsu, A. Napolitano, S. Briganti, J.C. Garcia-Borron, D. Kovacs, P. Meredith, A. Pezzella, M. Picardo, T. Sarna, J.D. Simon, S. Ito, Melanins and melanogenesis: Methods, standards, protocols. Pigm. Cell Melanoma Res. 26, 616-633, 2013. DOI= 10.1111/pcmr.12121

16. A. Pezzella, M. Barra, A. Musto, A. Navarra, M. Alfè, P. Manini, S. Parisi, A. Cassinese, V. Criscuolo, M. d'Ischia, Stem cell-compatible eumelanin biointerface fabricated by chemically controlled solid state polymerization. Mater. Horiz. 2, 212-220, 2015. DOI= 10.1039/C4MH00097H

17. L.G.S. Albano, E. Di Mauro, P. Kumar, F. Cicoira, C.F.O. Graeff, C. Santato, Novel insights on the physicochemical properties of eumelanins and their DMSO derivatives. Polym. Int. 65, 1315-1322, 2016. DOI= 10.1002/pi.5167

18. X. Yu, , H. Fan, Y. Liu, Z. Shi, Z. Jin, Characterization of carbonized polydopamine nanoparticles suggests ordered supramolecular structure of polydopamine. Langmuir 30, 5497-5505, 2014. DOI= 10.1021/la500225v

19. G. Albanese M. G. Bridelli A. Deriu, Structural dynamics of melanin investigated by Rayleigh scattering of Mössbauer radiation. Biopolymers 23, 1481-1498, 1984. DOI= 10.1002/bip.360230805

20. G. A. Swan, A. Waggott, Studies related to the chemistry of melanins. Part X. Quantitative assessment of different types of units present in dopa-melanin. J. Chem. Soc. C: Organic, 1409-1418, 1970. DOI= 10.1039/J39700001409

21. G. Koller, S. Berkebile, M. Oehzelt, P. Puschnig, C. Ambrosch-Draxl, F.P. Netzer, M.G. Ramsey, Intra- and intermodular band dispersion in an organic crystal. Science 317, 351-355, 2007. DOI 10.1126/science.1143239

22. C. Liu, K. Wang, X. Gong, A. J. Heeger, Low bandgap semiconducting polymers for polymeric photovoltaics. Chem. Soc. Rev. 45, 4825-4846, 2016. DOI= 10.1039/C5CS00650C

23. J. Roncali, C. Thobie-Gautier, An efficient strategy towards small bandgap polymers: The rigidification of the π-conjugated system. Adv. Mater. 6, 846-848, 1994. DOI= 10.1002/adma.19940061108

24. J. Roncali, Synthetic principles for bandgap control in linear π-conjugated systems. Chem. Rev. 97, 173-205, 1997. DOI= 10.1021/cr950257t

25. R. Hyogo, A. Nakamura, H. Okuda, K. Wakamatsu, S. Ito, T. Sota, Mid-infrared vibrational spectroscopic characterization of 5,6-dihydroxyindole and eumelanin derived from it. Chem. Phys. Lett. 517, 211-216, 2011. DOI= 10.1016/j.cplett.2011.10.043

26. V. Capozzi, G. Perna, A. Gallone, P.F. Biagi, P. Carmone, A. Fratello, G. Guida, P. Zanna, R. Cicero, Raman and optical spectroscopy of eumelanin films. J. Mol. Struct. 744-747, 717-721, 2005. DOI= 10.1016/j.molstruc.2004.11.074

27. A. Napolitano, A. Pezzella, G. Prota, R. Seraglia and P. Traldi, Structural Analysis of Synthetic Melanins from 5,6-Dihydroxyindole by Matrix-assisted Laser Desorption/Ionization Mass Spectrometry. Rapid Commun. Mass Spectrom., 10, 468-472. 1996. DOI= 10.1002/(SICI)1097-0231(19960315)10:4<468::AID-RCM506>3.0.CO;2-6

28. J.P. Bothma, J.de Boor, U. Divakar, P.E. Schwenn, P. Meredith, Device-Quality Electrically Conducting Melanin Thin Films. Adv. Mater. 20, 3539-3542, 2008. DOI= 10.1002/adma.200703141

29. E. Di Mauro, O. Carpentier, S. I. Yáñez Sánchez, N. Ignoumba Ignoumba, M. Lalancette-Jean, J. Lefebvre, S. Zhang, C. F. O. Graeff, F. Cicoira, C. Santato, Resistive switching controlled by the hydration level in thin films of the biopigment eumelanin. J. Mater. Chem. C 4, 9544-9553, 2016. DOI= 10.1039/C6TC02793H

30. S. Ito, K. Wakamatsu, M. d'ischia, A. Napolitano, A. Pezzella, in Melanins and Melanosomes: Biosynthesis, Biogenesis, Physiological, and Pathological Functions 167-185, 2011. DOI= 10.1002/9783527636150

31. M. Jastrzebska, A. Kocot, J. K.Vij, J. Zalewska-Rejdak, T. Witecki, Dielectric studies on charge hopping in melanin polymer. J. Mol. Struct. 606, 205-210, 2002. DOI= 10.1016/S0022-2860(01)00873-0

32. C. J. Jan, M. D. Walton, E. P. McConnell, W.S. Jang, Y.S. Kim, J. C. Grunlan, Carbon black thin films with tunable resistance and optical transparency. Carbon 44, 1974-1981, 2006. DOI= 10.1016/j.carbon.2006.01.021

33. A. Celzard, J. F. Marêché, F. Payot, G. Furdin, Electrical conductivity of carbonaceous powders. Carbon 40, 2801-2815, 2002. DOI= S0008-6223(02)00196-3

34. S. D. Namgung, J. Lee, I. R. Choe, T. Sung, Y.O. Kim, Y.S. Lee, K T. Nam, J. Y. Kwon, Increased electrical conductivity of peptides through annealing process. APL Materials 5, 2017. DOI= 10.1063/1.4997562

35. B. E. Barton, E. J. Hukkanen, G. F. Billovits, D. Schlader, M. J. Behr, D. Yancey, M. Rickard, X. Qiu, D. M. Mowery, L. Brehm, B. Haskins, W. Wang, M. S. Spalding, C. Derstine, Carbon, 130, 288-294, 2018. DOI= 10.1016/j.carbon.2018.01.031

36. T. H. Le, Y. Kim, H. Yoon, Electrical and electrochemical properties of conducting polymers. Polymers 9, 2017. DOI= 10.3390/polym9040150

4 Eumelanin as a photocatalytically-active bio-material

4.1 Introduction

Conversion of solar irradiation is widely acknowledged to be one of the most promising strategies for sustainable energy. Photovoltaic conversion of light directly into electricity is currently the most well-developed approach, however there exists a great demand to develop direct solar-to-chemical energy conversion schemes[1, 2]. The classic example is photo- or photoelectrochemical splitting of water into hydrogen and oxygen[3]. H_2 can be burned directly to release energy or used in fuel cells in a completely carbon-free energy cycle. An alternative concept, long-theorized to be thermodynamically as competitive as the H_2 energy cycle, is storing energy in hydrogen peroxide, H_2O_2. H_2O_2 has the significant advantage over H_2 as it exists as a stable aqueous solution. Hydrogen peroxide (H_2O_2) is at the center of a revolution in industrial green chemistry, but it may also hold the key to future efficient, inexpensive, and safe energy technology. It is celebrated as a sustainable reagent since its only byproducts are water and oxygen. Because of these thermodynamically stable byproducts, H_2O_2 contains a high free energy (120 kJ/mol). In turn, the energy contained within hydrogen peroxide can be released in manifold ways. Large amounts of heat can be released via H_2O_2 exothermic autocombustion into H_2O and O_2 steam. This reaction has for instance been used for years in liquid-fueled outer space rockets. A newer discovery is that the spontaneous reactions to produce H_2O and O_2 can be harnessed in fuel cells[4-6], acting in a single compartment where H_2O_2 is both the fuel and oxidizer. The peroxide energy cycle is thermodynamically nearly as efficient as burning H_2. A 50% aqueous solution packs an impressive 1.72 MJ/kg.

In this chapter will be discussed also the way to use eumelanin as photocatalyst for producing hydrogen, which is a relatively well-established fuel concept, and to pave the way for the hydrogen peroxide carbon-free energy cycle, which is something more still in early stages of development but with great potential.

Organic semiconductors are carbon-based materials which have been extensively develop for high performance and low-cost electronics, and are today ubiquitous in display technology, organic-light emitting diodes, and in devices such as copiers, scanners, and printers[7]. They are also the active component in low-cost photovoltaic technologies[8]. Despite the substantial research interest in organic semiconductors, they have been largely overlooked as potential photocatalytic materials. This is largely due to the fault of the fact that many archetypical organic semiconductors are known be sensitive to degradation in the presence of water and oxygen, especially under illumination[9]. Głowacki et al. demonstrated in 2016 organic semiconductor photocathodes for oxygen reduction to peroxide, fabricating a photoelectrochemical cell which generated electrical power and peroxide while illuminated with sunlight (Figure 4.1, left)[10]. We found that the photocatalytic properties of eumelanin were impressive, as it is capable of both peroxide and hydrogen production depending on the level of oxygenation of the environment (Figure 4.1, right).

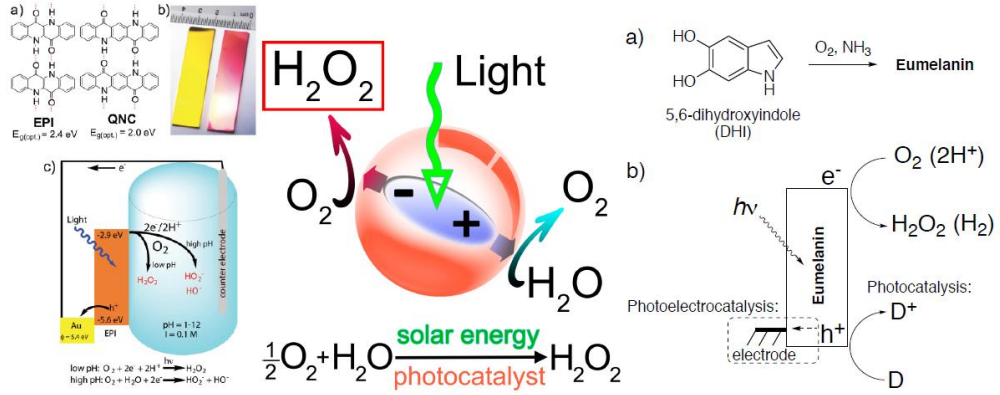

Fig. 4.1. (left) Organic semiconductor photocathodes for catalytic photogeneration of H_2O_2. This was the first example of a photoelectrochemical cell which generates peroxide and critically it is uniquely enabled by organic semiconductors[10] (middle) Nanoparticles of synthetic organic pigments have recently been shown by Gryszel et al.[11] to photocatalyze oxygen reduction selectively to peroxide, with concurrent oxidation of various substrates including water to oxygen. (right)

4.2 Stable Photocatalyst for oxygen reduction reaction (ORR) to hydrogen peroxide

Photoconductivity of eumelanin and its photochemical reactions with oxygen have been known for some time, eumelanins have not been regarded as photofaradaic materials. We find that eumelanin shows photocathodic behavior for both the oxygen reduction reaction and the hydrogen evolution reaction. Eumelanin films irradiated in aqueous solutions at pH 2 or 7 with simulated solar light photochemically reduce oxygen to hydrogen peroxide with accompanying oxidation of sacrificial oxalate, formate, or phenol. Autooxidation of the eumelanin competes with oxidation of donors. Deposition of thin films on electrodes yields photoelectrodes with higher photocatalytic stability compared with the case of pure photocatalysis, implicating the successful extraction of positive charges from the eumelanin layer. These results open up new potential applications for eumelanin as a photocatalytically-active biomaterial, and inform the growing fundamental body of knowledge about the physical chemistry of eumelanins.

The electrical properties of biomolecules such as proteins[12-14], DNA[15], polysaccharides[16, 17], and biopig-ments[18-20] have attracted a growing amount of scientific interest in recent years. This attention is motivated by expanding fundamental understanding of the roles electronic transport may play in biology, as well as the possibility of using bio-origin materials as active components in bioelectronics devices[21, 22]. The long history of research into eumelanins, the most common organic pigmentary materials found in nature, is as complex as the chemistry and physics of eumelanins themselves. From the biophysical perspective, the physiological roles played by eumelanins have been the topic of the most scrutiny[23]. Agreement exists that the primary purpose of eumelanin is as a photoprotectant, as it is ideally suited to absorbing potentially damaging high energy photons[24, 25]. Eumelanins have however been implicated in other important

biochemical processes, and are also crucial for mediating light management in the mammalian eye[26]. Since the seminal work of McGinness[27] on electrical transport in eumelanin in 1974, many have endeavored to exploit eumelanin as a natural active material for bioelectronics[21, 28-30]. Under-standing the nature of eumelanin conductivity is complicated by its heterogeneous nature, and two models for its structure exist: The extended heteromacromolecule model versus the stacked oligomer model, where planar molecular units assemble via π-π stacking. The nature of conductivity of eumelanin remains debated, though the recent consensus is that observations of macroscopic conductivity in eumelanin are primarily protonic in nature. Meredith et al. and Santato et al. have elaborated a charge transport model in a series of papers[31-33] showing the relationship between protons as the major charge carrier and the paramagnetic species observed in eumelanin, with the phenomenon of photoconductivity in eumelanin also being accounted for[34]. There are two distinct radical species in eumelanin, a carbon-centered and semiquinone one, with the latter being involved in protonic photoconductivity and implicated in potential photochemical reactivity[35]. Several devices exploiting protonic transport in eumelanin thin films have been demonstrated[33, 36], though there is also evidence that there may be electronic charge carrier mobility in eumelanin[37]. Eumelanin thin films can be electrochemically-addressed and intercalated with ions[38], thus they have been used in sodium ion batteries[29].

It has been recently demonstrated that some organic semiconducting small molecules can act as aqueous photocatalysts[11, 39] or photoelectrocatalysts[10, 40] for O_2 reduction to H_2O_2. A starting off question for this work is: Can eumelanin be a bio-origin material with intrinsic photocatalytic activity? The photo-chemical properties of eumelanins have been studied in the biological context. Sarna et al. discovered the photochemical production of hydrogen peroxide via oxygen reduction during eumelanin autooxidation[41, 42], inspiring detailed investigation into the role of eumelanin interactions with reactive oxygen species (ROS). In these works, the widely-accepted synthetic eumelanin[23, 33, 36] consisting of oxidatively-

polymerized 5,6-dihydroxyindole (DHI) was used. In his 1990 paper, Sarna noted that the molar quantity of H_2O_2 produced during the photochemical degradation of eumelanin was 20% higher than the molar equivalent of the starting DHI monomers. This foreshadows the possibility of a photochemical redox cycle where photoexcited electrons in eumelanin reduce oxygen to hydrogen peroxide, while the photogenerated positive species oxidize some other donor. It follows that these holes can be, in principle, thanks to the (photo)redox properties pigment, neutralized by electrons originating from an electrode to complete the cycle. In this work, we provide evidence that it is indeed the case that eumelanin behaves in a way analogous to a semiconductor photocatalyst, and is suitable for photoelectrodes as well. Eumelanin can behave as a photocathode in both oxygenated and deoxygenated conditions, demonstrating higher catalytic stability than in the case of pure photocatalytic conditions. This shows that eumelanin can be electrochemically addressed by an underlying electrode with an impressive effectiveness.

As a commonly-used standard eumelanin, we prepared synthetic eumelanin thin films by spin coating a 30 mg/mL 5,6-dihydroxyindole (DHI) methanolic solution onto PET foil substrates followed by the ammonia-induced solid-state polymerization[30] procedure (Fig. 4.2a). For photochemical experiments, eumelanin-coated foil circles were placed in solutions at two different pH values (pH=2, pH=7) in the presence and in absence of different sacrificial electron donors (Phenol, Formate, Oxalate). The "blank" condition, referring to electrolyte alone, indicates that oxygen reduction to hydrogen peroxide, or proton reduction to H_2, can be accompanied by the autooxidation of eumelanin itself. If a photocatalytic redox cycle can be supported, more peroxide should be produced in conditions with added donors, and the eumelanin must show higher stability. The hypothesized photo-redox processes with eumelanin as a photocatalyst are illustrated in Fig. 4.2b.

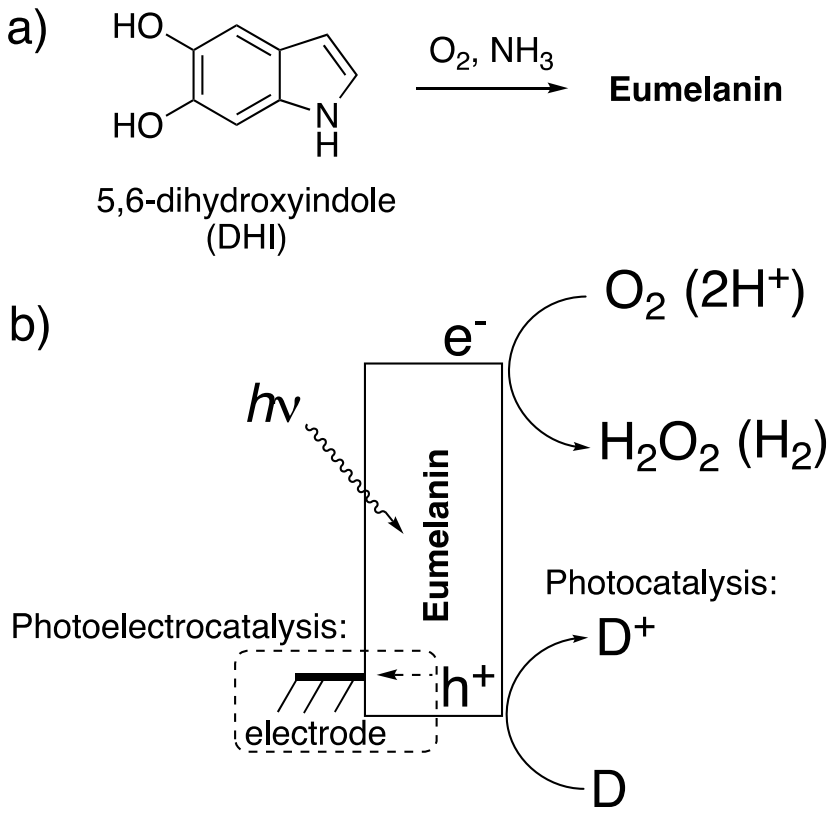

Figure 4.2. a) Eumelanin thin films obtained via oxidation of 5,6-dihydroxyindole (DHI) were used in this study as a model for natural eumelanin. b) Semiconductor model of eumelanin photocatalysis, where photogenerated electrons and holes participate in redox reactions. Reduction of oxygen to hydrogen peroxide proceeds in oxygenated conditions, or reduction of protons to hydrogen in deoxygenated conditions. Holes can oxidize suitable electron donors, or be neutralized by electron injected by an electrode in the case of photoelectrocatalysis. If the hole is not quenched by an electron-donor, it will lead to eumelanin autooxidation.

The two pH values were chosen since neutral pH is relevant to biological applications of melanin and also corresponds with the majority of existing experimental data on melanin photochemistry, and low pH was chosen to see if the proton-enhanced reaction of peroxide production (or hydrogen evolution) proceed more efficiently. High pH conditions cannot be tested for photochemical experiments, as the eumelanin degradates in alkali conditions (pH>9).

We first conducted photolysis experiments by irradiation of eumelanin films in water under a pure O_2 atmosphere, using solar simulator light source with an irradiance of 1.05 sun. (Fig. 4.3a). Aliquots of solution were periodically removed to test for the evolution of hydrogen peroxide using the tetramethyl benzidine/horseradish peroxidase (TMB/HRP) assay well known from biological applications (Fig. 4.3c)[43]. The results for hydrogen peroxide evolution over 12 hours are shown in Fig. 4.3b. Samples with added electron donors yield about twice as much peroxide as "blank" samples. To quantify the difference between the contribution of eumelanin autooxidation and the oxidation of donors, we calculated the catalytic turnover number (TON) expressed as nmol of H_2O_2 generated / nmol DHI (starting indole equivalent) regarding a simplified picture in which DHI acts as monomer and eumelanin as its polymer, although the picture would be more complex[23]. The amount of degraded DHI is calculated from measurement of the optical absorbance of the eumelanin in the film before and after the entire process and comparing to the absorbance of standard curves, as detailed in the experimental methods section. The TONs, along with max final [H_2O_2] values are given in Table 4.1. The presence of donors increases the TON in all cases, giving values 2-4 times higher than eumelanin alone (autooxidation). This result confirms the presence of a true photo-redox cycle in eumelanin (Fig. 4.3b).

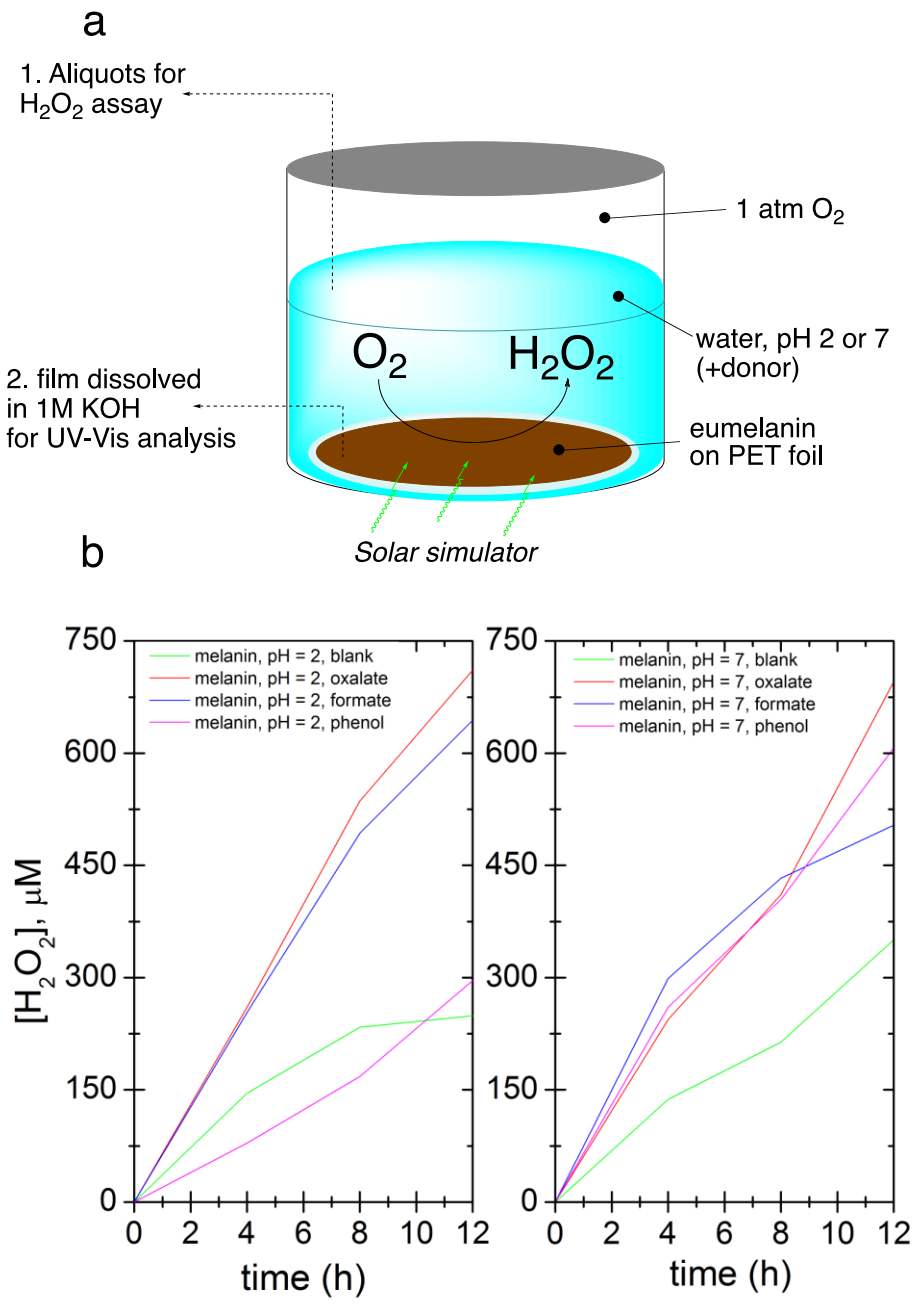
a
1. Aliquots for
H_2O_2 assay
1 atm O_2
water, pH 2 or 7
(+donor)
O_2
H_2O_2
2. film dissolved
in 1M KOH
for UV-Vis analysis
eumelanin
on PET foil
Solar simulator
b
$[H_2O_2]$, µM
time (h)
melanin, pH = 2, blank
melanin, pH = 2, oxalate
melanin, pH = 2, formate
melanin, pH = 2, phenol
melanin, pH = 7, blank
melanin, pH = 7, oxalate
melanin, pH = 7, formate
melanin, pH = 7, phenol

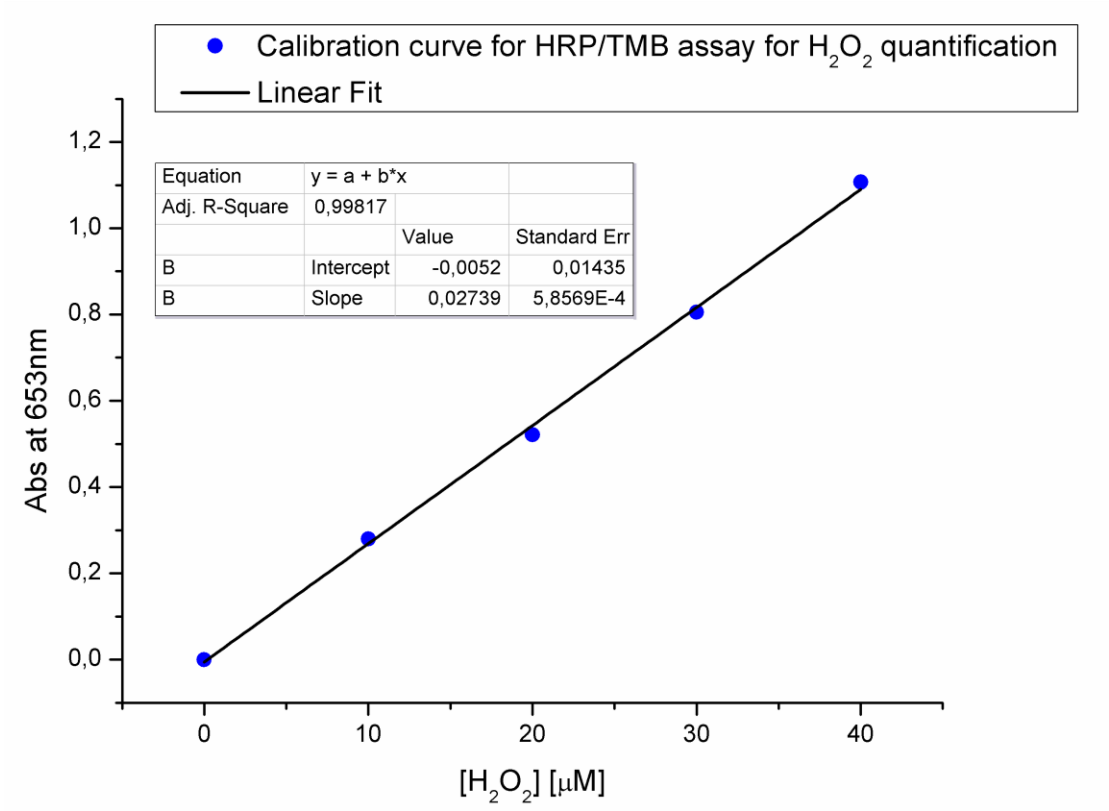

Figure 4.3. Photochemical evolution of hydrogen peroxide by eumelanin. a) The experiment involves irradiating eumelanin films in oxygenated aqueous solution with a broad-spectrum light source and removing aliquots to determine H_2O_2 concentration. At the end of the experiment, the film is removed and dissolved to determine the amount of degraded eumelanin by measuring optical absorption. b) The amount of evolved H_2O_2 over time for conditions of pH 2 and pH 7, without donor (blank case) and with readily-oxidizable donors oxalate, formate, and phenol. c) Example calibration curve for the horseradish peroxidase/tetramethyl benzidine peroxide assay.

pH	Donor	$[H_2O_2]$ in reaction [μM]	catalytic TON $[n_{H2O2\ generated} / n_{DHI\ monomer\ consumed}]$
2	Blank	248.8	1.0
	Oxalate	710.8	3.7
	Formate	644.0	1.7
	Phenol	295.8	1.6
7	Blank	350.6	1.5
	Oxalate	695.5	2.2
	Formate	503.9	3.3
	Phenol	606.8	3.9

Table 4.1. Photochemical evolution of hydrogen peroxide by eumelanin in terms of final peroxide concentration and turnover number (TON).

4.3 Eumelanin as Photoelectrocatalyst for efficient hydrogen peroxide photosynthesis

Concluding that a photochemical redox cycle is possible, and considering that eumelanin has been re-ported to possess photoconductivity[34, 35] it follows that it may also be possible to have a photoelectrochemical catalytic behavior. In this case, photoexcited electrons participate in oxygen reduction, or hydrogen evolution, while carriers originating from the underlying electrode neutralize the resultant positive holes. To this end, we deposited eumelanin films on fluorine-doped tin oxide (FTO), on which we found eumelanin had good adhesion. Photoelectrolysis was carried out with a three-electrode potentiostat using FTO/eumelanin as the working electrode, and the same light source as for the aforementioned photocatalysis experiments. The cathode chamber, containing an O_2 inlet and also an Ag/AgCl reference electrode, was separated from the anodic chamber (Pt wire anode) with a Nafion membrane (Fig. 4.6). The Nafion is critical to prevent the diffusion of H_2O_2 to the anode chamber, as it would otherwise be oxidized on the counter electrode. In chronoamperometric conditions at a potential of 0V, the eumelanin electrode was found to give a steady photocathodic current of about 8 $\mu A/cm^2$, which was found to decline by about 50% over 6 hours of continuous illumination. Measurement of aliquots from the cathode chamber confirmed that the photocathodic product was hydrogen peroxide, which was produced with a constant Faraday yield of ≈90% (Fig. 4.4a). Fig. 4.4a shows a long photoelectrolysis with a few periods where the light was turned off to check the level of the dark current. Regular frequency on/off cycles, with 45s illumination, are plotted in Fig. 4.4b, evidencing a rapid photoelectrochemical response from the eumelanin film. A turnover number of 5.13 was calculated for the eumelanin film used as the photocathode. This TON is higher than any of the photocatalytic cases,

indicating that holes must be quenched in the eumelanin layer by the FTO electrode more efficiently than they oxidize the various donor molecules discussed previously. Since the films are 150 nm thick, conductivity/photoconductivity of the eumelanin plays a key role.

The distinctive absorption of eumelanins has been seen as evidence that it is an amorphous semiconductor analogous to amorphous silicon, for instance; or it can be interpreted as originating from a mix of different discrete chromophores overlaying to create the absorption envelope of eumelanin[24]. One can question which of these chromophoric species is responsible for the photocatalytic processes. We measured the photocathodic current using a series of different narrow-band LEDs, calibrated to the same irradiance, in order to construct a photocurrent action spectrum (Fig. 4.4c). These results show that all wavelengths where the eumelanin absorbs photo-current is generated, and its magnitude follows the optical absorption of the eumelanin film. This behavior could be explained by a more complex picture in which there is a cooperative contribution of excited states of different potentials contributing to a single higher potential excited state as resultant after disproportionation/comproportionation reactions of different pigment constituents[32, 44, 45].

Despite the higher TON in eumelanin under oxygenated photocathodic conditions, it still degrades. The spectra obtained for pristine samples versus used samples, both as thin films (Fig. 4.4d), and after dissolution (Fig. 4.4e), confirm this. Neither the film nor the solution shows any additional peaks or otherwise changes in the shape of the spectra following irradiation. Only a monotonic decrease of each spectrum is seen, indicating that the eumelanin is uniformly degrading and not obviously producing another chromophoric byproduct. Degradation proceeds as in the photocatalytic case from the action of unquenched positive moieties, holes, leading to autooxidation. It is possible that the action of accumulating H_2O_2 may also play an additional role in accelerating degradation as the photoelectrolysis

proceeds and concentration of peroxide increases. In oxygenated electrolytes, the reaction of oxygen to hydrogen peroxide dominates.

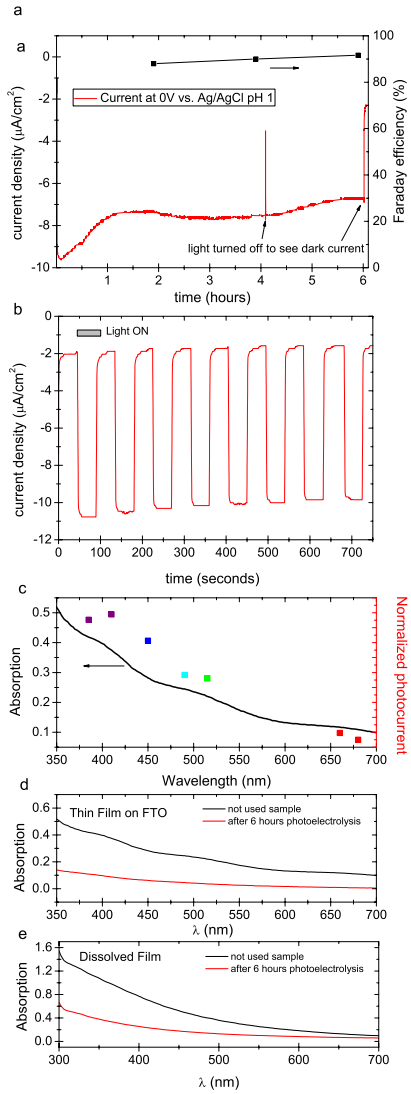

Figure 4.4. Photocathodic experiments in oxygenated conditions. a) Chronoamperometric photocurrent density for an FTO/eumelanin working electrode under solar simulator illumination, pH = 1, 0V vs. Ag/AgCl. Faraday efficiency of O_2 reduction to H_2O_2 is plotted on the right axis. b) Chronoamperometry of a eumelanin photocathode with 45s light on/off cycles. c) Photocurrent action spectrum measurement. eumelanin film on FTO absorption spectrum with accompanying photocurrents for seven different LEDs. d) UV-VIS comparison between dissolved eumelanin thin film used as blank (150nm) vs. dissolved eumelanin thin film used in photo(electro)catalytic oxygen reduction reaction for H_2O_2 evolution (50nm).

4.4 Application of DHI Eumelanin for hydrogen evolution reaction

Thorough deoxygenation of the electrolyte with argon for several hours followed by measurement under argon shows that a smaller photocurrent persists (Fig. 4.5a), on the order of 4 $\mu A/cm^2$ at a cathodic polarization of -0.25V. The photocurrent action spectrum follows the broad absorption of the eumelanin, exactly as in the oxygenated photocathode case (Fig. 4.5b). Sustained photocurrent in fully deoxygenated conditions can only be attributed to the hydrogen evolution reaction, where the photoexcited electrons reduce protons instead of oxygen. We find relatively stable photocurrent over 32 hours. Over this time, the eumelanin film was found to degrade by the same amount as the oxygenated conditions gave after 6 hours. This indicates that despite the photocurrent density being about 70% of the oxygenated photocurrent, the eumelanin is about five times more stable (Fig. 4.5 c,d). These photocurrent densities are too small to provide sufficient quantities of H_2 for reliable quantification, however the only possible alternative hypothesis for the observed photocurrent is a degradation reaction of the eumelanin itself, which is not consist with the observation of substantially improved stability. From this we infer that the hydrogen evolution reaction is indeed occurring, albeit with very limited efficiency.

From our results it emerges that synthetic eumelanin can produce peroxide not only from autooxidation, as previously established[42], but also as part of a redox cycle where a donor molecule is oxidized (as discussed in the case of pure photocatalysis), or where holes are neutralized by an electrode. This behavior is analogous to a classic semiconductor photocatalyst model, from the point of view of photochemical processes the semiconductor picture holds macroscopically. The

mechanisms at play specifically in eumelanin are more complex, and still need to be resolved in detail. Sarna et al. had proven that eumelanin can perform a single-electron photoreduction of oxygen to superoxide, which then becomes further reduced and protonated to yield peroxide[41]. These findings however are for conditions of UV irradiation. We would speculate that with lower energy photons, as in our case, the superoxide mechanism may be surpassed by the thermodynamically-favored two-electron reduction of oxygen directly to peroxide. Our present results on photocathodic current are consistent with either the one-electron, two-electron, or coexistence of both pathways. Our observation of eumelanin-catalyzed photooxidation of various electron-donors, as well as the stabilizing effect of having an electrode injecting electrons into eumelanin photocathodes, highlights the important role of the photogenerated positive species on eumelanin. In the traditional semiconductor model of photocathodes, photoinduced electrons reduce a species in solution, while the corresponding holes are transported away to the electrode. Previous studies have established that protons are the positive charge carrier in eumelanin[31, 34], this means that for eumelanin this photocathode model must be understood differently. A picture consistent with the prevailing knowledge on eumelanin is that photoreduction occurs, leaving behind a positive charge. This can be quenched by electron-carrying semiquinone species, which can be restored via injection of electrons from an underlying electrode. In the pure photocatalytic case, the positively-charged eumelanin moiety oxidizes electron donors directly. Our results confirm that oxygen accelerates photodegradation, and that in oxygen-free conditions a redox cycle involving hydrogen evolution is possible, with apparently better eumelanin stability.

These results are remarkable from the point of view of catalysis – eumelanin is a photocatalytic bio-material capable of peroxide evolution, hydrogen evolution, and photooxidation of various organic substrates. This invites not only exploration in

sustainability technologies with eumelanin as a bio-origin photocatalyst, but also has implications in the biological sciences. Photodynamic therapies exploiting these photoprocesses in eumelanin are intriguing. Recently, eumelanin particles have been explored for photodynamic therapy which harnesses photothermal heating of the particles[46], however our results suggest that photofaradaic reactions could also be used to achieve various physiological effects. Mechanistic understanding must still be improved. More detailed eumelanin photochemistry should be conducted to elucidate the role of one- and two-electron processes. Overall our results open a new side of understanding of the physical chemistry of eumelanins.

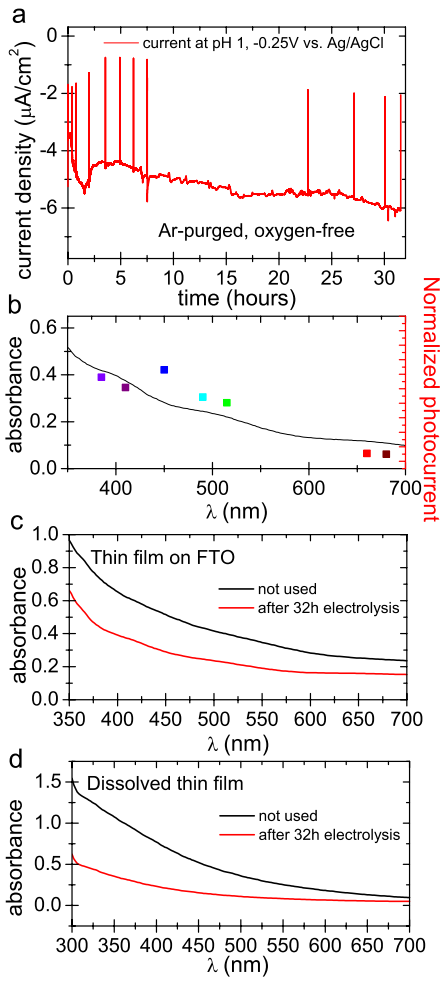

Figure 4.5. Photocathodic experiments in oxygen-free electrolyte. (a) Chronoamperometry with solar simulator illumination over 32 hours at -0.25 V vs. Ag/AgCl and deoxygenated pH =1 electrolyte. The positive spikes in the current trace are turning off of the light source in order to see the level of dark current in the sample (b) Photocurrent action spectrum overlaid with the absorption spectrum of eumelanin on FTO for deoxygenated photocurrent. (c) Direct UV-VIS comparison between DHI eumelanin thin film used as blank (150 nm) vs DHI eumelanin thin film used in the 32-hour photo(electro)catalytic experiment (150 nm); (d) UV-VIS comparison between dissolved eumelanin thin film used as blank vs. dissolved eumelanin thin film used in the same experiment.

4.5 Experimental section

Eumelanin sample preparation. All commercially available reagents were used as received and all the solvents were analytical grade quality. Anhydrous solvents were purchased from commercial sources. 5,6-Dihydroxindole (DHI) was prepared according to a reported procedure[47]. DHI thin films were pre-pared by spin coating with Laurell WS-650MZ-23NPP/LITE coater on round PET foils of 3.14 cm^2 and on square FTO glasses of 3.75cm^2 from concentrated methanol solutions (30 mg/mL) after filtering through a 0.2 μm Whatman membrane using a speed gradient of 2500 rpm for 30s. Appropriate volume deposition (100 - 150 μL) was used. The DHI films then were chemically polymerized following the AISSP procedure: Eumelanin thin films were obtained by exposing the DHI films (150-200 nm thickness) for 1 h to air-equilibrated gaseous ammonia from an ammonia solution (28% in water) in a sealed chamber at 1 atm pressure at controlled temperature (25 - 40°C).

Photocatalysis. Eumelanin films were put in vials in 1 mL solutions at two different pH (pH=2, pH=7) in presence and in absence of different sacrificial electron donors (Phenol, Formate, Oxalate) to test the possibility to increase, with suitable donors, the amount of peroxide produced during the photocatalytic oxygen reduction reaction. A white LED solar simulator with intensity of 1.05 sun was used to illuminate the substrates for a total time of 12 h. Before the exposure of these films to the light, every vial was filled with O_2 at the beginning and after every single H_2O_2 assay made every 4 h. The quantification of the produced hydrogen peroxide was done spectrophotometrically via the method of Horseradish Peroxidase/3,3′,5,5′-Tetramethylbenzidine (TMB) H_2O_2 quantification by

following the oxidation of TMB[43] at 653 nm using a Synergy/H1 microplate reader BioTek®. Aliquots of every single solution (10 μL) were afterwards added into a mixture of 30 μg mL^{-1} TMB (Sigma-Aldrich) and 0.750 ng mL^{-1} HRP (Sigma-Aldrich) in 0.1 M citrate-phosphate buffer pH 6.0, giving a volume of 1 mL. Quantification of the produced H_2O_2 was determined using extinction coefficient values for the TMB dimer and cross-checked with a calibration curve made by measuring solutions of known H_2O_2 (Merck). The TON was calculated with respect to the amount of DHI monomer in the sample. Eumelanin was quantified by dissolving thin films in 1M NaOH solution, and comparing absorption to a standard curve. The standard curve was produced by polymerizing DHI in suspensions using varying known starting quantities of DHI, and subsequently converting these polymer suspensions into solutions by adding NaOH. This gives a linear relationship between absorption and DHI content.

Photoelectrocatalysis. Photoelectrochemical measurements were conducted using an H-cell configuration as shown in Figure 3.6, using a Redox.me MM PEC H-CELL. Cyclic Voltammetry and chronoamperometry experiments were carried out using an Ivium technologies Vertex One potentiostat, with the eumelanin-modified FTO as the working electrode, a Pt wire as the counter electrode, and an Ag/AgCl (3M KCl) reference electrode. The electrodes were illuminated with a white LED light source with the power of 255 mW/cm^2. In our case we compared both oxygenated and deoxygenated (O2-bubbled, Ar-purged) conditions.

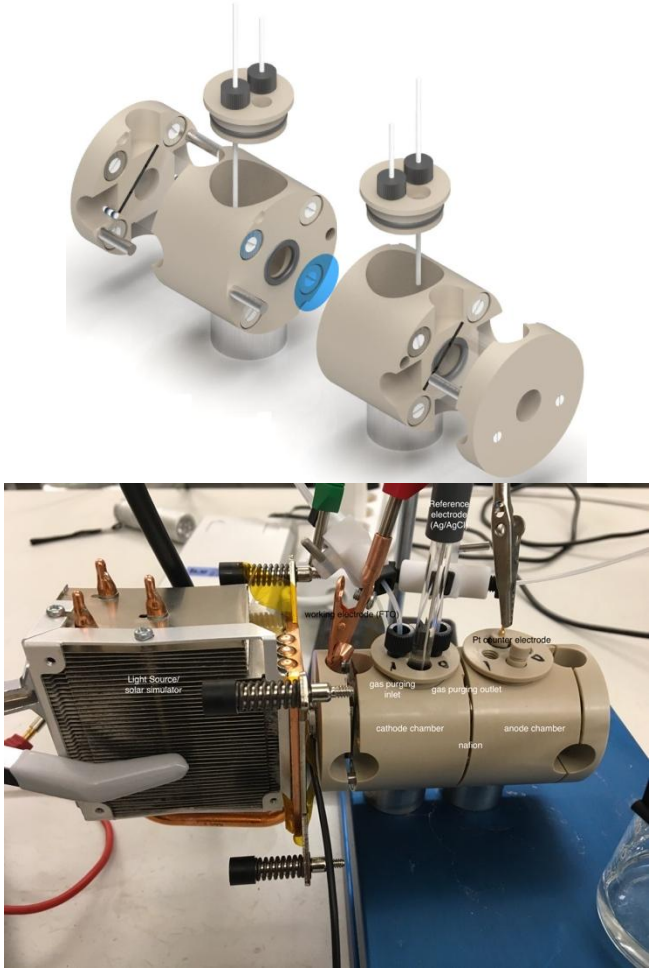

Figure 4.6. Photoelectrochemical H-cell measurement configuration with Eumelanin modified FTO as the working electrode. Aqueous electrolytes in the pH range 1-7 were used, purged with either O_2 or Ar.

4.6 References

1. O. Khaselev, J. A. Turner, A Monolithic Photovoltaic-Photoelectrochemical Device for Hydrogen Production via Water Splitting. Science, 280, 425–427, 1998. DOI= 10.1126/science.280.5362.425
2. T. Hisatomi, J. Kubota, K. Domen, Recent Advances in Semiconductors for Photocatalytic and Photoelectrochemical Water Splitting. Chem. Soc. Rev., 43, 7520–7535, 2014. DOI= 10.1039/C3CS60378D
3. Photoelectrochemical Water Splitting Materials, Processes and Architectures; H.-J. Lewerenz, L. Peter, Eds.; Royal Society of Chemistry: Cambridge, 2013. DOI= 10.1039/9781849737739
4. S. Fukuzumi, Y. Yamada, K. D. Karlin, Hydrogen Peroxide as a Sustainable Energy Carrier: Electrocatalytic Production of Hydrogen Peroxide and the Fuel Cell. Electrochim. Acta, 82, 493–511, 2012. DOI= 10.1016/j.electacta.2012.03.132
5. S. A. Mousavi Shaegh, N.-T. Nguyen, S. M. Mousavi Ehteshami, S. H. Chan, A Membraneless Hydrogen Peroxide Fuel Cell Using Prussian Blue as Cathode Material. Energy Environ. Sci., 5 (8), 8225–8228, 2012. DOI= 10.1039/c2ee21806b
6. K. Mase, M. Yoneda, Y. Yamada, S. Fukuzumi, Seawater Usable for Production and Consumption of Hydrogen Peroxide as a Solar Fuel. Nat. Commun., 7 (May), 11470, 2016. DOI= 10.1038/ncomms11470
7. Martin Pope; Swenberg, C. E. Electronic Processes In Organic Crystals and Polymers, 2nd ed.; Oxford University Press: Oxford, 1999. ISBN: 0195129636,9780195129632
8. S. Günes, H. Neugebauer, N. S. Sariciftci, Conjugated Polymer-Based Organic Solar Cells. Chem. Rev., 107 (4), 1324–1338, 2007. DOI= 10.1021/cr050149z
9. S. Scholz, D. Kondakov, B. Lüssem, K. Leo, Degradation Mechanisms and Reactions in Organic Light-Emitting Devices. Chem. Rev., 115, 8449–8503, 2015. DOI= 10.1021/cr400704v
10. M. Jakešová, D. H. Apaydin, M. Sytnyk, K. Oppelt, W. Heiss, N. S. Sariciftci, E. D. Głowacki, Hydrogen-Bonded Organic Semiconductors as Stable Photoelectrocatalysts

for Efficient Hydrogen Peroxide Photosynthesis. Adv. Funct. Mater., 26, 5248–5254, 2016. DOI= 10.1002/adfm.201601946

11. M. Gryszel, M. Sytnyk, M. Jakesova, G. Romanazzi, R. Gabrielsson, W. Heiss, E. D. Głowacki, General Observation of Photocatalytic Oxygen Reduction to Hydrogen Peroxide by Organic Semiconductor Thin Films and Colloidal Crystals. ACS Applied Materials and Interfaces, 16, 13253-13257, 2018. DOI= 10.1021/acsami.8b01295
12. D. D. Ordinario, L. Phan, W. G. Walkup IV, J.-M. Jocson, E. Karshalev, N. Hüsken, A. A. Gorodetsky, Bulk protonic conductivity in a cephalopod structural protein. Nat. Chem., 6, 596, 2014. DOI= 10.1038/nchem.1960
13. D. D. Ordinario, L. Phan, Y. Van Dyke, T. Nguyen, A. G. Smith, M. Nguyen, N. M. Mofid, M. K. Dao, A. A. Gorodetsky, Photochemical Doping of Protonic Transistors from a Cephalopod Protein. Chem. Mater., 2016. DOI= 10.1021/acs.chemmater.6b00336
14. N. Amdursky, X. Wang, P. Meredith, D. D. C. Bradley, M. M. Stevens, Long-Range Proton Conduction across Free-Standing Serum Albumin Mats. Adv. Mater., 28, 2692, 2016. DOI= 10.1002/adma.201505337
15. D. Porath, A. Bezryadin, S. de Vries, C. Dekker, Direct measurement of electrical transport through DNA molecules. Nature, 403, 635, 2000. DOI= 10.1038/35001029
16. C. Zhong, Y. Deng, A. F. Roudsari, A. Kapetanovic, M. P. Anantram, M. Rolandi, A polysaccharide bioprotonic field-effect transistor. Nat. Commun., 2, 476, 2011. DOI= 10.1038/ncomms1489
17. E. E. Josberger, Y. Deng, W. Sun, R. Kautz, M. Rolandi, Two-terminal protonic devices with synaptic-like short-term depression and device memory. Adv. Mater., 1, 2014. DOI= 10.1002/adma.201400320
18. C. W. Tang, A. C. Albrecht, Photovoltaic effects of metal-chlorophyll-a-metal sandwich cells. J. Chem. Phys., 62, 2139, 1975. DOI= 10.1063/1.430780
19. M. Irimia-Vladu, E. D. Głowacki, P. A. Troshin, G. Schwabegger, L. Leonat, D. K. Susarova, O. Krystal, M. Ullah, Y. Kanbur, M. A. Bodea, V. F. Razumov, H. Sitter, S. Bauer, N. S. Sariciftci, Indigo - A natural pigment for high performance ambipolar organic field effect transistors and circuits. Adv. Mater., 24, 375, 2012. DOI= 10.1002/adma.201102619

20. E. D. Głowacki, G. Voss, N. S. Sariciftci, 25th anniversary article: Progress in chemistry and applications of functional indigos for organic electronics. Adv. Mater., 25, 6783, 2013. DOI= 10.1002/adma.201302652
21. P. Meredith, C. J. Bettinger, M. Irimia-Vladu, A. B. Mostert, P. E. Schwenn, Electronic and optoelectronic materials and devices inspired by nature. Reports Prog. Phys., 76, 34501, 2013. DOI= 10.1088/0034-4885/76/3/034501
22. D. T. Simon, E. O. Gabrielsson, K. Tybrandt, M. Berggren, Organic Bioelectronics: Bridging the Signaling Gap between Biology and Technology. Chem. Rev., 116, 13009, 2016. DOI= 10.1021/acs.chemrev.6b00146
23. M. d'Ischia, K. Wakamatsu, A. Napolitano, S. Briganti, J. C. Garcia-Borron, D. Kovacs, P. Meredith, A. Pezzella, M. Picardo, T. Sarna, J. D. Simon, S. Ito, Melanins and melanogenesis: Methods, standards, protocols. Pigment cell Melanoma Res., 26, 616, 2013. DOI= 10.1111/pcmr.12121
24. M. D'Ischia, A. Napolitano, A. Pezzella, P. Meredith and T. Sarna, Angew. Chemie - Int. Ed., 2009, 48, 3914–3921. DOI= 10.1002/anie.200803786
25. A. Huijser, A. Pezzella and V. Sundström, Functionality of epidermal melanin pigments: current knowledge on UV-dissipative mechanisms and research perspectives. Phys. Chem. Chem. Phys., 13, 9119–9127, 2011. DOI= 10.1039/C1CP20131J
26. P. Meredith and T. Sarna, The physical and chemical properties of eumelanin. Pigment cell Res., 2006, 19, 572–594 DOI= 10.1111/j.1600-0749.2006.00345.x
27. J. McGinness, , P. Corry, P. Proctor, Amorphous semiconductor switching in melanins. Science 183, 853-855, 1974. DOI= 10.1126/science.183.4127.853
28. C. J. Bettinger, J. P. Bruggeman, A. Misra, J. T. Borenstein, R. Langer, Biocompatibility of biodegradable semiconducting melanin films for nerve tissue engineering. Biomaterials, 30, 3050, 2009. DOI= 10.1016/j.biomaterials.2009.02.018
29. Y. J. Kim, W. Wu, S.-E. Chun, J. F. Whitacre, C. J. Bettinger, Biologically derived melanin electrodes in aqueous sodium-ion energy storage devices. Proc. Natl. Acad. Sci. U. S. A., 110, 20912, 2013. DOI= 10.1073/pnas.1314345110
30. A. Pezzella, M. Barra, A. Musto, A. Navarra, M. Alfe, P. Manini, S. Parisi, A. Cassinese, V. Criscuolo, M. D'Ischia, Stem cell-compatible eumelanin biointerface

fabricated by chemically controlled solid state polymerization. Mater. Horizons, 2, 212, 2015. DOI= 10.1039/c4mh00097h

31. A. B. Mostert, B. J. Powell, I. R. Gentle, P. Meredith, On the Origin of Electrical Conductivity in the Bio-Electronic Material Melanin. Appl. Phys. Lett., 100 (9), 93701. 9, 2012. DOI= 10.1063/1.3688491
32. S. B. Rienecker, A. B. Mostert, G. Schenk, G. R. Hanson, P. Meredith, Heavy Water as a Probe of the Free Radical Nature and Electrical Conductivity of Melanin. J. Phys. Chem. B, 119 (48), 14994–15000, 2015. DOI= 10.1021/acs.jpcb.5b08970
33. J. Wünsche, Y. Deng, P. Kumar, E. Di Mauro, E. Josberger, J. Sayago, A. Pezzella, F. Soavi, F. Cicoira, M. Rolandi and C. Santato, Chem. Mater., 2015, 27, 436–442
34. A. B. Mostert, B. J. Powell, F. L. Pratt, G. R. Hanson, T. Sarna, I. R. Gentle, P. Meredith, Role of semiconductivity and ion transport in the electrical conduction of melanin. Proc. Natl. Acad. Sci. U. S. A. 109, 8943-8947, 2012. DOI: 10.1073/pnas.1119948109
35. S. B. Rienecker, A. B. Mostert, C. Noble, G. R. Hanson and P. Meredith, Sci. Adv., 2018, 4, 1–7
36. M. Sheliakina, A. B. Mostert and P. Meredith, An all-solid-state biocompatible ion-to-electron transducer for bioelectronics. Mater. Horizons, 5, 256–263, 2018. DOI= 10.1039/C7MH00831G
37. J. Wunsche, F. Cicoira, C. F. O. Graeff and C. Santato, J. Mater. Chem. B, 2013, 1, 3836–3842
38. Y. J. Kim, W. Wu, S. E. Chun, J. F. Whitacre, C. J. Bettinger, Catechol-mediated reversible binding of multivalent cations in eumelanin half-cells. Adv. Mater., 26, 6572, 2014. DOI= 10.1002/adma.201402295
39. M. K. Węcławski, M. Jakešová, M. Charyton, N. Demitri, B. Koszarna, K. Oppelt, S. Sariciftci, D. T. Gryko, E. D. Głowacki, Biscoumarin-containing acenes as stable organic semiconductors for photocatalytic oxygen reduction to hydrogen peroxide. J. Mater. Chem. A, 5, 20780, 2017. DOI= 10.1039/c7ta05882a
40. M. Warczak, M. Gryszel, M. Jakešová, V. Đerek, E. D. Głowacki, Organic semiconductor perylenetetracarboxylic diimide (PTCDI) electrodes for electrocatalytic

reduction of oxygen to hydrogen peroxide. Chem. Commun., 54, 1960, 2018. DOI= 10.1039/c7cc08471d

41. W. Korytowski, B. Pilas, T. Sarna, B. Kalyanaraman, Photoinduced generation of hydrogen peroxide and hydroxyl radicals in melanins. Photochem. Photobiol., 45, 185, 1987. DOI= 10.1111/j.1751-1097.1987.tb05362.x
42. W. Korytowski, T. Sarna, Bleaching of melanin pigments. Role of copper ions and hydrogen peroxide in autooxidation and photooxidation of synthetic dopa-melanin. J. Biol. Chem., 265, 12410, 1990. PubMed ID : 2165063
43. P. D. Josephy, T. Eling, R. P. Mason, The horseradish peroxidase-catalyzed oxidation of 3,5,3',5'-tetramethylbenzidine. Free radical and charge-transfer complex intermediates.. J. Biol. Chem., 257, 3669, 1982. PubMed ID : 6277943
44. A. Pezzella, O. Crescenzi, L. Panzella, A. Napolitano, E. J. Land, V. Barone, M. D'Ischia, Free radical coupling of o-semiquinones uncovered. J. Am. Chem. Soc., 135, 12142–12149, 2013. DOI= 10.1021/ja4067332
45. A. J. Clulow, A. B. Mostert, M. Sheliakina, A. Nelson, N. Booth, P. L. Burn, I. R. Gentle, P. Meredith, The structural impact of water sorption on device-quality melanin thin films. Soft Matter, 13, 3954–3965, 2017. DOI= 10.1039/c6sm02420c
46. M. Kim, H. S. Kim, M. A. Kim, H. Ryu, H. J. Jeong, C. M. Lee, Thermohydrogel Containing Melanin for Photothermal Cancer Therapy. Macromol. Biosci., 17, 1, 2017. DOI= 10.1002/mabi.201600371
47. R. Edge, M. D'Ischia, E. J. Land, A. Napolitano, S. Navaratnam, L. Panzella, A. Pezzella, C. A. Ramsden, P. A. Riley, Dopaquinone redox exchange with dihydroxyindole and dihydroxyindole carboxylic acid. Pigment cell Res., 19, 443, 2006. DOI= 10.1111/j.1600-0749.2006.00327.x

Conclusions and future directions

From all of this work, as result of this finding, we demonstrate new potentialities of Eumelanin in organic-electronics and bio-electronics field, developing new methods and new recipes either to increase electrical conductivity in order to exploit this material for several applications and purposes either to use it as photocatalytically-active material. The results concerning photo(electro)catalysis are remarkable from the point of view of catalysis – eumelanin is a photocatalytic bio-material capable of peroxide evolution, hydrogen evolution, and photooxidation of various organic substrates. This invites not only exploration in sustainability technologies with eumelanin as a bio-origin photocatalyst, but also has implications in the biological sciences. Photodynamic therapies exploiting these photoprocesses in eumelanin are intriguing. Recently, eumelanin particles have been explored for photodynamic therapy which harnesses photothermal heating of the particles, however our results suggest that photofaradaic reactions could also be used to achieve various physiological effects. Although a conclusive picture about the conductor vs semiconductor behavior of the eumelanins and insights about the mobility of charge carriers will require further investigations, results related to annealed thin films of Eumelanin, here reported, radically modify the actual picture of the eumelanin charge transport properties, reversing the paradigm according to which eumelanin conductivity increases with the water content of the pigment. Indeed, when eumelanin molecular constituents are rearranged in conductive layers, the contribution of electronic current is demonstrated to be largely preeminent with respect to the ionic one, allowing to get unprecedented conductivity and to consider the mammalian pigment as an actual conductor and remarks the possibility to use this material in several different applications in organic(bio)-electronics, for example as conductive layer in organic light

emitting diode devices working on the transparency and modulating the conductivity of the layer.

List of Publications

1. Aqueous photo(electro)catalysis with eumelanin thin films

L. Migliaccio, M. Gryszel, V. Đerek, A. Pezzella, E. Głowacki

MATERIALS HORIZONS; 2018 DOI 10.1039/c8mh00715b

IF 13.183 JRank Q1 CHEMISTRY,MULTIDISCIPLINARY citation n. 0

2. Eumelanin coating of silica aerogel by supercritical carbon dioxide deposition of a 5,6-Dihydroxyindole thin film

G. Caputo, I. Bonadies, **L. Migliaccio**, M. F. Caso, A. Pezzella

Materials; 2018 DOI: 10.3390/ma11091494

IF 3.325 JRank Q2 CHEMISTRY,MULTIDISCIPLINARY citation n. 0

3. Eumelanin–PEDOT:PSS Complementing En Route to Mammalian-Pigment- Based Electrodes: Design and Fabrication of an ITO-Free Organic Light-Emitting Device

L. Migliaccio, S. Aprano, L. Iannuzzi, M. G. Maglione, P. Tassini, C. Minarini, P. Manini, and A. Pezzella

Advanced Electronic Materials; 2017 DOI:10.1002/aelm.201600342

IF 5.466 JRank Q1 CHEMISTRY,MULTIDISCIPLINARY citation n. 5

4. Eumelanin-Based Organic Bioelectronics: Myth or Reality

M. Barra, I. Bonadies, C. Carfagna, A. Cassinese, F. Cimino, O. Crescenzi, V. Criscuolo, M. d'Ischia, M. G. Maglione, P. Manini, **L. Migliaccio**, A. Musto, A. Napolitano, A. Navarra, L. Panzella, S. Parisi, A. Pezzella, C. T. Prontera and P. Tassini

MRS Advances; 2016 DOI: 10.1557/adv.2015.49

IF JRank CHEMISTRY,MULTIDISCIPLINARY citation n. 1

Submitted Articles

1. Impact of eumelanin-PEDOT blending: increased PEDOT crystalline order and packing-conductivity relationship in ternary (PEDOT:PSS:eumelanin) thin films

L. Migliaccio, D. Altamura, C. Giannini, F. Gesuele, P. Manini, M.G. Maglione, P. Tassini, A. Pezzella

Advanced Electronic Materials; 2018 Submitted

IF 5.466 JRank Q1 CHEMISTRY,MULTIDISCIPLINARY

2. Quasi-metallic conductivity in mammalian pigment based eumelanin thin films after simple thermal vacuum annealing

L. Migliaccio, P. Manini, D. Altamura, C. Giannini, M.G. Maglione, P. Tassini, C. Minarini, A. Pezzella

Journal of Materials Chemistry C; 2018 Submitted

IF 5.976 JRank Q1 CHEMISTRY,MULTIDISCIPLINARY

Communications at conferences

1. **Ludovico Migliaccio**, Paola Manini, Maria Grazia Maglione, Paolo Tassini, Irene Bonadies, Francesca Cimino, Cosimo Carfagna, Alessandro Pezzella, "Eumelanin molding: toward human pigment based devices for bioelectronics", BioEl 2016, Kirchberg, Austria. Poster communication
2. **Ludovico Migliaccio**, Paola Manini, Maria Grazia Maglione, Paolo Tassini, Irene Bonadies, Francesca Cimino, Cosimo Carfagna, Alessandro Pezzella, "Eumelanin molding: toward human pigment based devices for bioelectronics", SCI 2016, Mestre, Italy. Poster communication
3. **Ludovico Migliaccio,** Salvatore Aprano, Luca Iannuzzi, Maria Grazia Maglione, Paolo Tassini, Carla Minarini, Paola Manini, Alessandro Pezzella, " Organic Synergisms: Eumelanin/PEDOT(PSS) integration for ITO-free electrodes in bioelectronics and nanomedicine", innoLAE 2017, Genome Campus, Cambridge, UK. Poster communication
4. Salvatore Aprano, Luca Iannuzzi, **Ludovico Migliaccio**, Claudia Diletto, Maria Grazia Maglione, Paolo Tassini, Carla Minarini, Paola Manini, Alessandro Pezzella, Alfredo Rubino, " Metal hexagonal grids and transparent conductors for OLEDs anodes" innoLAE 2017, Genome Campus, Cambridge, UK. Poster communication
5. **Ludovico Migliaccio**, Salvatore Aprano, Luca Iannuzzi, Maria Grazia Maglione, Paolo Tassini, Carla Minarini, Paola Manini, Alessandro Pezzella, "Eumelanin-PEDOT:PSS integration for an ITO-free Organic Light Emitting Diode", XIV Convegno Nazionale AIMAT 2017, Ischia Porto, Italy. Poster communication
6. **Ludovico Migliaccio**, Paola Manini, Carla Minarini, Paolo Tassini , Maria Grazia Maglione, Alessandro Pezzella, "Quasi metallic conductivity in eumelanin thin films", BioEl 2018, Kirchberg, Austria., Poster communication

7. **Ludovico Migliaccio**, Salvatore Aprano, Luca Iannuzzi, Maria Grazia Maglione, Paolo Tassini, Carla Minarini, Paola Manini, Alessandro Pezzella, “Organic Synergisms: Eumelanin/PEDOT(PSS) integration for ITO-free electrodes in bioelectronics”, ORBITALY 2018, Milano, Italy. Poster communication

List of schools seminaries and courses

1. "BIOECONOMY AND CIRCULAR ECONOMY" ORGANIZED BY SCUOLE DI DOTTORATO DELLA SCUOLA POLITECNICA E DELLE SCIENZE DI BASE, ON 29/01/2016, AT C.U. OF MONTE SANT'ANGELO. SEMINAR
2. " LA FOTOCHIMICA: PRINCIPI E APPLICAZIONI" ORGANIZED BY UNIVERSITY OF NAPLES, DEPARTMENT OF CHEMICAL SCIENCES, HELD BY PROF M.R. IESCE. COURSE (10/02/2016). 3 C.F.U.
3. " INDUSTRIA E RICERCA NEL SETTORE BIOFARMACEUTICO: BISOGNI ATTUALI E SVILUPPI FUTURI" ORGANIZED BY UNIVERSITY OF NAPLES, DEPARTMENT OF CHEMICAL SCIENCES, ON 25/02/2016 HELD BY DOTT. SARA CARILLO. SEMINAR.
4. "3rd INTERNATIONAL WINTERSCHOOL ON BIOELECTRONICS, BioEl 2016" FROM 12/03/2016 TO 19/03/2016 IN KIRCHBERG IN TYROL, AUSTRIA. WINTERSCHOOL. 3 C.F.U.
5. " THE VERSATILITY OF MESOSCOPIC SOLAR CELLS" ORGANIZED BY UNIVERSITY OF NAPLES, DEPARTMENT OF CHEMICAL SCIENCES, ON 14/04/2016 HELD BY PROF A. HAGFELDT. SEMINAR
6. " METODI DI STRUTTURA ELETTRONICA PER MATERIALI ALLO STATO SOLIDO" ORGANIZED BY UNIVERSITY OF NAPLES, DEPARTMENT OF CHEMICAL SCIENCES, HELD BY PROF. A. B. MUNOZ-GARCIA. COURSE (21/06/2016). 3 C.F.U.
7. "AGGIORNAMENTO AVANZATO SULLA TECNOLOGIA DEL VUOTO E ULTRA-ALTO VUOTO" ORGANIZED BY RESEARCH CENTER ENEA IN PORTICI (ITALY) HELD BY PFEIFFER VACUUM ITALY S.p.A.. COURSE. (04/10/2016). 3 C.F.U.
8. "LEAK DETECTION" ORGANIZED BY RESEARCH CENTER ENEA IN PORTICI (ITALY) HELD BY PFEIFFER VACUUM ITALY S.p.A.. COURSE. (04/10/2016).
9. "SICUREZZA NELL'USO DI GAS COMPRESSI - CRIOGENICI - TOSSICI" ORGANIZED BY RESEARCH CENTER ENEA IN PORTICI (ITALY) HELD BY RIVOIRA INDUSTRIAL & SPECIALITY GASES. COURSE. (05/10/2016).

10. "MOLTEPLICITY OF MORPHOLOGIES IN POLY(L-LACTIDE) BIORESORBABLE VASCULAR SCAFFOLDS" ORGANIZED BY RESEARCH CENTER ENEA IN PORTICI (ITALY), ON 07/06/2017, HELD BY PROF. I. A. KORNFIELD. SEMINAR

11. "PRIMA SCUOLA NAZIONALE SENSORI CHIMICI" ORGANIZED BY SCUOLE DI DOTTORATO DELLA SCUOLA POLITECNICA E DELLE SCIENZE DI BASE, FROM 24/05/2017 TO 26/05/2017, AT C.U. OF MONTE SANT'ANGELO. SCHOOL. 4 C.F.U.

12. "XIV Convegno Nazionale AIMAT 2017, FROM 12/07/2017 TO 18/07/2017 IN ISCHIA PORTO, ITALY. SUMMERSCHOOL. 3 C.F.U.

13. " SYNTHESIS, STRUCTURE AND APPLICATIONS OF NATURAL AND MODIFIED OIGONUCLEOTIDES" ORGANIZED BY UNIVERSITY OF NAPLES, DEPARTMENT OF CHEMICAL SCIENCES, HELD BY PROF. D. MONTESARCHIO. COURSE (21/07/2017). 3 C.F.U.

14. "ORGANIC AND BIO-ORGANIC SYSTEMS FOR SOLAR ENERGY CONVERSION AND CO_2 RECYCLING" ORGANIZED BY LINKOPINGS UNIVERSITET (SWEDEN), ON 17/01/2018, HELD BY PROF. N. S. SARICIFTCI. SEMINAR.

15. "METROLOGICAL AFM AND ITS APPLICATIONS" ORGANIZED BY LINKOPINGS UNIVERSITET (SWEDEN), ON 20/02/2018, HELD BY DOTT. M. HAVLICEK. SEMINAR.

16. "5th INTERNATIONAL WINTERSCHOOL ON BIOELECTRONICS, BioEl 2018" FROM 10/03/2016 TO 17/03/2016 IN KIRCHBERG IN TYROL, AUSTRIA. WINTERSCHOOL. 3 C.F.U.

Aknowledgements (Italian version)

Ringraziamenti

Prima di tutto vorrei ringraziare i miei due instancabili supervisori, Alessandro Pezzella e Paolo Tassini, senza i quali ogni singolo esperimento sarebbe stato difficile e dalle complicate risposte scientifiche. So ancora di dovere imparare tanto da loro, ma durante questi anni ho cercato di rubare tante idee che spero mi serviranno per il mio futuro da ricercatore. Inoltre risulta essere doveroso ringraziare Mariagrazia Maglione e Paola Manini che mi hanno aiutato anche in situazioni che esulavano dagli esperimenti relativi alla mia tematica di dottorato e che sono state sempre in prima linea durante l'intero percorso.

Una piccola parentesi del mio dottorato, che poi si è rivelata essere una modifica della mia vita, è stata l'esperienza svolta come studente visitatore presso il LOE group in Norrköping (Sweden), per la quale opportunità ringrazio Alessandro Pezzella che ha creduto in me e mi ha saputo bene indirizzare, ed è doveroso ringraziare anche Eric Głowacki che è stato il mio supervisor durante questo periodo ed il suo gruppo che mi ha accolto e considerato come parte integrante del team. Per tutto ciò che hanno fatto, è più che giusto ringraziarli singolarmente, per cui vorrei ringraziare Vedran Đerek, uno degli scienziati più meticolosi che abbia mai incontrato nel mio percorso, praticamente un factotum con un cervello non comune. Vorrei ringraziare anche Marie Jakešová, una vera amica ed una persona splendida non solo scientificamente ma anche umanamente. E ringrazio anche Maciej Gryszel, il mio compagno di esperimenti, col quale, nonostante gli innumerevoli momenti di desolazione, siamo stati in grado anche di ridere durante gli esperimenti. E’ stato un periodo davvero bello che mi ha reso più forte. Non è stato semplice per me lottare contro il freddo, la neve, il buio e quant'altro, per me che se mi affaccio dall'ufficio vedo il mare, però ha aiutato a migliorare me stesso

perchè sono del parere che prima di essere dei buoni scienziati, bisogna essere delle brave persone ed apprezzare le cose che si hanno di fronte. Per questo vorrei ringraziare il pezzo più grande del mio cuore, la mia " Bella famiglia", che mi è stata accanto dai giorni più felici a quelli più tristi di questo percorso. Non era semplice per loro combattere contro il mio brutto carattere risultante da giornate di esperimenti inconclusivi, ma non me lo hanno mai fatto pesare e ne approfitto qui per scusarmi con loro di questo mio atteggiamento. Però uno dei momenti più belli della giornata era proprio ritornare a casa, la mia fortezza, con le mie persone fidate ed amate, per cui vorrei ringraziarli riportando alcune righe dal discorso iniziale del film "Patch Adams", che ho visto quando ero in Svezia e subito ho condiviso quel pensiero e significato attribuito a casa e nel mio caso famiglia:

"Per tutti la vita è un ritorno a casa: commessi viaggiatori, segretari, minatori, apicoltori, mangiatori di spade, per tutti. Tutti i cuori irrequieti del mondo, cercano tutti la strada di casa.

È difficile descrivere cosa provassi allora… immaginatevi di camminare in un turbine di neve senza neppure accorgervi di camminare in tondo: la pesantezza delle gambe nei cumuli, le vostre grida che scompaiono nel vento con la sensazione di essere piccoli e immensamente lontani da casa. Casa. Il dizionario la definisce sia come un luogo di origine sia come uno scopo o una destinazione… e la bufera, la bufera era tutta nella mia mente. O come dice Dante, il divino poeta: «Nel mezzo del cammin di nostra vita, | mi ritrovai per una selva oscura | ché la diritta via era smarrita.» Alla fine ho trovato la diritta via, ma nel posto più improbabile."

Ovviamente ringrazio i miei amici storici, Antonio, Carlo e Nicola, persone con le quali sono cresciuto e benchè abbiamo intrapreso strade diverse per prefiggerci

obiettivi diversi, non c’è stato giorno in cui non ci siamo visti e divertiti per rendere le giornate più felici. Li ringrazio perchè mi hanno sempre sostenuto in tutto quello che ho fatto, credendo in me e rafforzando la mia costanza ed audacia in tutte le attività che svolgevo.

Infine ringrazio "Lei", LA MUSICA, la dama di accompagnamento perfetta di ogni singolo istante della mia vita. Mi reputo essere una persona abbastanza solitaria, la musica e la Chitarra però mi hanno ingentilito e sono di una compagnia che non stanca mai, dalle corse per prendere i treni, alle lunghe camminate di ritorno a casa, ai voli aerei, agli innumerevoli esperimenti.

La musica sensibilizza, ascoltatela, fatevelo dire da un solitario topo di laboratorio come me.